

The dual GLP-1/glucagon receptor agonist G49 mimics bariatric surgery effects by inducing metabolic rewiring and inter-organ crosstalk

Received: 7 April 2021

Accepted: 1 November 2024

Published online: 28 November 2024

 Check for updates

A list of authors and their affiliations appears at the end of the paper

Bariatric surgery is effective for the treatment and remission of obesity and type 2 diabetes, but pharmacological approaches which exert similar metabolic adaptations are needed to avoid post-surgical complications. Here we show how G49, an oxyntomodulin (OXM) analog and dual glucagon/glucagon-like peptide-1 receptor (GCGR/GLP-1R) agonist, triggers an inter-organ crosstalk between adipose tissue, pancreas, and liver which is initiated by a rapid release of free fatty acids (FFAs) by white adipose tissue (WAT) in a GCGR-dependent manner. This interactome leads to elevations in adiponectin and fibroblast growth factor 21 (FGF21), causing WAT beiging, brown adipose tissue (BAT) activation, increased energy expenditure (EE) and weight loss. Elevation of OXM, under basal and postprandial conditions, and similar metabolic adaptations after G49 treatment were found in plasma from patients with obesity early after metabolic bariatric surgery. These results identify G49 as a potential pharmacological alternative sharing with bariatric surgery hormonal and metabolic pathways.

In the last two decades, glucagon-like peptide-1 receptor (GLP-1R) and glucagon receptor (GCGR) dual agonists (dualAGs) have emerged as potential pharmacological approaches to treat obesity and overcome the risks associated with bariatric surgery¹, as well as limitations in implementing a healthy life-style in population living with obesity. The native peptide oxyntomodulin (OXM), which increases in plasma after Roux-en-Y gastric bypass (mRYGB) bariatric surgery^{2,3}, activates both GLP-1R and GCGR although with reduced affinity compared with their cognate ligands⁴. However, its short half-life in circulation limits its therapeutic utility⁵ and, therefore, more stable dualAGs have been developed. Poci et al.⁶ demonstrated reductions in body weight, hyperglycemia, total fat mass, hepatic steatosis, and improvement of insulin sensitivity in mice upon diet-induced obesity (DIO) treated with a dualAG for 2 weeks. In a subsequent study, they found superior efficacy by increasing GCGR tone in dualAGs, but with adverse consequences in glucose control⁷, emphasizing the importance of developing a balanced activity across GLP-1R and GCGR. Another study

showed reductions in body weight, but not in glycated hemoglobin A1c (HbA_{1c}), in patients with obesity treated with JNJ-64565111 dualAG⁸. Reductions in blood glucose together with increased energy expenditure (EE) and decreased food intake, resulting in loss of fat mass, were reported for a different dualAG (chimeric GLP-1/GCG peptide) following one-month treatment⁹ and for BI456906 dualAG in DIO mice treated during 4 weeks and in phase 1 and 2 trials^{10,11}. Another dualAG administered for 8 weeks also decreased body weight, food intake and fat mass, as well as reduced blood glucose and improved glucose tolerance and lipid metabolism¹².

We have demonstrated the beneficial effect of G49, a dualAG, in resolving metabolic-dysfunction associated steatohepatitis (MASH) and improving liver regeneration under this pathological condition in C57BL/6j mice by targeting multiple homeostatic mechanisms including inflammation, oxidative/endoplasmic reticulum stress, mitochondrial dysfunction, and shifting glucose metabolism¹³. Likewise, another dualAG named cotadutide (MEDI0382) was more

✉ e-mail: pvaldecantos@iib.uam.es; avalverde@iib.uam.es

effective than obeticholic acid in improving liver metabolism and ameliorating MASH and fibrosis in C57BL/6J or *ob/ob* mice on a high trans-fat/fructose/cholesterol diet¹⁴, as well as decreased liver inflammation and apoptosis in adipocytes¹⁵. In a clinical setting, cotadutide improved postprandial glucose excursions and reduced body weight and hepatic fat in obese or overweight individuals with obesity or overweight people with type 2 diabetes^{16,17}, showing the potential to deliver clinically meaningful effects. In a phase 2b trial, cotadutide reduced glycemia and body weight and improved metabolic-dysfunction associated steatotic liver disease (MASLD)¹⁸. On the other hand, the dual GLP-1-glucose-dependent insulinotropic peptide (GIP) receptor agonist LY3298176 (Tirzepatide) provided substantial and sustained reductions in body weight in a 72-week trial in individuals with obesity¹⁹. Remarkably, addition of CGCR co-agonism to GLP-1/GIP increased EE in obese mice^{20,21} and in a phase 2 trial showed improvements in weight loss of 15% in 60%, 75% and 83% adults with obesity receiving 4, 8 and 12 mg, respectively²².

Despite these preclinical and therapeutic advancements in gut-derived peptides, particularly multiagonists, the molecular mechanisms driving metabolic reprogramming and remodeling of target tissues in the context of an inter-organ crosstalk that leads to fat mass reduction and increased EE have not been addressed. In this work, by using different *in vivo* approaches, we provided evidence of white adipose tissue (WAT) lipolysis as a trigger of the G49 dualAG action. Together with its subsequent effects on the pancreas-liver axis and beige/brown fat, G49 orchestrates a coordinated metabolic reprogramming that increased EE and promotes body weight loss and metabolic fitness.

Results

One-week treatment of DIO mice with G49 rapidly increases lipolysis and induces a beige immune signature in visceral WAT

In our previous study, we reported the efficacy of G49 (100 nmol/kg) in DIO mice treated for 3 weeks in reducing steatosis and hepatic inflammation in parallel with a reduction in body weight and improvement in liver regeneration¹³. Herein we focused in deciphering, at the molecular level, the metabolic reprogramming triggered by G49 on its target tissues, an issue not investigated before with a multiagonist. Initially, a dose-response study was conducted in male mice fed a high-fat diet (HFD) for 12 weeks followed by G49 treatment (*s.c.* injection every 2 days) for 1 week. Figure 1A shows that G49 (100 nmol/kg) acutely reduced body weight ($15.6 \pm 1.27\%$) to levels comparable with those of age-matched mice fed a chow diet (CHD). Notably, food intake was reduced after the first G49 injection concurrently with an increase in cFos-positive POMC neurons in the arcuate (ARC) nucleus of the hypothalamus (Fig. S1B–D). Food intake progressively normalized, and no differences were observed between vehicle and G49-treated mice after 1 week of treatment (Figs. 1A and S1B), time at which the percentage of activated POMC neurons was reduced (Fig. S1C, D). A higher dose of G49 (500 nmol/kg) strongly reduced body weight and suppressed cumulative food intake in DIO mice, but this treatment was not further considered to comply with animal welfare guidelines, whereas a lower dose (20 nmol/kg) reduced weight loss by $6.9 \pm 0.89\%$ (Fig. 1A). Remarkably, a correlation was observed between the initial body weight and body weight loss during 1-week treatment with G49 (100 nmol/kg) in different cohorts of DIO mice (Fig. 1B). Body weight loss in the absence of a reduction in cumulative food intake was also found in DIO female mice treated with G49 for 1 week (Fig. S2A, B). When we conducted the 1-week treatment with G49 in male mice on a reversed light/dark cycle (RC), body weight loss was more pronounced compared to that of mice on normal cycle ($20.1 \pm 0.49\%$ versus $16.1 \pm 0.72\%$) in parallel with a

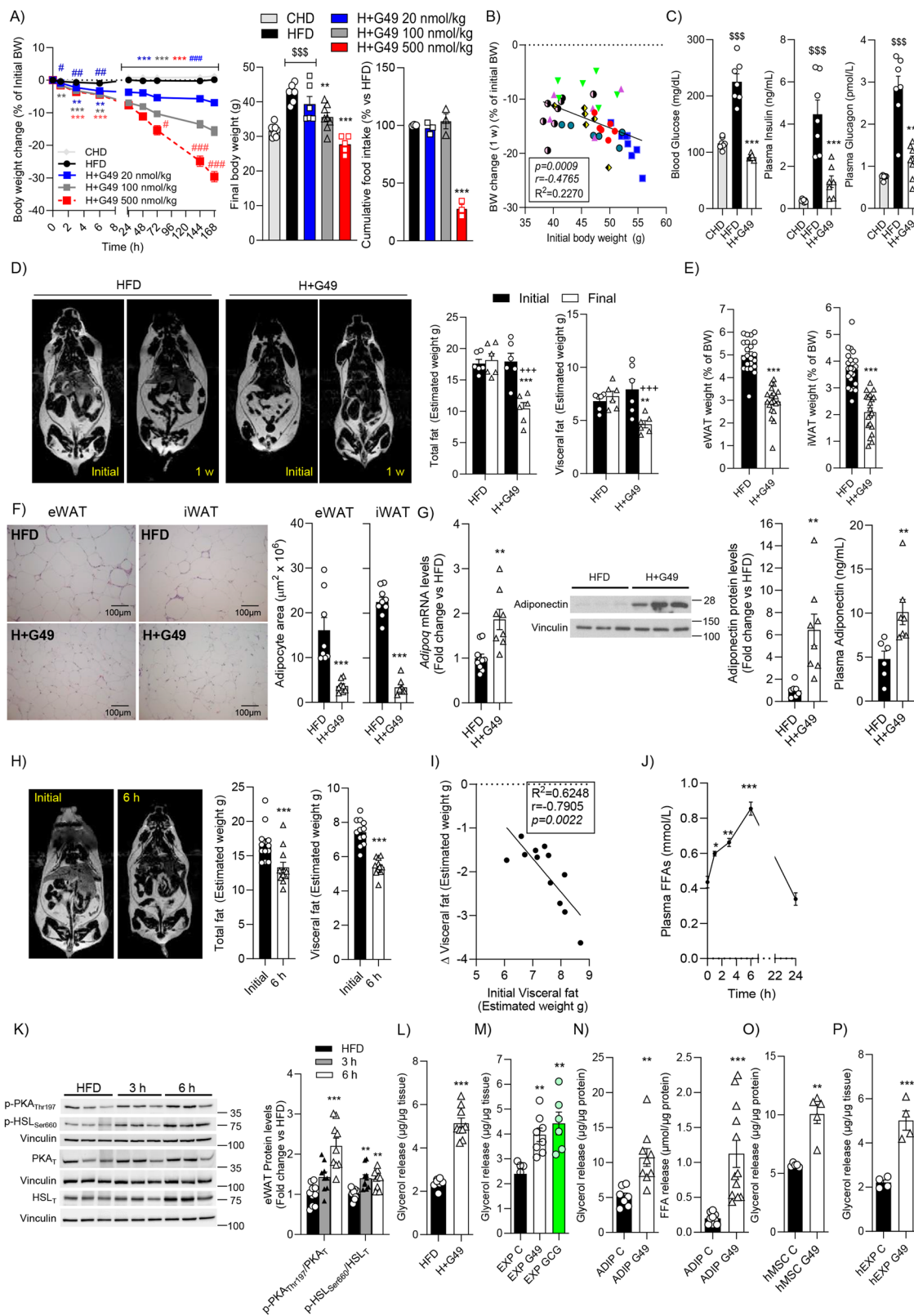
reduction in cumulative food intake (Fig. S2D). To decipher the specific effects of G49 in switching metabolism independently of its anorexigenic effect, subsequent studies were conducted in male mice treated with this dualAG at 100 nmol/kg during the light phase.

Metabolic profiling revealed substantial decreases in blood glucose, plasma insulin, and glucagon in DIO mice receiving G49 treatment (Fig. 1C). Analysis of body composition showed a reduction in total and visceral fat concurrently with a reduction in epididymal (eWAT) and subcutaneous inguinal (iWAT) WAT weight, adipocyte size, and an increase in adiponectin levels in eWAT and plasma of DIO mice treated 1 week with G49 (Fig. 1D–G). Interestingly, the increase in adiponectin was observed as early as 24 h post-injection (Fig. S2E). The efficacy of G49 in reducing blood glucose and adiposity was also found in female mice (Fig. S2C) and in male mice housed at thermoneutrality (Fig. S2F–I).

Next, the effect of G49 was compared to that of a single GLP-1R agonist (Fc-GLP1)²³. Mice were injected Fc-GLP1 at 50 nmol/kg, a dose adjusted to account for differences in binding affinity to GLP-1R compared to G49 (100 nmol/kg) (Fig. S1A). Comparable peptide plasma levels were found in DIO mice 24 h-post injection of each peptide (105.1 ± 18.33 nM for Fc-GLP1, $n = 6$ and 121.7 ± 12.88 nM for G49, $n = 5$). After 1 week of treatment, Fc-GLP1-injected mice showed an attenuated loss of body weight ($11.0 \pm 0.46\%$ versus 19.2 ± 1.02) and adiposity compared to mice receiving G49 (Fig. S3A). This phenotype was accompanied by reduced cumulative food intake (Fig. S3B) and an increase in cFos positive POMC neurons (Fig. S1C, D) in mice treated with Fc-GLP1, but not G49. Notably, a lesser reduction in blood glucose was found in Fc-GLP1-treated animals during 1 week (Fig. S3C).

Detailed evaluation of reduction in eWAT depots as early as 6 h post-G49 injection revealed a decrease in total and visceral fat that correlated with the initial visceral fat content (Fig. 1H, I). Further, plasma free fatty acids (FFAs) peaked at 6 h post-G49 treatment (Fig. 1J), pointing to a lipolytic effect of this dualAG. At the molecular level, eWAT lipolysis, monitored by protein kinase A (PKA)_{Thr197} and hormone sensitive lipase (HSL)_{Ser660} phosphorylation (Fig. 1K), supported the release of FFAs by this fat depot. This lipolytic molecular signature was also found in iWAT, but not in brown adipose tissue (BAT) (Fig. S4A, B). Lipolysis was also evident by an increase in glycerol released to the medium in eWAT explants from mice treated with G49 and sacrificed after 6 h and confirmed by *ex vivo* treatment of eWAT explants from DIO mice with G49 (500 nM) for 4 h (Fig. 1L, M). Notably, glucagon, used at 10 nM, increased lipolysis in eWAT explants (Fig. 1M). Likewise, treatment of isolated adipocytes from eWAT with G49 increased glycerol and FFA release (Fig. 1N). Further, G49 increased glycerol release in human mesenchymal stem cells (hMSC)-derived adipocytes and in human explants from omental fat (Fig. 1O, P). By contrast, elevation of FFAs was not observed in Fc-GLP1-treated mice for 6 h (Fig. S3D).

Histological evaluation of eWAT sections at 6 h post-G49 injection revealed rapid changes in adipocyte features with increased number of smaller adipocytes together with presence of TUNEL positive cells and elevations in fibroblast growth factor 21 (*Fgf21*) mRNA levels (Fig. 2A, B). Remodeling of eWAT by G49 was also assessed by a transient increase in *Acta2*, *Tgfb*, and *Mmp9* mRNA levels that declined at day 7 (Fig. 2B). Surprisingly, F4/80 and Tyrosine Hydroxylase (TH) positive immune cells were found in some eWAT areas in mice treated with G49 for 6 h (Fig. 2C) and gene expression analysis revealed upregulated mRNA levels of M2 markers (*Arg1*, *Il10*, *Tgfb*) as well as *Th* (Fig. 2D). Likewise, an increase of *Th* mRNA at 6 h and a peak of *Il14*, *Il10*, and *Il13* that declined at 24 h post-G49 treatment were found in the stromal vascular fraction (SVF). Flow cytometry analysis of the SVF of eWAT from G49-treated animals for 6 h confirmed a beige-related immune signature. This was evidenced by infiltration of eosinophils determined as SiglecF⁺/Cd11b⁺/Cd11c⁻ cell population, particularly the IL4⁺ subpopulation, as previously described²⁴ (Fig. 2E). Also an increase



in M2 (Cd206⁺) subpopulation, concomitantly with a decrease in M1 (Cd11c⁺) cells gated from the macrophages (Cd11b⁺F4/80⁺) (Fig. 2F) and a reduction in neutrophil infiltration (Cd11b⁺Ly6g⁺) (Fig. 2G) were found. Interestingly, G49 increased the Cd206⁺/Cd11c⁺ ratio in the neutrophil population (Fig. 2H). Likewise, invariant NKTs (TCR β ⁺NK1.1⁺Cd3⁺), also related to the beiging process²⁵, were increased in eWAT from G49-treated mice (Fig. 2I).

One-week treatment of DIO mice with G49 induces a transient lipid overload in the liver, increases ketogenesis and FGF21 levels

Due to the rapid increase (1–6 h) in circulating FFAs in G49-treated mice (Fig. 1J), we measured liver triglycerides (TGs) which were elevated at 3–12 h post-injection, peaking at 6 h, in parallel with an increase in hepatic neutrophil infiltration (Fig. 3A), and coincident with

Fig. 1 | One-week treatment of DIO mice with G49 rapidly increases lipolysis in eWAT and white adipocytes. **A** Body weight (BW) evolution (CHD, $n = 8$; HFD, $n = 5$; H + G49 20 nmol/kg, $n = 6$; H + G49 100 nmol/kg, $n = 9$; H + G49 500 nmol/kg, $n = 6$), final body weight (CHD, $n = 8$; HFD, $n = 6$; H + G49 20 nmol/kg, $n = 6$; H + G49 100 nmol/kg, $n = 8$; H + G49 500 nmol/kg, $n = 5$) and cumulative food intake ($n = 3$). BW change: p values in Source data file. Final BW: HFD vs. H + G49 100 nmol/kg, $^{**}p = 0.0024$; HFD vs. H + G49 500 nmol/kg, $^{***}p < 0.0001$; CHD vs. HFD, $^{***}p < 0.0001$; CHD vs. H + G49 20 nmol/kg, $^{***}p = 0.0010$. Cumulative food intake: HFD vs. H + G49 500 nmol/kg, $^{***}p < 0.0001$. Two-way repeated measures (RM) ANOVA with Bonferroni post hoc test for BW evolution. One-way ANOVA with Bonferroni post hoc test for final BW and cumulative food intake. **B** BW loss vs. initial BW (independent cohorts in different colors), Pearson correlation test ($n = 45$, $p = 0.0009$). **C** Blood glucose ($n = 7$), plasma insulin ($n = 7$) and glucagon ($n = 7$ in CHD and HFD; $n = 9$ in H + G49) at 1 week. Glucose: HFD vs. H + G49, $^{***}p < 0.0001$; CHD vs. HFD, $^{***}p < 0.0001$. Insulin: HFD vs. H + G49, $^{***}p < 0.0001$; CHD vs. HFD, $^{***}p < 0.0001$. Glucagon: HFD vs. H + G49, $^{***}p < 0.0001$; CHD vs. HFD, $^{***}p < 0.0001$. One-way ANOVA with Bonferroni post hoc test. **D** MRI images, total fat, visceral fat and lean mass ($n = 6$ at initial; $n = 6$ at 1 week, same mice). Total fat: HFD vs. H + G49, Final $^{***}p < 0.0001$; Initial vs. Final, H + G49 $^{***}p < 0.0001$. Visceral fat: HFD vs. H + G49, Final $^{**}p = 0.0084$; Initial vs. Final, H + G49 $^{***}p = 0.0001$. Two-way RM ANOVA with Bonferroni post hoc test. **E** eWAT and iWAT weight (HFD, $n = 22$; H + G49, $n = 20$). eWAT, $^{***}p < 0.0001$; iWAT, $^{***}p < 0.0001$. Unpaired two-tailed t -test. **F** eWAT and iWAT H&E images and adipocyte area (eWAT $n = 8$; iWAT $n = 9$ in HFD, $n = 8$ in H + G49). Scale bar 100 μm . eWAT adipocyte area, $^{***}p = 0.0007$; iWAT adipocyte area, $^{***}p < 0.0001$. Unpaired two-tailed t -test. **G** eWAT *Adipoq* mRNA

(HFD, $n = 10$; H + G49, $n = 8$), adiponectin protein (HFD, $n = 7$; H + G49, $n = 8$) and plasma adiponectin (HFD, $n = 6$; H + G49, $n = 7$) levels. *Adipoq* mRNA, $^{**}p = 0.0060$; eWAT adiponectin, $^{**}p = 0.0038$; plasma adiponectin, $^{**}p = 0.0023$. Unpaired two-tailed t -test. **H** MRI of total and visceral fat before and 6 h post-G49 injection ($n = 12$ at initial; $n = 12$ at 6 h, same mice). Total fat, $^{***}p < 0.0001$; Visceral fat, $^{***}p < 0.0001$. Paired two-tailed t -test. **I** Δ Visceral fat vs. initial visceral fat ($n = 12$ at initial; $n = 12$ at 6 h, same mice), $p = 0.0022$. Pearson correlation test. **J** Plasma FFAs (t_0 , $n = 9$; t_1 – t_3 h, $n = 6$; t_6 h, $n = 15$; t_{24} h, $n = 11$). Time vs. t_0 : 1 h, $^{*}p = 0.0365$; 3 h, $^{**}p = 0.0018$; 6 h, $^{***}p < 0.0001$. One-way ANOVA with Bonferroni post hoc test. **K** Representative Western blots and quantification: p-PKA_{Thr197}/PKA (HFD, $n = 10$; t_3 – t_6 h, $n = 9$), p-HSL_{Ser660}/HSL (HFD, $n = 9$; t_3 h, $n = 10$; t_6 h, $n = 9$). p-PKA_{Thr197}: 6 h vs. 0 h, $^{***}p < 0.0001$. p-HSL_{Ser660}: 3 h vs. 0 h, $^{**}p = 0.0021$; 6 h vs. 0 h, $^{**}p = 0.0040$. One-way ANOVA with post hoc test. **L** Glycerol released during 4 h in eWAT explants (vehicle or G49, 6 h) (HFD, $n = 7$; H + G49, $n = 9$). $^{***}p < 0.0001$ vs. HFD. Unpaired two-tailed t -test. **M** Glycerol release in eWAT explants untreated (EXP C, $n = 6$) or treated (EXP G49, $n = 8$) with G49 (500 nM) or glucagon (EXP GCG, $n = 6$) (10 nM) for 4 h. EXP C vs. EXP G49, $^{**}p = 0.0052$; EXP C vs. EXP GCG, $^{**}p = 0.0011$. One-way ANOVA with post hoc test. **N** Glycerol (ADIP C, $n = 7$; ADIP G49, $n = 9$) and FFA release (ADIP C, $n = 9$; ADIP G49, $n = 12$) in mouse adipocytes (500 nM G49, 4 h). Glycerol, $^{**}p = 0.0026$. FFA, $^{***}p < 0.0001$. Unpaired two-tailed t -test. **O** Glycerol release in hMSC-derived adipocytes (500 nM G49, 4 h) ($n = 5$ independent cell vials). $^{**}p = 0.0056$. Unpaired two-tailed t -test. **P** Glycerol release in human WAT explants (500 nM G49, 24 h) ($n = 4$, explants from independent individuals). $^{***}p = 0.0008$. Unpaired two-tailed t -test. Data are mean \pm SEM. Source data are provided as a Source Data file.

an increase in lipid accumulation analyzed by H&E and oil-red O staining of liver sections, liver-to-body weight ratio, and alanine aminotransferase (ALT) activity (Fig. 3B–D). To assess a contribution of de novo lipogenesis to this transient hepatic lipid overload, *Srebfl* and *Fasn* mRNA levels were analyzed and both were elevated at 6 h post-G49 treatment (Fig. 3E). This peak was coincident with a rise in plasma insulin (Fig. 3F), which was also observed by ex vivo treatment of pancreatic islets from DIO mice with G49 (500 nM) for 1 or 24 h (Fig. 3G). Treatment with Fc-GLP1 induced a lower insulin peak (Fig. S3E) suggesting a contribution of FFAs as insulin secretagogues as reported²⁶. Both transient hepatic lipid overload (Fig. 3A, B) and lipogenic gene expression (Fig. 3E) decreased thereafter in parallel with an increase in circulating TGs that reached maximal levels at 24 h and decreased to basal levels at 48 h post-G49 treatment (Fig. 3H). To characterize the overall impact of these acute metabolic effects we conducted indirect calorimetry. DIO mice were placed into metabolic cages 2 days prior receiving the first dose of G49 and metabolic parameters were recorded for the following 3 days. As shown in Fig. 3I, a rapid decrease in the respiratory exchange ratio (RER) was detected 6 h post-first and second injection of G49, and this effect was maintained in the following day in both light and dark phases. Interestingly, RER decreased in mice receiving G49 concurring with a concomitant increase in hepatic *Cpt1a* and *Ppara* mRNAs (Fig. 3J) and fatty acid oxidation (FAO) (Fig. 3K). Accordingly, elevations in hepatic *Hmcs2* (encoding mitochondrial 3-hydroxy-3-methylglutaryl CoA (HMG-CoA) synthase) expression and blood ketone bodies were observed 12 h post-first G49 dose (Fig. 3L), time-point coincident with the drop of insulin (Fig. 3F). These changes in ketogenic markers were augmented by the second injection, peaking at 72 h, but decreased thereafter concomitantly with reduced hepatic TG content (Fig. 3A). An increase in blood ketone bodies was also found in female mice treated with G49 for 72 h (Fig. S2C). Since liver ketogenesis is a major source of FGF21²⁷, we studied the modulation of this hepatokine by G49 via GCGR based on previous work²⁸. *Fgf21* expression in liver tissue and FGF21 plasma levels reached significant increases at 12 h post-first G49 dose followed by a similar regulatory pattern than that of ketogenic parameters (Fig. 3M). Since ketogenesis was not elevated in mice receiving Fc-GLP1 (Fig. S3F), these results point to a major contribution of GCGR in the eWAT (lipolysis)-pancreas (insulin secretion)-liver (FAO/ketogenesis/

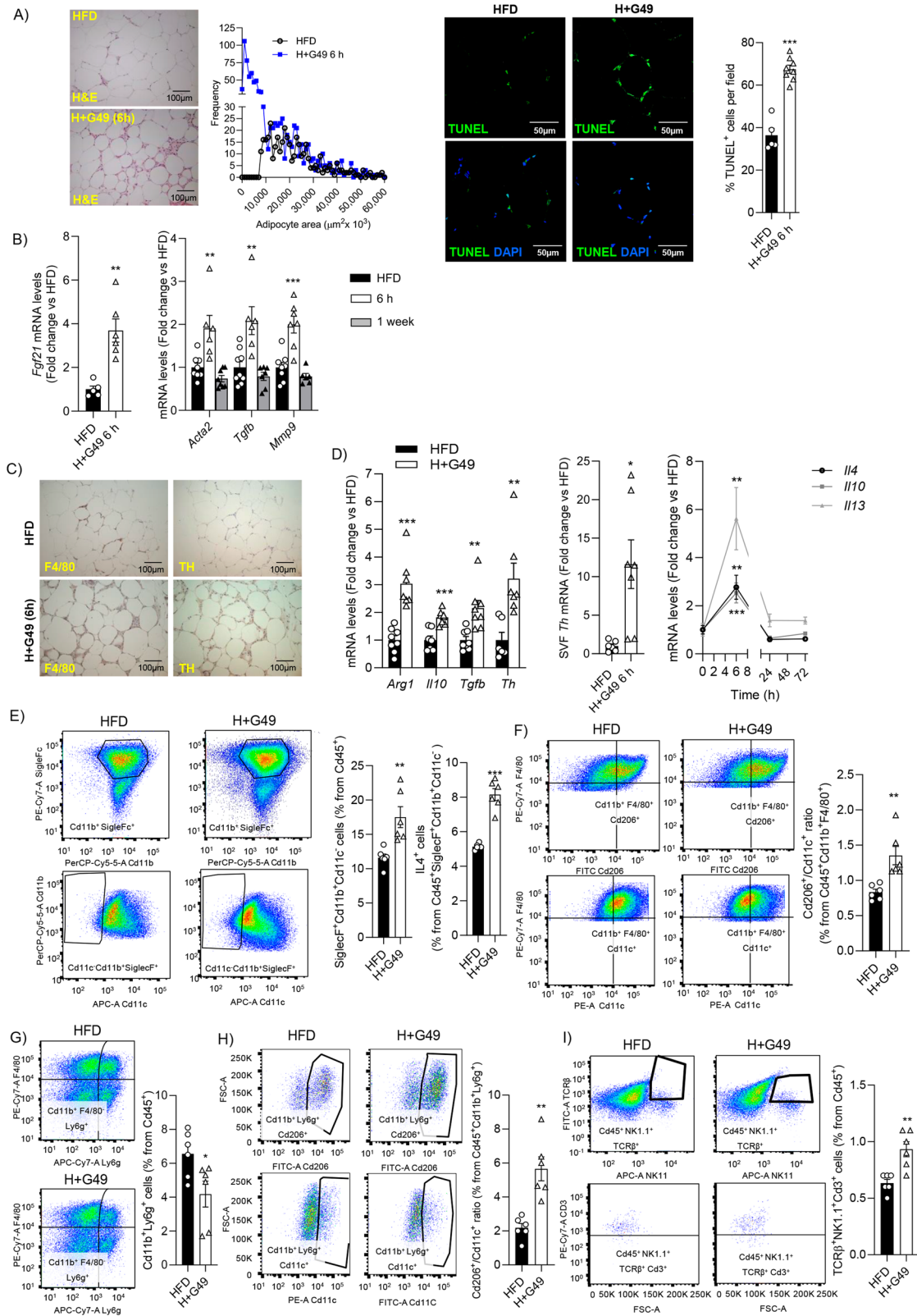
FGF21) interactome as an early event in G49 action that drives the metabolic flexibility described in this study.

Next, in vitro experiments in primary hepatocytes from DIO mice were performed to unravel possible cell autonomous effects of G49. G49 (500 nM) treatment for 16 h increased *Cpt1a* mRNA levels and FAO, an effect concurrent with increased FGF21 levels released to the culture medium and *Sir2* expression, a gene related to mitochondrial function (Fig. S5A–C). Further, in primary mouse hepatocytes isolated from DIO mice, pre-treatment with G49 increased insulin sensitivity manifested by elevations in insulin-induced AKT_{Ser473} phosphorylation (Fig. S5D).

Activation of BAT, WAT beiging and increased energy expenditure in DIO mice treated with G49

Due to the rapid effect of G49 in eWAT we questioned whether 1-week treatment with this dualAG was also able to activate BAT and WAT beiging. Elevation of 2 °C in the BAT skin area following 1-week G49 treatment was found in parallel with an increase in thermogenic-related genes (*Cpt1b*, *Dio2*, *Cox1vii*, *Ucp1*, *Th*, *Fgf21*) and protein levels of UCPI and TH in BAT (Fig. 4A–D). Interestingly, neither UCPI nor BAT temperature were increased by Fc-GLP1 (Fig. S3G, H). A more detailed analysis revealed that BAT temperature and thermogenic-related genes were already elevated by G49 at day 3 (Fig. S5E, left panel), a time-point at which mice presented a significant increase in EE (in both light and dark phases) (Fig. 4E). G49 treatment for 3 days increased basal and maximal respiration in BAT explants (Fig. 4F). To further assess the essential role of UCPI in BAT activation by G49, a cohort of UCPI^{-/-} and UCPI^{+/-} mice fed a HFD were treated for 1 week. Both groups exhibited similar reductions in body weight up to 72 h post-G49 injection. However, UCPI^{-/-} mice did not lose weight beyond this time-point (Fig. 4G). Moreover, G49-treated UCPI^{-/-} mice showed elevations in FFAs (at 6 h) and FGF21 (at 72 h) (Fig. 4H). Of note, these mice also exhibited elevated basal FGF21 in plasma as previously reported²⁹. As expected, no features of BAT activation were found at the end of the treatment in mice lacking UCPI (Fig. 4I).

Next we evaluated a possible cell-autonomous effect of G49 in brown adipocytes (BA). Seahorse analysis of differentiated BA treated with G49 for 16 h showed an increase in mitochondrial respiration (Fig. S6A). Moreover, G49 increased *Cpt1b* gene expression and FAO



and up-regulated lipolysis, thermogenic gene expression (*Ucp1*, *Ppargc1a*, *Sir2*) and UCP1 protein levels in BA (Fig. S6B, C). To further investigate the effects of liver-derived FGF21 (Fig. 3M) in response to G49 in BAT activation, we performed crosstalk experiments in cell culture. Treatment of differentiated BA with medium supplemented with the serum collected from mice receiving G49 for 72 h, which was

enriched in FGF21 (Fig. 3M), increased *Ucp1* mRNA and UCP1 protein levels (Fig. S6D).

The rapid metabolic response of DIO mice to G49 due to eWAT remodeling (Fig. 2A, B) led us to study the beiging process. Increases in angiogenesis (*Vegf*) and beiging-related genes (*Cidea*, *Prdm16*, *Cox11l*, *Ucp1*, *Th*, *Cpt1a*) were found in eWAT of mice receiving G49 for 1 week

Fig. 2 | A single dose of G49 rapidly induces a beiging immune signature in eWAT from DIO mice. **A** Representative H&E staining images and morphometric analysis of adipocyte area ($n = 8$ mice in HFD and H + G49). Scale bar 100 μm . Representative TUNEL images and quantification (HFD, $n = 5$; H + G49, $n = 8$). Scale bar 50 μm . $***p < 0.0001$. Unpaired two-tailed t -test. **B** *Fgf21* mRNA (HFD, $n = 5$; H + G49, $n = 6$) $**p = 0.0015$. Unpaired two-tailed t -test. mRNA levels of remodeling-related genes (*Acta2*, HFD, $n = 8$; 6 h, $n = 6$; 1 week, $n = 8$; *Tgfb*, HFD, $n = 9$; 6 h, $n = 6$; 1 week, $n = 7$; *Mmp9*, HFD, $n = 8$; 6 h, $n = 7$; 1 week, $n = 6$) in eWAT from DIO mice treated with G49 for 6 h or 1 week. *Acta2*: 0 h vs. 6 h, $**p = 0.0023$. *Tgfb*: 0 h vs. 6 h, $**p = 0.0012$. *Mmp9*: 0 h vs. 6 h, $***p = 0.0001$. One-way ANOVA with Bonferroni post hoc test. **C** Representative F4/80 and TH immunostaining images in eWAT ($n = 4$). Scale bar 100 μm . **D** Gene expression-related beiging signature analyzed 6 h after G49 injection. Left panel eWAT: *Arg1*, HFD, $n = 8$; H + G49, $n = 7$, $***p < 0.0001$; *Il10*, HFD, $n = 7$; H + G49, $n = 8$, $***p = 0.0003$; *Tgfb*, HFD, $n = 8$; H + G49, $n = 8$,

$**p = 0.0021$; *Th*, HFD, $n = 6$; H + G49, $n = 7$, $**p = 0.0012$. Unpaired two-tailed t -test. Middle panel SVF: *Th*, HFD, $n = 6$; H + G49, $n = 7$, $*p = 0.0149$. Unpaired two-tailed t -test. Right panel SVF gene expression at different time-points *Il4*, 0 h, $n = 6$; 6 h, $n = 7$; 24 h, $n = 5$; 72 h, $n = 6$. *Il10*, 0 h, $n = 6$; 6 h, $n = 6$; 24 h, $n = 5$; 72 h, $n = 6$. *Il13*, 0 h, $n = 5$; 6 h, $n = 7$; 24 h, $n = 5$; 72 h, $n = 7$. *Il4*: 0 h vs. 6 h, $**p = 0.0015$. *Il10*: 0 h vs. 6 h, $***p = 0.0007$. *Il13*: 0 h vs. 6 h, $**p = 0.0017$. One-way ANOVA with Bonferroni post hoc test. **E–I** Immune cell populations in SVF from eWAT at 6 h post-G49 injection ($n = 6$ in HFD; H + G49). SiglecF⁺Cd11b⁺Cd11c⁺ ($**p = 0.0099$) and IL4⁺ cells ($***p < 0.0001$) (**E**), Cd11b⁺F4/80⁺Cd206⁺ and Cd11b⁺F4/80⁺Cd11c⁺ cells and ratio between these populations ($**p = 0.0036$) (**F**), Cd11b⁺Ly6g⁺ cells ($*p = 0.0331$) (**G**), Cd11b⁺Ly6g⁺Cd206⁺ and Cd11b⁺Ly6g⁺Cd11c⁺ cells and ratio between these populations ($**p = 0.0031$) (**H**), and TCR β ⁺NK1.1⁺Cd3⁺ cells ($**p = 0.0024$) (**I**). **E–I** Unpaired two-tailed t -test. Data are mean \pm SEM. Source data are provided as a Source Data file.

(Fig. 4J), some of which were elevated as early as 48–72 h after the first injection (Fig. S5E, right panel), and these changes in eWAT also concurred with higher UCPI and TH protein content (Fig. 4K). UCPI expression was also analyzed in iWAT of G49-treated mice and a similar improvement was found (Fig. 4L).

The increase of circulating OXM and FGF21 levels in patients after mRYGB correlate with body weight loss

Since OXM is one of the incretins elevated after bariatric surgery, we measured fasting OXM levels in plasma of individuals with severe obesity before and 4 weeks after restrictive or metabolic gastric bypass (mRYGB) bariatric surgery. As previously reported³⁰, mRYGB resulted in greater body weight loss after 1 year compared to restrictive surgery (Fig. 5A). Fasting OXM levels increased at 4 weeks only in patients undergoing mRYGB (Fig. 5B) and were associated with body weight loss one year after surgery. This correlation was confirmed in an independent cohort (Fig. 5C). In the confirmatory cohort we also analyzed the meal-related response of OXM before and 4 weeks after bariatric surgery and patients showed a flat response during the meal test which was restored 4 weeks post-bariatric surgery (Fig. 5D). Notably, a correlation was observed between OXM response, measured as area under the curve (AUC) during the meal test, and the loss of body weight after one year. Interestingly, these associations were not found between body weight loss one year after surgery and GLP-1 plasma levels under basal and in response to the meal test (Fig. 5E, F).

We attempted to further explore the translation of data from the effects of G49 described above by measuring non-esterified FFAs, FGF21 and adiponectin levels in serum from patients with obesity 4 weeks after bariatric surgery. FFAs increased and positively correlated with 4-week body weight loss in mRYGB patients (Fig. 5G). Moreover, FGF21 increased exclusively in patients undergoing mRYGB and, importantly, it significantly correlated with the fat mass before surgery, plasma TG levels 4 weeks after surgery and one year-body weight loss and reduction of waist circumference (Fig. 5H). In agreement with the transient lipid overload found in DIO mice treated with G49 (Fig. 3A), plasma gamma-glutamyl transferase (GGT) activity was transiently elevated in patients undergoing mRYGB at 4 weeks post-surgery and correlated with serum FGF21 (Fig. 5I, J). The increase in serum FGF21 was also found in the independent cohort (Fig. 5K). Likewise, serum adiponectin was elevated in patients undergoing mRYGB 4 weeks after surgery and correlated with 1-year body weight loss (Fig. 5L). Whereas insulin levels decreased in the 2 bariatric surgery groups, the decrease in glucagon was more evident in mRYGB patients (Fig. 5M). These results point to a translational relevance of the pre-clinical data in G49-treated DIO mice.

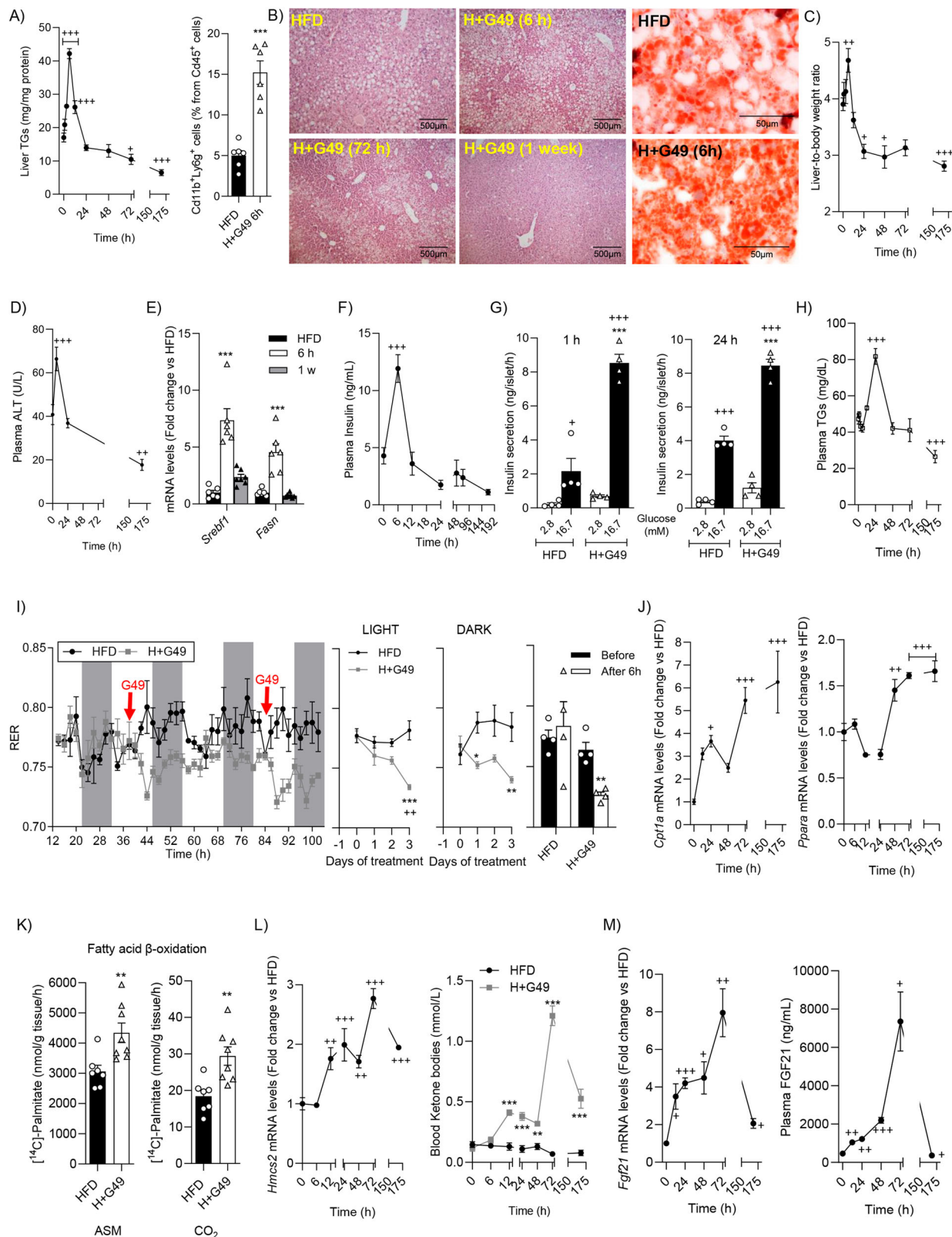
Hepatic FGF21 and adiponectin are required to fully achieve BAT activation by G49

To gain more insights into FGF21 as a mediator of G49 actions in BAT activation, a cohort of hepatocyte-specific FGF21-deficient

(*FGF21^{Alb-KO}*) mice and their controls (*Alb^{Cre}*) fed a HFD were treated with G49 for 1 week. Of note, no differences in body weight were observed up to 48 h of treatment (Fig. 6A). Interestingly, body weight stabilized in G49-treated *FGF21^{Alb-KO}* mice in the period of 3–7 days. G49 did not change cumulative food intake in either genotype treated for 1 week, although an increase in food intake in *FGF21^{Alb-KO}* regardless G49 treatment was observed (Fig. 6A), as reported in mice with global FGF21 deletion³¹. Notably, at 6 h post-G49 injection, plasma FFAs and insulin increased in both genotypes (Fig. 6B, C). However, in *FGF21^{Alb-KO}* mice, blood ketone bodies were not elevated at 72 h compared to the effect of G49 in the *Alb^{Cre}* group (Fig. 6D). These results concurred with a partial reduction of eWAT and iWAT depots and a lower effect of G49 in increasing in UCPI protein levels in BAT (Fig. 6E, F). Likewise, marked differences were found in the effect of G49 on BAT temperature (Fig. 6G). Surprisingly, plasma FGF21 levels in G49-treated *FGF21^{Alb-KO}* mice increased after 72 h (Fig. 6H), suggesting an extrahepatic contribution to circulating FGF21 in response to G49. In this regard, *Fgf21* mRNA levels were upregulated in eWAT and iWAT from *FGF21^{Alb-KO}* mice at 72 h of G49 treatment (Fig. 6I). Noteworthy, *Fgf21* mRNA upregulation was not observed in BAT.

Next, FGF21 reconstitution was conducted by injecting recombinant murine FGF21 (0.05 mg/kg) in HFD-fed *FGF21^{Alb-KO}* mice at 48, 60 and 72 h post-G49 injections. This injection period was chosen based on the transient elevation of plasma FGF21 in DIO mice in response to G49 (Fig. 3M). The efficacy of exogenous FGF21 administration was verified by analyzing its levels in plasma (Fig. 6J). Under these experimental conditions, G49 reduced body weight in the period 3–7 days of treatment (Fig. 6K) and markedly increased UCPI protein levels and BAT temperature (Fig. 6L, M).

Since adiponectin, which is elevated in plasma in G49-treated mice (Figs. 1G and S2E), decreases hepatic lipogenesis and increases β -oxidation through adipoR-mediated PPAR α ³², we next addressed its contribution to G49 effects in DIO mice. To achieve this, a cohort of DIO adiponectin-deficient (*Adipoq^{-/-}*) and control (*Adipoq^{+/+}*) mice were treated with G49 for 1 week. As found in G49-treated *FGF21^{Alb-KO}* mice (Fig. 6A), body weight stabilized in the period of 3–7 days in *Adipoq^{-/-}* mice (Fig. S7A). In these mice, this effect was reflected by the lower reduction in visceral fat at 1 week of treatment compared to *Adipoq^{+/+}* mice (Fig. S7B). The analysis of plasma FFAs at 6 h post-G49 injection revealed similar elevations in both genotypes of mice pointing to preservation of WAT lipolysis (Fig. S7C). However, hepatic FAO and plasma FGF21 analyzed at 72 h post-G49 injection were reduced in *Adipoq^{-/-}* mice (Fig. S7D, E) and, in agreement, G49-mediated increase in BAT temperature was reduced and no increase in UCPI protein levels was found (Fig. S7F). Overall these results demonstrate that elevations in FGF21 and adiponectin are required to fully achieve BAT activation and weight loss by G49.



Both GCGR and GLP-1R are necessary for the full effect of G49 in body weight loss and BAT activation

We next performed experiments aimed to identify the relative contribution of GCGR and GLP-1R to the rapid responses of G49 mediated by the inter-organ crosstalk that favors EE through BAT/beiging activation. To achieve this, we blocked GLP-1R or GCGR with the antagonists exendin 9-39 (Ex9-39) and des-His1-[Glu9]-

Glucagon (1-29) amide (GCGRant), respectively. A cohort of DIO mice was randomized in 8 experimental groups. Half of the mice did not receive G49 and were distributed in groups receiving: vehicle (HFD), GCGR antagonist (H + GCGRant), GLP-1R antagonist (H + Ex9-39) and the 2 antagonists (H + Ex9-39 + GCGRant). The other half received G49 with or without antagonists as follows: H + G49, H + Ex9-39 + G49, H + GCGRant + G49 and H + Ex9-39 + GCGRant +

Fig. 3 | G49 induces a rapid and transient lipid overload in the liver and increases ketogenesis and FGF21. **A** TGs (t_0 , $n = 9$; t_1 –3 h, $n = 7$; t_6 h, $n = 9$; t_{12} h, $n = 5$; t_{24} h, $n = 7$; t_{48} –72 h, $n = 6$; t_{168} h, $n = 7$) and $Cd11b^+Ly6g^+$ cells ($n = 6$) in livers. Liver TGs: 0 h vs. 3 h, $^{***}p < 0.0001$; 0 h vs. 6 h, $^{***}p < 0.0001$; 0 h vs. 12 h, $^{***}p = 0.0004$; 0 h vs. 72 h, $^*p = 0.0118$; 0 h vs. 168 h, $^{***}p < 0.0001$. One-way ANOVA with Bonferroni post hoc test. $Cd11b^+Ly6g^+$ cells, $^{***}p < 0.0001$. Unpaired two-tailed t -test. **B** Representative H&E (Scale bar 500 μ m) and oil red O (Scale bar 50 μ m) staining images ($n = 4$). **C** Liver-to-body weight ratio (t_0 , $n = 12$; t_1 h, $n = 6$; t_3 h, $n = 7$; t_6 h, $n = 15$; t_{12} –24 h, $n = 6$; t_{48} –72 h, $n = 5$; t_{168} h, $n = 10$). 0 h vs. 6 h, $^{**}p = 0.0023$; 0 h vs. 24 h, $^*p = 0.0172$; 0 h vs. 48 h, $^*p = 0.0106$; 0 h vs. 168 h, $^{***}p < 0.0001$. One-way ANOVA with Bonferroni post hoc test. **D** Plasma ALT (t_0 , $n = 8$; t_6 h, $n = 9$; t_{24} h, $n = 7$; t_{68} h, $n = 8$). 0 h vs. 6 h, $^{***}p = 0.0004$; 0 h vs. 168 h, $^{**}p = 0.0016$. One-way ANOVA with Bonferroni post hoc test. **E** mRNA levels (HFD, $n = 6$; t_6 h, $n = 6$; t_1 week, $n = 7$). *Srebf1*: 0 vs. 6 h, $^{***}p < 0.0001$. *Fasn*: 0 vs. 6 h, $^{***}p < 0.0001$. One-way ANOVA with Bonferroni post hoc test. **F** Plasma insulin (t_0 , $n = 7$; t_6 h, $n = 10$, t_{12} –168 h, $n = 6$). 0 h vs. 6 h, $^{***}p < 0.0001$. One-way ANOVA with Bonferroni post hoc test. **G** GSIS in pancreatic islets from DIO mice treated ex vivo with G49 ($n = 4$ islets from independent mice). Left panel. HFD vs. H + G49: 16.7 mM, $^{***}p < 0.0001$; 2.8 vs. 16.7 mM: HFD, $^*p = 0.0277$; H + G49, $^{***}p < 0.0001$. Right panel. HFD vs. H + G49: 16.7 mM, $^{***}p < 0.0001$; 2.8 vs. 16.7 mM: HFD, $^{***}p < 0.0001$; H + G49, $^{***}p < 0.0001$. Two-way ANOVA with Bonferroni post hoc test. **H** Plasma TGs (t_0 , $n = 8$; t_1 –3 h, $n = 6$; t_6 h, $n = 9$; t_{12} h, $n = 6$; t_{24} –48 h, $n = 8$; t_{72} h, $n = 6$; t_{168} h, $n = 8$). 0 h vs. 24 h, $^{***}p < 0.0001$; 0 h vs. 168 h, $^{***}p = 0.0002$. One-way ANOVA with

Bonferroni post hoc test. **I** RER during 3 days of treatment ($n = 4$ HFD; H + G49). Light: HFD vs. H + G49: $^{***}p < 0.0001$ at day 3; H + G49: day 0 vs. day 3, $^{**}p = 0.0059$. Dark: HFD vs. H + G49: $^*p = 0.0246$ at day 1, $^{**}p = 0.0042$ at day 3. RER analyzed 6 h after first and second G49 injection ($n = 4$). HFD vs. H + G49: $^{**}p = 0.0066$ after 6 h. Two-way ANOVA with Bonferroni post hoc test. **J** *Cpt1a* (t_0 , $n = 6$; t_{12} –24 h, $n = 8$; t_{48} –168 h, $n = 7$). 0 h vs. 24 h, $^*p = 0.0247$; 0 h vs. 72 h, $^{***}p = 0.0001$; 0 h vs. 168 h, $^{***}p < 0.0001$. *Ppara* (t_0 , $n = 7$; t_6 h, $n = 9$; t_{12} h, $n = 6$; t_{24} h, $n = 5$; t_{48} h, $n = 6$; t_{72} h, $n = 5$; t_{168} h, $n = 6$). 0 h vs. 48 h, $^{**}p = 0.0015$; 0 h vs. 72 h, $^{***}p < 0.0001$; 0 h vs. 168 h, $^{***}p < 0.0001$. One-way ANOVA with Bonferroni post hoc test. **K** Fatty acid oxidation (FAO) in livers at 72 h (HFD, $n = 7$; H + G49, $n = 8$). ASM, $^{**}p = 0.0068$; CO_2 , $^{**}p = 0.0037$. Unpaired two-tailed t -test. **L** *Hmcs2* (t_0 , $n = 6$; t_6 h, $n = 9$; t_{12} –24 h, $n = 6$; t_{48} –168 h, $n = 7$). 0 h vs. 12 h, $^{**}p = 0.0045$; 0 h vs. 24 h, $^{***}p = 0.0001$; 0 h vs. 48 h, $^{**}p = 0.0063$; 0 h vs. 72 h, $^{***}p < 0.0001$; 0 h vs. 168 h, $^{***}p = 0.0002$. Blood ketone bodies (HFD t_0 , $n = 15$; t_6 h, $n = 11$; t_{12} –72 h, $n = 10$; t_{168} h, $n = 9$ and H + G49 t_0 , $n = 10$; t_6 h, $n = 12$; t_{12} –72 h, $n = 10$; t_{168} h, $n = 8$). HFD vs. H + G49: 12 h, $^{***}p < 0.0001$; 24 h, $^{***}p < 0.0001$; 48 h, $^{**}p = 0.0026$; 72, 168 h, $^{***}p < 0.0001$. Two-way ANOVA with Bonferroni post hoc test. **M** *Fgf21* (t_0 , $n = 5$; t_{12} –168 h, $n = 7$). 0 h vs. 12 h, $^*p = 0.0432$; 0 h vs. 24 h, $^{***}p < 0.0001$; 0 h vs. 48 h, $^*p = 0.0289$; 0 h vs. 72 h, $^{**}p = 0.0070$; 0 h vs. 168 h, $^*p = 0.0255$. Plasma FGF21 (t_0 , $n = 6$; t_{12} –168 h, $n = 7$). 0 h vs. 12 h, $^{**}p = 0.0078$; 0 h vs. 24 h, $^{**}p < 0.0064$; 0 h vs. 48 h, $^{***}p = 0.0002$; 0 h vs. 72 h, $^*p = 0.0101$; 0 h vs. 168 h, $^*p = 0.0258$. Brown–Forsythe and Welch ANOVA with Dunnett’s T3 post hoc test. Data are mean \pm SEM. Source data are provided as a Source Data file.

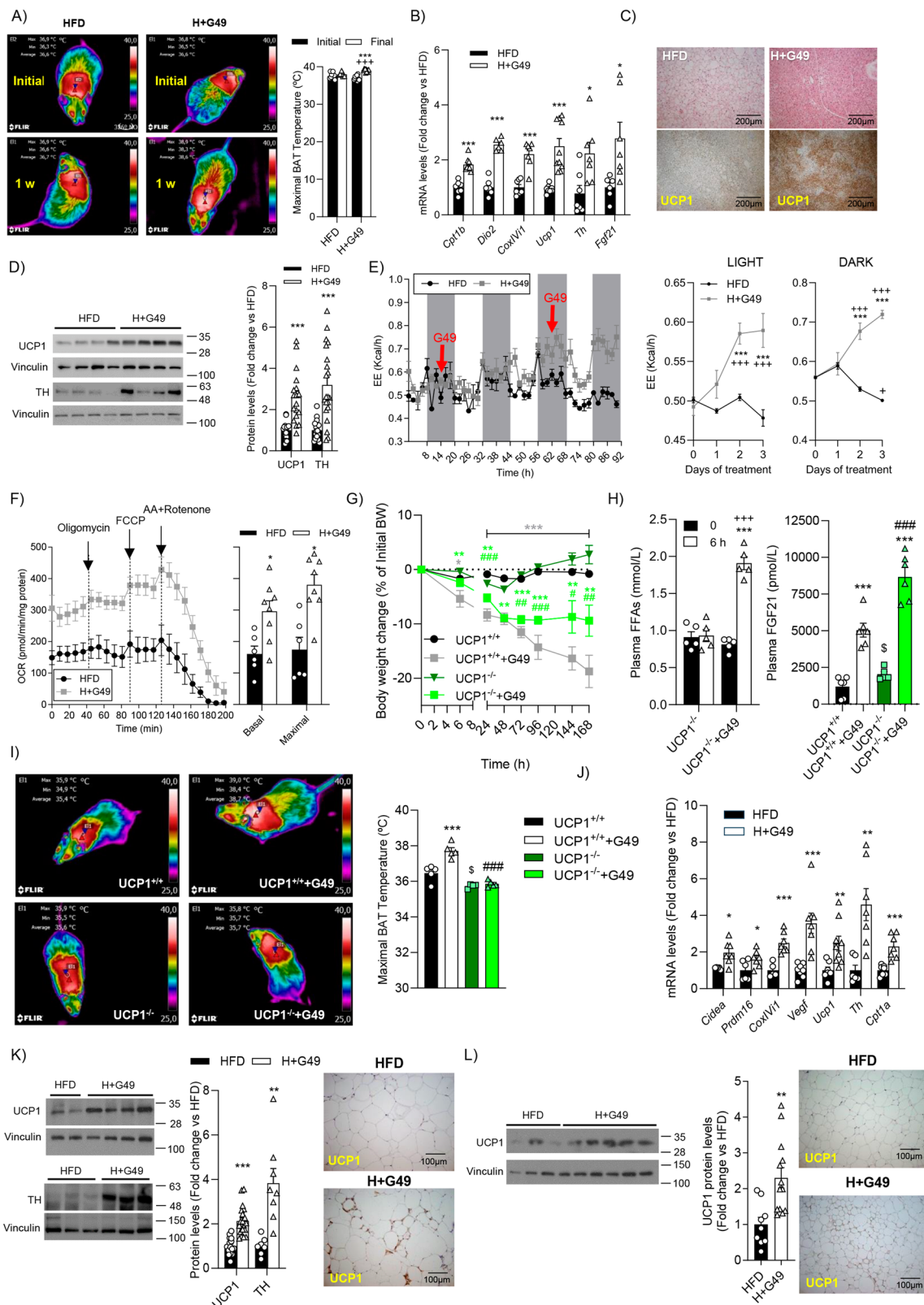
G49. Mice received the first dose of each or both antagonists 3 h prior to G49 administration and injections were repeated every day up to day 7 (Fig. S8A). We first tested the effect of the antagonists either alone or in combination in DIO mice due to their potential effects by blocking endogenous glucagon or GLP-1. Regarding mice injected Ex9-39, no significant effects on body weight and food intake were found (Fig. S8B, C), as well as in metabolic parameters (Fig. S8D, E). By contrast, mice receiving GCGRant either alone or in combination with Ex9-39 showed $6.8 \pm 0.46\%$ and $6.0 \pm 0.67\%$ body weight loss, respectively, that was not related to changes in food intake (Fig. S8B, C) although metabolic parameters did not change except plasma FGF21 that was decreased in the presence of GCGRant (Fig. S8D, E). Of note, no changes in EE were found in DIO mice receiving either antagonist (Fig. S8F). Next, we analyzed the effect of G49 in the presence of the receptor antagonists. To achieve this, we compared data from G49-treated mice in the presence of either or both antagonists to their respective control groups (antagonists in the absence of G49). As shown in Fig. 7A, administration of G49 together with Ex9-39 resulted in less body weight loss at day 7 ($9.3 \pm 0.85\%$ in H + Ex9-39 + G49 versus $23.2 \pm 1.45\%$ in H + G49). Likewise, body weight loss in mice receiving G49 plus GCGRant was $8.8 \pm 0.73\%$. However, G49 failed to decrease body weight in the presence of both antagonists, suggesting the contribution of both receptors to achieve the full effect of G49 in reducing obesity. Importantly, although G49 did not affect cumulative food intake at day 7 (Fig. 1A), in the presence of GCGRant it suppressed cumulative food intake by $26.1 \pm 1.84\%$ versus the HFD group (Fig. 7B), reinforcing the modulation of food intake by G49 through the GLP-1R. Regarding adiposity and estimated weight of total and visceral fat mass and eWAT and iWAT weight, which markedly decreased at day 7 by G49 as expected (Fig. 7C, D), its administration with antagonists, either alone or in combination, totally blocked this effect. Of note, the effect of G49 plus GCGRant regarding body weight loss and visceral adiposity was in line with the effect of Fc-GLP1 (Fig. S3A). Moreover, eWAT beige signature (Fig. 7E), BAT activation (Fig. 7F, G) and EE (Fig. 7H) were suppressed in mice injected G49 in the presence of either or both antagonists although in BAT the blockade of GCGR maintained G49-mediated increase in *Th* mRNA levels. The relevance of both GLP-1R and GCGR in the effects of G49 during 1-week treatment in reducing body weight and adiposity was reinforced by an alternative experimental approach in which receptors were blocked with monoclonal

antibodies (mAb). In this protocol, mAbs were administered 24 h before the first G49 injection (Fig. S9A–D).

GCGR-mediated effects of G49 are essential for triggering the inter-organ crosstalk between WAT and liver

Due to the superior efficacy of G49 in targeting obesity compared to Fc-GLP1 we focused on deciphering the role of GCGR in the inter-organ crosstalk responsible for the full effects of this dualAG. Of note, the GCGRant was able to block the effect of glucagon in elevating glucose levels in lean mice (Fig. S10A), as well as the effect of G49 in increasing hepatic gluconeogenic gene expression in DIO mice after 1-week treatment (Fig. S10B). Notably, the combination of G49 plus GCGRant abolished the acute effects of G49 in reducing total and visceral adiposity at 6 h post-injection and FFA elevation (Fig. 8A, B). By contrast, G49 retained its effect in elevating FFAs in the presence of Ex9-39 in line with the absence of FFA elevation by Fc-GLP1 (Fig. S3D), pointing to a GCGR-mediated effect on G49 action in triggering WAT lipolysis. This was supported by the loss of the beige immune signature of the SVF from eWAT and also by the reduced glycerol released by eWAT explants treated ex vivo with G49 plus GCGRant (Fig. 8C, D). A step further, the peak in insulin secretion induced by G49 subsequently to WAT lipolysis was partially blocked by the GCGRant and, as expected, Ex9-39 totally abolished this increase (Fig. 8E). Likewise, *Fasn* and *Srebf1* mRNA levels in the liver were reduced by the presence of GCGRant (Fig. 8F) and, accordingly, hepatic lipid overload and ALT elevation were not observed (Fig. 8G). Moreover, the peaks of circulating TGs (24 h) (Fig. 8H), hepatic *Cpt1a* and *Hmcs2* mRNAs and blood ketone bodies (72 h) (Fig. 8I) induced by G49 were also abolished by the GCGRant. Notably, injection of DIO mice with G49 plus GCGRant abrogated the increase in plasma FGF21 (Fig. 8J). Interestingly, blockade of GLP-1R by Ex9-39 retained almost 50% of the G49 effects on the transient elevation of TGs levels at 24 h (Fig. 8H) and FGF21 levels at 72 h (Fig. 8J), but only reduced G49-mediated increases in plasma ketone bodies by 32.5%. These results suggest the essential contribution of GLP-1R-mediated insulin secretion in the pancreas–liver axis necessary for the subsequent effects of G49. In agreement with the above-mentioned effects of the blockade of GCGR in BAT activation (Fig. 7F, G), DIO mice treated with G49 in the presence of GCGRant did not present an increase in UCPI protein levels (Fig. 8J).

Considering the controversy on the role of GCGR in mediating eWAT lipolysis³³ and taking into account that the blockade of GCGR



suppressed FFA elevations by G49 and its subsequent effects in the liver, WAT lipolysis was measured in global *Gcgr*^{-/-} mice. It is noteworthy to highlight that those mice are resistant to obesity³⁴ and, therefore, lipolysis was measured in lean mice. As shown in Fig. 8K, a single injection of G49 did not elevate plasma FFAs at 1–6 h in *Gcgr*^{-/-} mice. These results were confirmed in WAT explants treated with G49 for 4 h (Fig. 8L). In order to investigate cell autonomous effects

of G49 in WAT lipolysis, we isolated white adipocytes and, as shown in Fig. 8M, those from *Gcgr*^{-/-} mice did not respond to G49 in inducing lipolysis. These results point to a potential role of G49 through GCGR engagement in inducing early WAT lipolysis in DIO mice. In fact, glucagon administration to lean mice led to an increase of circulating FFAs at 6 h post-injection and, importantly, this effect was not detected at 1 h (Fig. S5F).

Fig. 4 | Effect of 1-week treatment of DIO mice with G49 in BAT. **A** Representative thermography images and maximal BAT temperature (HFD, $n = 9$; H + G49, $n = 11$). HFD vs. H + G49: final, $***p = 0.0006$; Initial vs. final: H + G49, $***p < 0.0001$. Two-way ANOVA with Bonferroni post hoc test. **B** Thermogenic-related genes in BAT at 1 week: *Cpt1b* (HFD $n = 7$; H + G49, $n = 8$), $***p < 0.0001$; *Dio2* (HFD $n = 7$; H + G49, $n = 6$), $***p < 0.0001$; *Cox11* (HFD, H + G49, $n = 7$), $***p < 0.0001$; *Ucp1* (HFD $n = 9$, H + G49, $n = 10$), $***p = 0.0003$; *Th* (HFD, H + G49, $n = 7$), $*p = 0.0128$; *Fgf21* (HFD, $n = 6$; H + G49, $n = 7$), $*p = 0.0242$. Unpaired two-tailed *t*-test. **C** Representative BAT UCPI images at 1 week ($n = 4$). Scale bar 200 μm . **D** Representative Western blots and quantification. UCPI (HFD $n = 17$; H + G49, $n = 18$), $***p < 0.0001$. TH (HFD $n = 17$; H + G49, $n = 21$), $***p < 0.0001$. Unpaired two-tailed *t*-test. **E** Energy expenditure (EE) ($n = 4$ HFD; H + G49). Light: HFD vs. H + G49: day 2, $***p = 0.0004$; day 3, $***p < 0.0001$. day 0 vs. day 2: H + G49, $***p < 0.0001$. day 0 vs. day 3: H + G49, $***p < 0.0001$. Dark: HFD vs. H + G49: day 2, $***p < 0.0001$; day 3, $***p < 0.0001$. day 0 vs. day 2: H + G49, $***p = 0.0001$. day 0 vs. day 3: HFD, $*p = 0.0177$; H + G49, $***p < 0.0001$. Two-way ANOVA with Bonferroni post hoc test. **F** Seahorse in BAT explants from mice treated 72 h with G49 (HFD, $n = 6$; H + G49, $n = 8$ explants from independent mice). Basal, $*p = 0.0101$; Maximal, $*p = 0.0151$. Unpaired two-tailed *t*-test. **G** BW evolution in UCPI^{+/+} and UCPI^{-/-} mice (UCPI^{+/+} $n = 8$, UCPI^{+/+} + G49, $n = 9$; UCPI^{-/-} $n = 4$, UCPI^{-/-} + G49, $n = 5$). Mixed-effect analysis test with Bonferroni post hoc test. *p* values detailed in Source data file. **H** Plasma FFAs at 6 h ($n = 5$ at 0 h;

$n = 5$ at 6 h, same mice). UCPI^{-/-} vs. UCPI^{-/-} + G49: 6 h, $***p < 0.0001$; 0 h vs. 6 h: UCPI^{-/-} + G49, $***p < 0.0001$. Plasma FGF21 at 72 h (UCPI^{+/+} $n = 6$, UCPI^{+/+} + G49, $n = 6$; UCPI^{-/-} $n = 5$, UCPI^{-/-} + G49, $n = 6$). Vehicle vs. G49: UCPI^{+/+}, $***p < 0.0001$; UCPI^{-/-}, $***p < 0.0001$; UCPI^{+/+} + G49 vs. UCPI^{-/-} + G49, $***p < 0.0001$. Two-way ANOVA with Bonferroni post hoc test. UCPI^{+/+} vs. UCPI^{-/-}, $*p = 0.0409$ with unpaired two-tailed *t*-test. **I** Representative thermography images and maximal BAT temperature after 1-week (UCPI^{+/+} $n = 5$, UCPI^{+/+} + G49, $n = 5$; UCPI^{-/-} $n = 4$, UCPI^{-/-} + G49, $n = 5$). UCPI^{+/+} vs. UCPI^{+/+} + G49, $***p < 0.0001$; UCPI^{-/-} vs. UCPI^{-/-}, $*p = 0.0103$; UCPI^{+/+} + G49 vs. UCPI^{-/-} + G49, $***p < 0.0001$. Two-way ANOVA with Bonferroni post hoc test. **J** Beiging-related genes at 1 week (*Cidea*, HFD, $n = 5$; H + G49, $n = 7$, $*p = 0.0303$. *Prdm16*, HFD, $n = 6$; H + G49, $n = 7$, $*p = 0.0416$. *Cox11*, HFD, $n = 5$; H + G49, $n = 7$, $***p = 0.0005$. *Vegf*, HFD, $n = 8$; H + G49, $n = 8$, $***p = 0.0005$. *Ucp1*, HFD, $n = 7$; H + G49, $n = 9$, $***p = 0.0064$. *Th*, HFD, $n = 6$; H + G49, $n = 7$, $**p = 0.0047$. *Cpt1a*, HFD, $n = 7$; H + G49, $n = 7$, $***p = 0.0004$. Unpaired two-tailed *t*-test. **K** eWAT UCPI representative Western blot and quantification (HFD, $n = 15$; H + G49, $n = 20$, $***p < 0.0001$) and TH (HFD, $n = 7$, H + G49, $n = 8$, $**p = 0.0018$). Unpaired two-tailed *t*-test. Representative eWAT UCPI images ($n = 4$). Scale bar 100 μm . **L** Representative iWAT UCPI Western blot and quantification (HFD, $n = 9$; H + G49, $n = 13$). $**p = 0.0029$. Unpaired two-tailed *t*-test. Representative iWAT UCPI images ($n = 4$). Scale bar 100 μm . Data are mean \pm SEM. Source data are provided as a Source Data file.

WAT lipolysis mediated by G49 is essential for BAT activation and weight loss

Due to the rapid lipolytic effect of G49 in DIO mice (Fig. 1J, K), we blocked this metabolic process with Atglistatin (ATGLi), an inhibitor of adipose triglyceride lipase (ATGL)³⁵. To achieve this, DIO mice were treated with ATGLi by oral gavage 3 h prior to G49 injection and mice were sacrificed at 72 h. At this time-point, ATGLi reduced the effect of G49 in body weight loss ($5.7 \pm 0.31\%$ versus $11.8 \pm 0.51\%$) (Fig. 9A) despite its marked effects in the inhibition of cumulative food intake ($43.6 \pm 0.91\%$ in H + G49 + ATGLi group and $28.30 \pm 2.61\%$ in H + G49 group versus each vehicle). This effect occurred without reduction in fat depots (Fig. 9B). As expected, the peak of plasma FFAs and the reduction in total and visceral fat at 6 h post-G49 injection were absent in G49 plus ATGLi-treated mice (Fig. 9C, D). Detailed analysis of eWAT revealed the absence of the eWAT beiging signature at this early time-period in G49-treated mice in the presence of ATGLi (Fig. 9E), suggesting that lipolysis is required for eWAT remodeling and the beiging signature by G49. To determine if lipolysis triggers eWAT beiging immune signature in response to G49, DIO mice were injected G49 after receiving an irradiation to deplete immune cells (Fig. S10C). As shown in Fig. S10D, the elevation of FFAs was preserved, indicating that lipolysis is necessary for the immunomodulation in eWAT induced by G49.

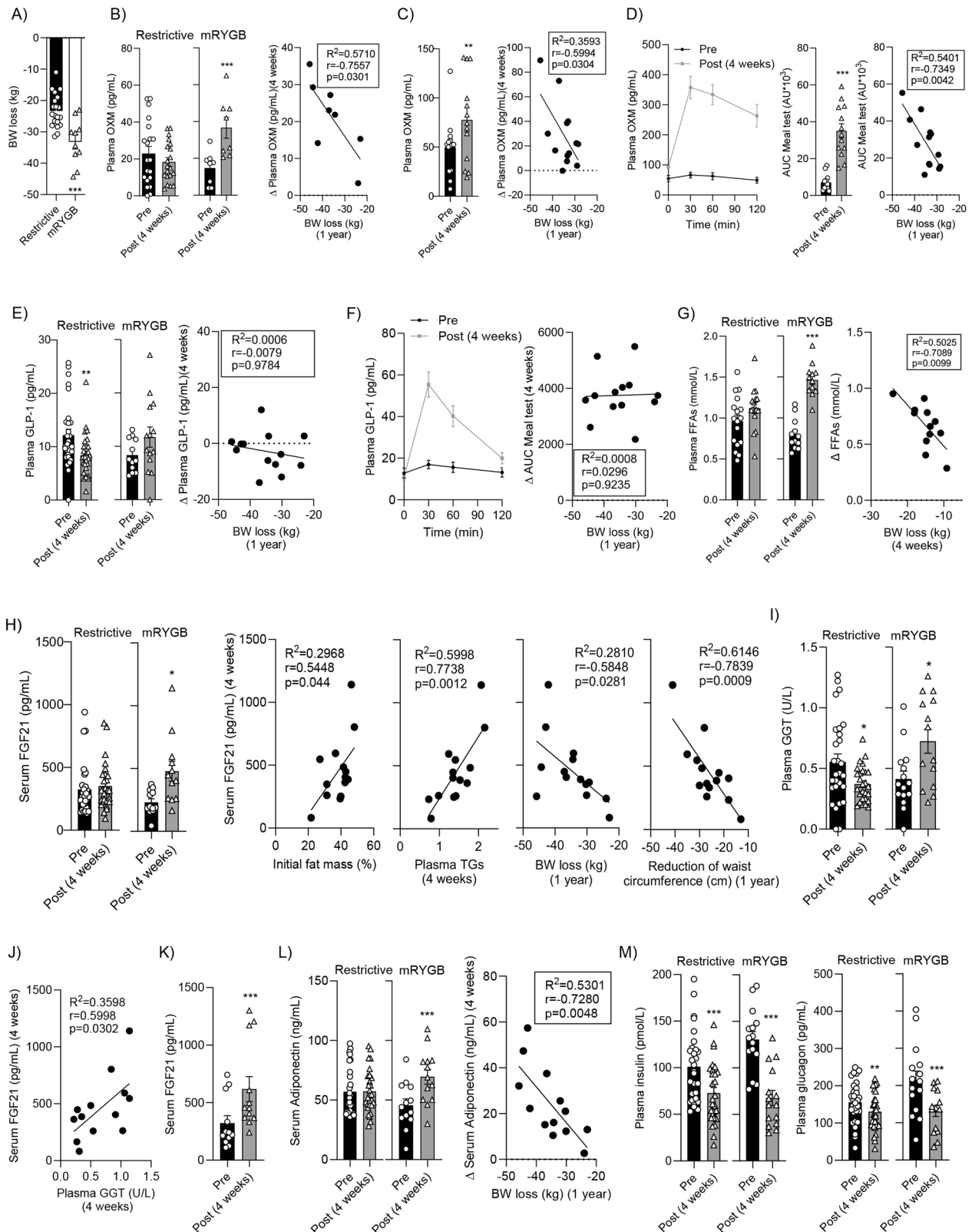
Further, plasma insulin was partly reduced by G49 in ATGLi-treated mice due to preserved GLP-1R-mediated effect on insulin secretion (Fig. 9F). In the liver, the lipid overload found in G49-treated mice was absent in mice co-treated with ATGLi and *Srebf1* and *Fasn* mRNAs were reduced (Fig. 9G). Likewise, the increase in markers of FAO and ketogenesis in the liver, as well as blood ketone bodies, were not observed in mice co-treated with ATGLi (Fig. 9H). Notably, G49-mediated *Fgf21* mRNA upregulation in the liver was also abolished (Fig. 9I) and the analysis of BAT revealed suppression of G49 effects on UCPI expression and BAT temperature (Fig. 9J, K).

Since the ATGLi blocks lipolysis in other tissues, including the liver, we conducted the G49 treatment in mice with *Atgl* deletion exclusively in adipocytes (ATGL^{adipoCre}) to elucidate the effect of G49 in WAT lipolysis-mediated beiging signature in eWAT and to decipher whether WAT lipolysis accounts for BAT activation and weight loss upon G49 treatment. HFD-fed ATGL^{adipoCre} mice treated with G49 for 1 week presented attenuated body weight loss than their vehicle-treated controls (ATGL^{flax/flax}) ($8.7 \pm 0.93\%$ versus $16.2 \pm 0.82\%$) without reduction in adiposity (Fig. 10A, B). Moreover, the pattern of reduction in food intake by G49 was similar in both genotypes (Fig. S11A), pointing

to a contribution of reduced food intake to the residual weight loss in ATGL^{adipoCre} mice. As occurred with the ATGLi, in ATGL^{adipoCre} mice plasma FFAs were not elevated and visceral and total adiposity was not affected by 6 h treatment with G49 (Fig. 10C, D). Moreover, the G49-mediated elevation of plasma insulin was partially abolished in ATGL^{adipoCre} mice (Fig. 10E), as occurred with the G49/GCGRant co-treatment (Fig. 8E) and, notably, in these mice plasma ALT was not elevated (27.2 ± 3.01 U/L in ATGL^{adipoCre} + G49 versus 37.3 ± 2.48 U/L in ATGL^{adipoCre} vehicle group, $n = 5$) compared to the elevations found in the control group (71.5 ± 6.92 U/L in ATGL^{flax/flax} + G49 versus 37.2 ± 2.91 U/L in ATGL^{flax/flax} vehicle group, $n = 5$). Regarding the eWAT beiging immune signature, the elevations of the anti-inflammatory *Il10*, *Il13* and *Th* mRNAs, as readouts, found in ATGL^{flax/flax} were absent in the SVF of ATGL^{adipoCre} mice (Fig. 10F) and the immune cell infiltrates were not observed (Fig. 10G). Likewise, G49-mediated effects in increasing hepatic *Cpt1a* expression, FAO, *Hmcs2* expression, blood ketone bodies and also *Fgf21* expression in liver and FGF21 plasma levels were lost in ATGL^{adipoCre} mice (Fig. 10H, I). In this line, the drop in RER measured at 6 h post-first and second G49 injection was not observed in ATGL^{adipoCre} mice (Fig. 10J). Then, we analyzed BAT activation and the effect of G49 in elevating *Ucp1* mRNA and protein levels and BAT temperature was blunted in ATGL^{adipoCre} mice (Fig. 10K, L) and, in agreement, G49 failed to increase EE (Figs. 10M and S11B). Similar weight loss, elevations in FFAs and BAT activation by G49 were observed in Adipo^{Cre} control mice (Fig. S11C–E). Remarkably, comparable results regarding BAT activation were found in mice treated with Fc-GLP1 in which eWAT lipolysis was not elevated (Fig. S3D, G, H). Finally, the effect of G49 in lean mice was mild and changes were found only in the short-term body weight loss, the early lipolytic response and the reduction of eWAT (Fig. S12).

Discussion

Bariatric surgery is currently the most effective treatment for obesity and type 2 diabetes remission although post-operative complications often occur increasing mortality and morbidity risks. Therefore, pharmacological alternatives are highly needed. One of the key features of bariatric surgery benefits is the recovery in the response to gut-derived peptides³⁶, including OXM, the native dualAG, that positively impacts on whole-body metabolism and energy balance^{3,37,38}. Our results herein confirmed the postprandial elevations of OXM previously reported 4 weeks after mRYGB². In addition, in two independent cohorts, higher basal OXM was found at this early time-period post-mRYGB and associated with body weight loss. Moreover,



postprandial OXM was elevated in patients with obesity as early as 4 weeks post-mRYGB and this response correlated with body weight loss after one year. Of note, the above-mentioned study showed elevation of basal and postprandial OXM levels 6 months post-mRYGB. Herein we show these beneficial effects at an early time-period after surgery, suggesting that OXM secretion by the gut is rapidly elevated following mRYGB and might play a key role in body weight loss.

We have characterized at the molecular level a time-course comprising inter-organ crosstalk driving the metabolic adaptations induced by G49, an OXM-like dualAG, with proven efficacy in reducing body weight and improving insulin sensitivity in DIO mice as we previously reported¹³. Herein we demonstrated that G49 administered at 100 nmol/kg acutely reduced body weight and adiposity during 1-week treatment with superior efficacy than of Fc-GLP1 and in a range

Fig. 5 | Elevation of plasma OXM, FGF21 and adiponectin in patients upon bariatric surgery. **A** BW loss 1 year after restrictive ($n = 20$ individuals) and mRYGB surgery ($n = 10$ individuals), *** $p = 0.0004$, unpaired two-tailed t -test. **B** Plasma OXM before (Pre) and 4 weeks after (Post) restrictive ($n = 20$ individuals) and mRYGB ($n = 8$ individuals, *** $p = 0.0004$, paired two-tailed t -test) surgery and correlation with BW loss 1 year after mRYGB ($n = 8$ individuals, $p = 0.0301$, Pearson correlation test). **C** Plasma OXM before (Pre) and 4 weeks after (Post) mRYGB ($n = 13$ individuals Pre and Post, ** $p = 0.0029$, paired two-tailed t -test) and correlation with BW loss 1 year after mRYGB in an independent cohort ($n = 13$ individuals, $p = 0.0304$, Pearson correlation test). **D** Plasma OXM during meal test 4 weeks after mRYGB and area under the curve (AUC) (left and middle panels) ($n = 13$ individuals). AUC: *** $p < 0.0001$, paired two-tailed t -test. Correlation with 1-year BW loss (right panel) ($n = 13$ individuals, $p = 0.0042$, Pearson correlation test). **E** Plasma GLP-1 before (Pre) and 4 weeks after (Post) restrictive ($n = 29$ individuals, ** $p = 0.0010$) and mRYGB ($n = 12$ individuals (Pre), $n = 14$ individuals (Post) surgery and correlation with BW loss 1 year after mRYGB ($n = 13$ individuals). **F** Plasma GLP-1 during meal test 4 weeks after mRYGB ($n = 14$ individuals) and correlation with 1-year BW loss ($n = 13$ individuals). **G** Plasma FFAs before ($n = 17$ restrictive, $n = 12$ mRYGB) and 4 weeks after restrictive or mRYGB bariatric surgery ($n = 16$ individuals restrictive, $n = 12$ individuals mRYGB). mRYGB: *** $p < 0.0001$, unpaired two-tailed t -test. Correlation with 4-week BW loss in mRYGB ($n = 12$ individuals, $p = 0.0099$, Pearson correlation test). **H** Serum FGF21 before and 4 weeks after restrictive or mRYGB

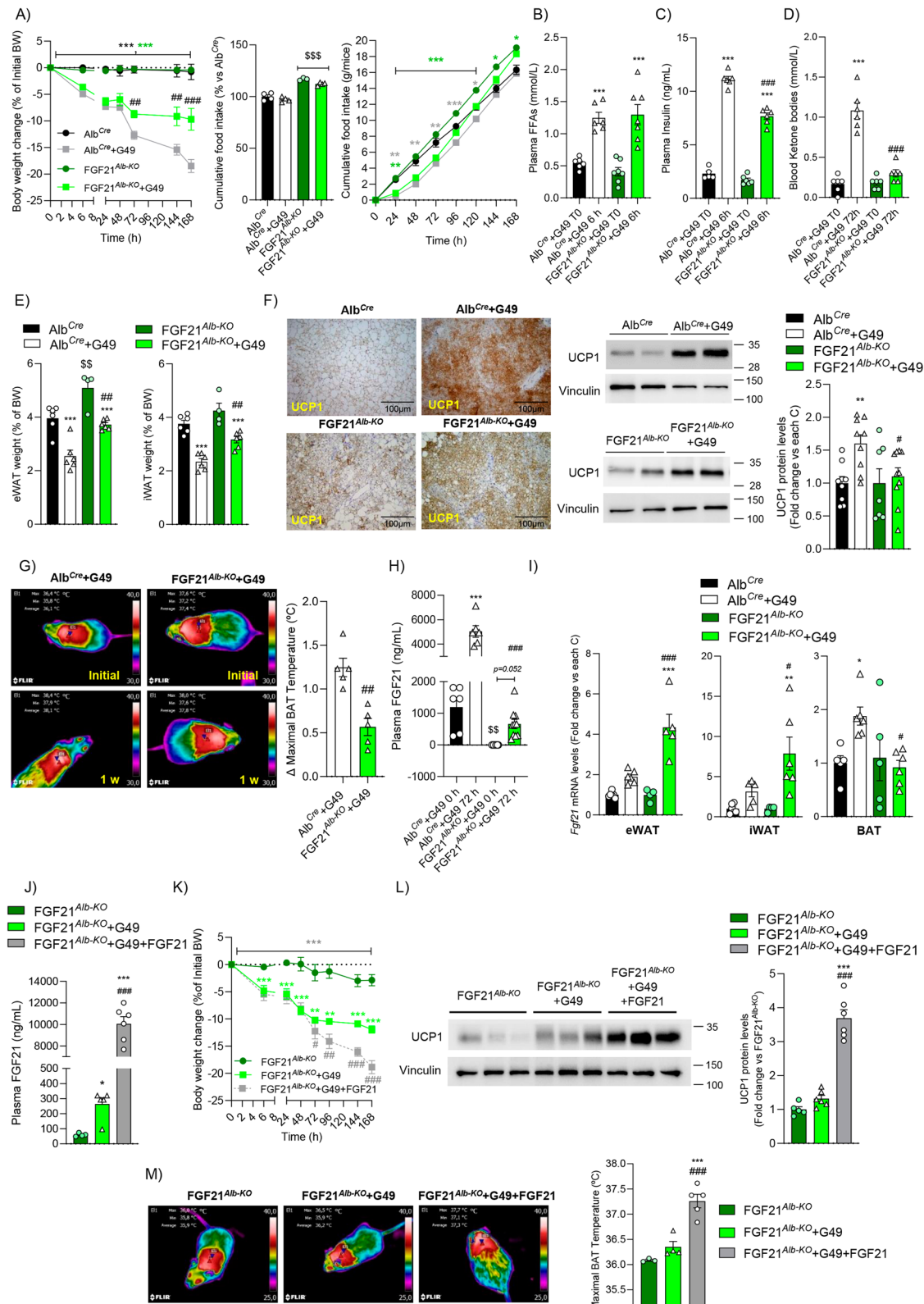
bariatric surgery ($n = 28/12$ individuals restrictive and mRYGB, respectively). mRYGB, * $p = 0.0176$, paired two-tailed t -test. Correlations between serum FGF21 levels at 4 weeks after surgery with initial fat mass ($p = 0.044$) and plasma TGs 4 weeks after surgery ($p = 0.0012$). Correlations between serum FGF21 levels at 4 weeks after surgery and BW loss ($p = 0.0281$) and reduction in waist circumference ($p = 0.0009$) after 1 year in mRYGB ($n = 14$). Pearson correlation test. **I** Plasma GGT activity before (Pre) ($n = 28$ individuals restrictive, $n = 15$ individuals mRYGB) and 4 weeks after (Post) ($n = 27$ individuals restrictive, $n = 14$ individuals mRYGB) surgery. Restrictive, * $p = 0.0154$; mRYGB, * $p = 0.0126$, unpaired two-tailed t -test. **J** Correlation of plasma GGT with serum FGF21 4 weeks after mRYGB ($n = 13$ individuals, $p = 0.0302$, Pearson correlation test). **K** Serum FGF21 in the independent cohort ($n = 12$ individuals, *** $p = 0.0002$, paired two-tailed t -test). **L** Serum adiponectin before and 4 weeks after restrictive or mRYGB bariatric surgery and correlation of serum adiponectin 4 weeks after mRYGB surgery and 1-year BW loss ($n = 29/13$ individuals in restrictive and mRYGB groups, respectively). mRYGB, *** $p = 0.0001$, paired two-tailed t -test. Correlation ($n = 13$ individuals), $p = 0.0048$, Pearson correlation test. **M** Plasma insulin ($n = 29$ individuals restrictive, *** $p = 0.0004$, $n = 15$ individuals mRYGB, *** $p < 0.0001$, paired two-tailed t -test) and glucagon ($n = 30$ individuals restrictive, ** $p = 0.0026$, $n = 15$ individuals mRYGB, *** $p = 0.0002$, paired two-tailed t -test) before (pre) and 4 weeks after restrictive or mRYGB surgery. Data are mean \pm SEM. Source data are provided as a Source Data file.

comparable to the effect of tirzepatide at this period of treatment reported by Coskun et al.²⁰ when administered in the reversed light/dark cycle. Of relevance and related to the anorexigenic effect of Fc-GLP1, food intake was reduced by G49 after the first injection, but it was normalized progressively, no differences being observed at 1 week between vehicle- and G49-treated mice. This differential effect of G49 and Fc-GLP1 was supported by the analysis of cFos positive POMC neurons in the ARC, indicating that G49-mediated effects on EE significantly contribute to the body weight loss. In this line, the present work reports the short-term whole-body metabolic adaptations, spatio-temporal coordination of the organ-specific responses, and the contribution of each receptor to the metabolic effects of a dualAG, the latter being achieved in vivo by using antagonists or mAbs to avoid possible metabolic adaptations due to genetic deletion of *Glp1r* or *Gcgr*^{39,40}.

Importantly, we have unraveled a key role of visceral WAT, not analyzed in-depth in previous studies, as an early target of our dualAG that triggers subsequent metabolic responses in the pancreas and liver, leading to BAT activation and WAT beiging. The fact that in DIO mice visceral WAT rapidly responds to G49, monitored by (1) a marked reduction of visceral fat mass that positively correlated with the initial visceral fat mass; (2) elevations in PKA/HSL phosphorylation and increases in plasma FFAs as early as at 3 h post-injection and, (3) the efficacy in reducing body weight, points to a therapeutic opportunity for morbid obesity. In this regard, Leitner et al.⁴¹ have recently reported a human “BATlas” in lean and obese individuals revealing that obese men have substantial quantities of “brownable” fat in different depots including those with abdominal location that may have a greater potential for expansion upon an appropriate pharmacological intervention.

Of relevance, the elevation of FFAs occurs transiently in a GCGR-dependent manner in DIO mice receiving an injection of G49, as evidenced by co-administration with the GCGR antagonist and by the lack of effect of Fc-GLP1 in this response. In agreement, G49 also induced lipolysis at 6 h post-injection in lean wild-type, but not *Gcgr*^{-/-} mice. The lipolytic effect of G49 was also found ex vivo in mice and human WAT explants and, importantly, this effect was absent in WAT explants from *Gcgr*^{-/-} mice. This rapid elevation of FFAs paralleled to a peak in plasma insulin, likely due to a direct effect of G49 in the pancreas via GLP-1R as OXM does⁴². This effect was demonstrated by the increase in glucose-stimulated insulin secretion in islets from DIO mice treated ex vivo with G49. Also, new

insights on the already known acute effect of FFAs as insulin secretagogues⁴³ have arisen from a recent study in mice treated with a β 3-agonist demonstrating insulin secretion in a WAT lipolysis-dependent manner²⁶, pointing to an indirect effect of G49 in enhancing insulin secretion through WAT lipolysis that likely boosts the GLP-1R-mediated effect as reflected by the lower insulin secretagogue effect of Fc-GLP1, as well as by the reduced effect of G49 when administered to mice lacking ATGL in adipose tissue. In fact, the transient elevation of plasma insulin by G49 was reduced by blockade of its direct insulin-secretagogue capacity (Ex9-39) or by suppressing the secretagogue action of FFAs (GCCGRant). The lipolytic effect of G49 was autonomous as demonstrated in primary adipocytes and hMSC-derived adipocytes. Notably, adipocytes from *Gcgr*^{-/-} mice failed to induce lipolysis upon G49 treatment, suggesting a lipolytic action, at least in part, via GCGR as it will be discussed below. In this regard, the role of the GCGR in mediating lipolysis is controversial. Whereas clinical studies using physiological doses of glucagon did not find elevation in plasma FFAs in humans⁴⁴, supraphysiological glucagon administration increased FFA concentration⁴⁵. In subsequent studies glucagon was shown to induce lipolysis in healthy human volunteers, patients with type 1 diabetes, mice and rats with STZ-induced diabetes, adipocytes isolated from diabetic and non-diabetic animals⁴⁶ and, in agreement with our results, in human adipocytes from healthy volunteers⁴⁷. It is noteworthy to highlight that Vasileva et al.³³ recently reported that adipocyte *Gcgr* expression did not affect fasting-induced lipolysis in lean mice and the lack of effect of glucagon in lipolysis ex vivo in WAT explants from wild-type or adipocyte-specific GCGR-deficient mice. In our settings, glucagon, even used at a supraphysiological dose (100 nmol/kg), did not increase lipolysis at 1 h, time at which Vasileva and co-workers analyzed lipolysis using glucagon at 5 μ g/kg (approx. 1.3 nmol/kg). However, our results show that glucagon increased lipolysis in vivo at 6 h. Likewise, glucagon used at 10 nM increased ex vivo lipolysis in WAT explants at 4 h whereas Vasileva et al. analyzed ex vivo lipolysis at 1 h. Regarding G49, when administered either to lean or DIO mice, it increased lipolysis at 6 h, but not at 1 h post-injection. Further, G49 failed to induce lipolysis in vivo in *Gcgr*^{-/-} mice and ex vivo in WAT explants or adipocytes from *Gcgr*^{-/-} mice at the time-periods in which we found a lipolytic effect in wild-type controls. Altogether, our results, not contradictory with this previous study, shed light to the role of GCGR in G49-mediated WAT lipolysis. However, we cannot exclude central



G49 effects mediated by GCGR as reported in the case of glucagon^{48,49}.

The observation of immune cell infiltration in eWAT as early as 6 h post-G49 injection that resembled the eWAT features reported by *Fabriano et al.*⁵⁰ in calorie-restricted mice, prompted us to analyze in detail the SVF. In agreement with results in iWAT from mice under cold-exposure²⁴ or caloric restriction⁵⁰, enrichment in eosinophils and,

importantly, a rise of the IL4⁺ subpopulation, was found in both SVF and eWAT from G49-treated DIO mice together with elevated *Il4* and *Il13* gene expression, a M2 immune signature related to being⁵⁰. Taken together, our results strongly suggest an effect of G49 in the recruitment of eosinophils and macrophages populations into eWAT, thereby promoting eosinophil-driven M2 polarization of macrophages. As expected, we found increased *Th* mRNA in SVF and eWAT as

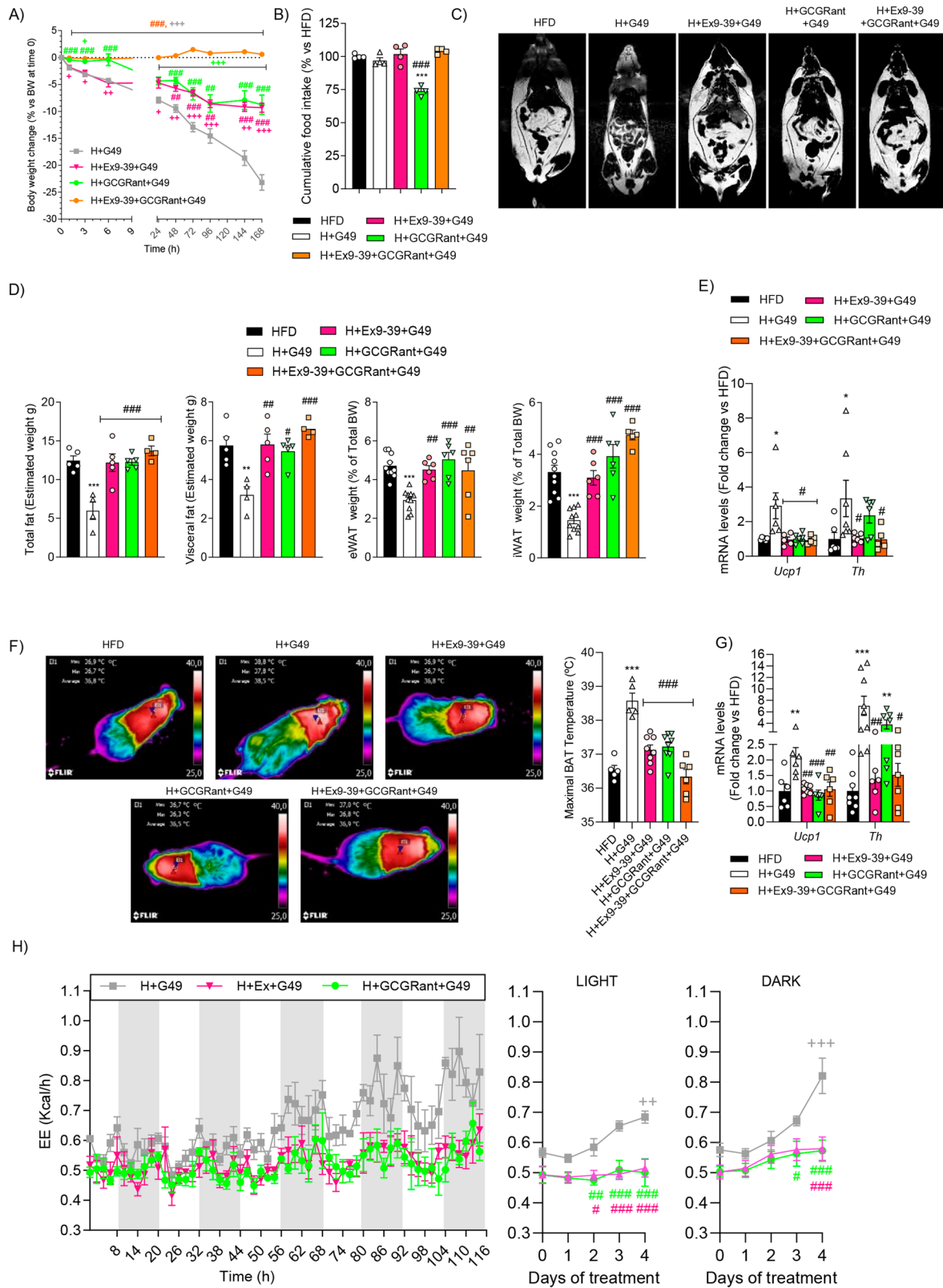
Fig. 6 | Hepatic FGF21 is required to fully achieve BAT activation by G49. **A** BW evolution (Alb^{Cre} *n* = 6, Alb^{Cre} + G49 *n* = 10; FGF21^{Alb-KO} *n* = 4, FGF21^{Alb-KO} + G49 *n* = 6). Two-way RM ANOVA with Bonferroni post hoc test. *p* values detailed in Source data file. Cumulative food intake (*n* = 4 except in FGF21^{Alb-KO} *n* = 3). Alb^{Cre} vs. FGF21^{Alb-KO}: \$\$\$*p* < 0.0001; Alb^{Cre} + G49 vs. FGF21^{Alb-KO} + G49, \$\$\$*p* < 0.0001. Cumulative food intake evolution. Two-way RM ANOVA with Bonferroni post hoc test. *p* values detailed in Source data file. **B** Plasma FFAs (Alb^{Cre} *n* = 6, Alb^{Cre} + G49 *n* = 6; FGF21^{Alb-KO} *n* = 7, FGF21^{Alb-KO} + G49 *n* = 7). 0 vs. 6 h: Alb^{Cre}, ****p* = 0.0002; FGF21^{Alb-KO}, ****p* < 0.0001. **C** Plasma insulin (*n* = 6 except Alb^{Cre} + G49 *t*0, *n* = 5). 0 vs. 6 h: Alb^{Cre}, ****p* < 0.0001; FGF21^{Alb-KO}, ****p* < 0.0001; Alb^{Cre} vs. FGF21^{Alb-KO}, 6 h, ###*p* < 0.0001. **D** Blood ketone bodies (*n* = 6 at *t*0; *n* = 6 at *t*72 h). 0 vs. 72 h: Alb^{Cre}, ****p* < 0.0001; Alb^{Cre} vs. FGF21^{Alb-KO}, 72 h, ###*p* < 0.0001. **E** eWAT and iWAT weight at 1-week (*n* = 6 except FGF21^{Alb-KO} *n* = 4). eWAT: Alb^{Cre} vs. Alb^{Cre} + G49, ****p* = 0.0002; FGF21^{Alb-KO} vs. FGF21^{Alb-KO} + G49, ****p* = 0.0007; Alb^{Cre} vs. FGF21^{Alb-KO}, \$\$*p* = 0.0040; Alb^{Cre} + G49 vs. FGF21^{Alb-KO} + G49, ##*p* = 0.0011. iWAT: Alb^{Cre} vs. Alb^{Cre} + G49, ****p* < 0.0001; FGF21^{Alb-KO} vs. FGF21^{Alb-KO} + G49, ****p* = 0.0005; Alb^{Cre} + G49 vs. FGF21^{Alb-KO} + G49, #*p* = 0.0021. **F** Representative BAT UCPI images (*n* = 3). Scale bar 100 μm. Western Blot and quantification (Alb^{Cre} *n* = 9, Alb^{Cre} + G49, *n* = 9; FGF21^{Alb-KO} *n* = 7, FGF21^{Alb-KO} + G49, *n* = 10) at 1 week. Alb^{Cre} vs. Alb^{Cre} + G49, ***p* = 0.0097; Alb^{Cre} + G49 vs. FGF21^{Alb-KO} + G49, #*p* = 0.0292. **G** Representative thermography images and maximal BAT temperature (*n* = 5 Alb^{Cre} + G49; *n* = 5 FGF21^{Alb-KO} + G49), #*p* = 0.0014. Unpaired two-tailed *t*-test. **H** Plasma FGF21 (Alb^{Cre} + G49 *t*0 and 72 h, *n* = 6, FGF21^{Alb-KO} + G49 *t*0 h, *n* = 9 and 72 h, *n* = 10) Alb^{Cre} + G49 *t*0 h vs. Alb^{Cre} + G49 72 h, ****p* < 0.0001; FGF21^{Alb-KO} + G49 *t*0 h vs. FGF21^{Alb-KO} + G49 72 h, *p* = 0.0520; Alb^{Cre} + G49 *t*0 h vs. FGF21^{Alb-KO} + G49 *t*0 h,

\$\$*p* = 0.0020; Alb^{Cre} + G49 72 h vs. FGF21^{Alb-KO} + G49 72 h, ###*p* < 0.0001. **I** Fgf21 in eWAT (Alb^{Cre}, Alb^{Cre} + G49 *n* = 6; FGF21^{Alb-KO} *n* = 4, FGF21^{Alb-KO} + G49 *n* = 5), iWAT (Alb^{Cre} *n* = 6, Alb^{Cre} + G49 *n* = 5; FGF21^{Alb-KO} *n* = 4, FGF21^{Alb-KO} + G49 *n* = 6) and BAT (Alb^{Cre} *n* = 5, Alb^{Cre} + G49 *n* = 6; FGF21^{Alb-KO} *n* = 5, FGF21^{Alb-KO} + G49 *n* = 6) at 72 h. eWAT: FGF21^{Alb-KO} vs. FGF21^{Alb-KO} + G49, ****p* < 0.0001; Alb^{Cre} + G49 vs. FGF21^{Alb-KO} + G49, ###*p* < 0.0001. iWAT: FGF21^{Alb-KO} vs. FGF21^{Alb-KO} + G49, ***p* = 0.0033; Alb^{Cre} + G49 vs. FGF21^{Alb-KO} + G49, #*p* = 0.0282. BAT: Alb^{Cre} vs. Alb^{Cre} + G49, **p* = 0.0325; Alb^{Cre} + G49 vs. FGF21^{Alb-KO} + G49, #*p* = 0.0143. Two-way ANOVA with Bonferroni post hoc test in (**A** (middle), **B–F**, **H**, **I**). **J–M** FGF21^{Alb-KO} mice received recombinant murine FGF21 at 48, 60 and 72 h post-G49 injection. **J** Plasma FGF21 (FGF21^{Alb-KO} *n* = 4, FGF21^{Alb-KO} + G49, *n* = 5, FGF21^{Alb-KO} + G49 + FGF21, *n* = 6). FGF21^{Alb-KO} vs. FGF21^{Alb-KO} + G49, **p* = 0.0221; FGF21^{Alb-KO} vs. FGF21^{Alb-KO} + G49 + FGF21, ****p* < 0.0001; FGF21^{Alb-KO} + G49 vs. FGF21^{Alb-KO} + G49 + FGF21, ###*p* < 0.0001. Brown–Forsythe and Welch ANOVA with Dunnett's T3 post hoc test. **K** BW (FGF21^{Alb-KO} *n* = 4, FGF21^{Alb-KO} + G49, *n* = 6, FGF21^{Alb-KO} + G49 + FGF21, *n* = 6). Two-way RM ANOVA with Bonferroni post hoc test. *p* values are detailed in Source data file. **L** Representative BAT UCPI Western blot and quantification (FGF21^{Alb-KO} *n* = 5, FGF21^{Alb-KO} + G49, *n* = 6, FGF21^{Alb-KO} + G49 + FGF21, *n* = 6). FGF21^{Alb-KO} vs. FGF21^{Alb-KO} + G49 + FGF21, ****p* < 0.0001; FGF21^{Alb-KO} + G49 vs. FGF21^{Alb-KO} + G49 + FGF21, ###*p* < 0.0001. **M** BAT temperature (FGF21^{Alb-KO} *n* = 3, FGF21^{Alb-KO} + G49, *n* = 4, FGF21^{Alb-KO} + G49 + FGF21, *n* = 5). FGF21^{Alb-KO} vs. FGF21^{Alb-KO} + G49 + FGF21, ****p* = 0.0002; FGF21^{Alb-KO} + G49 vs. FGF21^{Alb-KO} + G49 + FGF21, ###*p* = 0.0008. One-way ANOVA with Bonferroni post hoc test in (**L**, **M**). Data are mean ± SEM. Source data are provided as a Source Data file.

early as 6 h post-G49 injection, together with the presence of infiltrated TH⁺ cells in eWAT sections. On the other hand, SVF from G49-treated mice was enriched in iNKTs, an effect that concurred with a rise in *Fgf21* in eWAT. This population has been analyzed in detail by Lynch et al.²⁵ that found reductions in body weight and adiposity in mice treated with α-galactosyl ceramide (α-GalCer) that presented enrichment in iNKTs in WAT, an effect abolished by depleting this immune population. Moreover, this study showed that the presence of activated iNKTs in iWAT was paralleled to local increases in FGF21 and, in this line, mice deficient in *Fgf21* treated with α-GalCer failed to decrease body weight. Interestingly, these authors also found that iNKTs activation is required for maximal weight loss effect in liraglutide therapy that also concurred with an increase in *Fgf21* expression in eWAT. At present, we can not certainly assess the putative mechanism of recruitment of M2 macrophages/eosinophil/iNKTs in eWAT by G49. In this regard, a role for lipolysis in adipose tissue macrophages recruitment and accumulation has been demonstrated in DIO mice with calorie restriction⁵¹ and, more importantly, the above-mentioned study shows synchronized temporal changes between the peaks in plasma FFAs and macrophage number in eWAT, an effect suppressed in global *Atgl*^{-/-} mice. In this line, the immune signature in eWAT in response to G49 was absent in mice with defective lipolysis either by co-treatment of G49 with Atglstatin or GCGRant. These data were supported by the absence of M2-like profile in the SVF from ATGL^{adipoCre} mice. Moreover, the preservation of G49-induced lipolysis in irradiated mice supports the hypothesis that FFAs and, potentially, other adipocyte-derived lipid species promote the recruitment of immune cells related to eWAT beiging. Thus, considering our results in conjunction with previous studies^{24,25}, eWAT beiging in response to G49 could be due, at least in part, to an early switch of the immune signature in this fat depot triggered by lipolysis. Additionally, the presence of TUNEL positive cells in eWAT at 6 h post-G49 injection suggests that apoptosis due to excessive FFA release might also contribute to the recruitment of immune cells. In this regard it has been shown that apoptotic cell clearance induces the expression of various M2-activation-associated molecules in macrophages including IL-10, TGFβ and CD206⁵². Remarkably, G49-mediated beiging was blocked by GCGRant or Atglstatin that, in addition to lipolysis, also suppressed the increase in *Ucp1* expression in eWAT, again linking lipolysis with eWAT browning. Moreover, the fact that the elevation of *Th* in eWAT was counteracted by Ex9-39 suggests a GLP-IR-mediated contribution

to this effect probably via sympathetic innervation, also important to increase *Ucp1* mRNA and protein expression in eWAT. Altogether, our results support a key role of lipolysis in inducing dualAG-mediated M2-like immune signature and eWAT beiging although this relevant issue deserves further investigation in the setting of dualAG therapy.

The increase in circulating FFAs found in DIO mice after G49 injection also concurred with a hepatic lipid overload likely because of either FFA uptake, since the study of Heine et al.²⁶ showed accumulation of TGs in the liver at 4 h post-injection of a β3-receptor agonist that was absent in *Atgl*^{-/-} mice, and/or insulin-mediated de novo lipogenesis due to elevated *Srebf1* and *Fasn* hepatic gene expression detected at 6 h post-G49 injection. Interestingly, this transient TG increase paralleled with neutrophil infiltration as demonstrated in neutropenic mice⁵³. We addressed the rapid clearance of this transient hepatic lipid accumulation that could be due to the strong and acute activation of lipid export, manifested by the rise of plasma TGs that transiently peaked at 24 h post-injection. Interestingly, GCGR antagonism totally suppressed this response in agreement with the suppression of eWAT lipolysis. Moreover, GLP-1R antagonism partly reduced plasma TGs and this effect could be explained by the GLP-1R-mediated insulin secretagogue effect of G49 that likely accounts for insulin-mediated de novo lipogenesis rather than a direct effect of G49 actions in the liver through the GLP-1R which is nearly absent as reported⁵⁴. On the other hand, expression levels of hepatic *Cpt1a*, *Ppara*, *Hmcs2* and *Fgf21*, and circulating ketone bodies and FGF21 found highly elevated at 72 h in G49-treated mice are indicative of the contribution of FFA catabolism and ketogenesis to the lipid clearance. This was confirmed by elevated FAO in primary hepatocytes and livers of G49-treated mice. Furthermore, lipid utilization was clearly reflected by the rapid decrease in RER in mice receiving G49. These results are in line with the previous work of Pociu et al.⁶ that showed elevated hepatic *Cpt1a* and *Fgf21*, and plasma β-hydroxybutyrate in DIO mice treated with an OXM-like molecule with comparable GCGR affinity to G49. Likewise, our results demonstrating increased in vivo FAO in G49-treated DIO mice extend previous data of Boland et al.¹⁴ on the enhancement of mitochondrial functionality and the upregulation of FAO-related genes by the dualAG Cotadutide which alleviates steatohepatitis in mice. Although not directly supported, the above-mentioned study suggests that this rapid metabolic switch was mediated by the GCGR. Importantly, our results directly demonstrate lipolysis and GCGR-mediated effects of G49 in ketogenesis and plasma



FGF21 elevation, the latter likely derived from the liver in agreement with a recent study demonstrating glucagon-induced upregulation of *Fgf21* mRNA translation associated with suppressed activity of the mechanistic target of rapamycin complex 1⁵⁵. In addition, Inagaki et al.⁵⁶ reported an effect of hepatic FGF21 in inducing WAT lipolysis, suggesting that the early lipolytic effect of G49 can be boosted by liver-

derived FGF21 whose increase in plasma was detected from 12 h post-injection peaking at 72 h. Moreover, an autocrine effect of WAT FGF21 can also contribute to G49 lipolysis.

FGF21 is secreted by the hepatocytes⁵⁷ in a GCG-dependent manner, a response necessary to reduce body weight and increase EE by a GCGR agonist that lost its efficacy in global FGF21-deficient mice⁵⁸.

Fig. 7 | Both GCGR and GLP-1R mediate the inter-organ crosstalk and metabolic effects of G49 in DIO mice. **A** BW (H + G49, $n = 11$ and $n = 6$ in other groups). Two-way RM ANOVA with Bonferroni post hoc test. p values are detailed in Source data file. **B** Cumulative food intake ($n = 4$ in all groups). HFD vs. H + GCGRant + G49, $***p < 0.0001$; H + G49 vs. H + GCGRant + G49, $***p < 0.0001$. One-way ANOVA with Bonferroni post hoc test. **C** Representative MRI images. **D** Quantification of total fat and visceral fat (HFD, $n = 5$; H + G49, $n = 4$; H + Ex9-39 + G49, $n = 5$; H + GCGRant + G49, $n = 5$; H + Ex9-39 + GCGRant + G49, $n = 4$), eWAT weight ($n = 10$ in HFD and H + G49; $n = 6$ for other groups) and iWAT weight ($n = 10$ in HFD and H + G49; $n = 6$ in H + Ex9-39 + G49 and H + GCGRant + G49; $n = 5$ in H + Ex9-39 + GCGRant + G49) at 1 week. Total fat: HFD vs. H + G49, $***p = 0.0002$; H + G49 vs. H + Ex9-39 + G49, $***p = 0.0004$; H + G49 vs. H + GCGRant + G49, $***p = 0.0003$; H + G49 vs. H + Ex9-39 + GCGRant + G49, $***p < 0.0001$. Visceral fat: HFD vs. H + G49, $**p = 0.0034$; H + G49 vs. H + Ex9-39 + G49, $**p = 0.0028$; H + G49 vs. H + GCGRant + G49, $*p = 0.0102$; H + G49 vs. H + Ex9-39 + GCGRant + G49, $***p = 0.0003$. eWAT weight: HFD vs. H + G49, $***p = 0.0001$; H + G49 vs. H + Ex9-39 + G49, $**p = 0.0028$; H + G49 vs. H + GCGRant + G49, $***p < 0.0001$; H + G49 vs. H + Ex9-39 + GCGRant + G49, $**p = 0.0037$. iWAT weight: HFD vs. H + G49, $***p < 0.0001$; H + G49 vs. H + Ex9-39 + G49, $***p = 0.0006$; H + G49 vs. H + GCGRant + G49, $***p < 0.0001$; H + G49 vs. H + Ex9-39 + GCGRant + G49, $***p < 0.0001$. One-way ANOVA with Bonferroni post hoc test. **E** eWAT *Ucp1* ($n = 6$ in HFD, H + G49, H + GCGRant + G49 and $n = 5$ in other groups) and *Th* ($n = 6$ in HFD, H + Ex9-39 + G49 and H + GCGRant + G49; $n = 7$ in H + G49; $n = 5$ in H + Ex9-39 + GCGRant + G49) mRNAs at 1 week. *Ucp1*: HFD vs. H + G49, $*p = 0.0200$; H + G49 vs. H + Ex9-39 + G49, $*p = 0.0163$; H + G49 vs.

H + GCGRant + G49, $*p = 0.0175$; H + G49 vs. H + Ex9-39 + GCGRant + G49, $*p = 0.0139$. *Th*: HFD vs. H + G49, $*p = 0.0300$; H + G49 vs. H + Ex9-39 + G49, $*p = 0.0496$; H + G49 vs. H + Ex9-39 + GCGRant + G49, $*p = 0.0308$. Kruskal–Wallis with Dunn's post hoc test. **F** Representative thermographic images and maximal BAT temperature at 1 week ($n = 5$ in HFD and H + G49; $n = 8$ in H + Ex9-39 + G49 and H + GCGRant + G49; $n = 6$ in H + Ex9-39 + GCGRant + G49). HFD vs. H + G49, $***p < 0.0001$; H + G49 vs. H + Ex9-39 + G49, $***p < 0.0001$; H + G49 vs. H + GCGRant + G49, $***p < 0.0001$; H + G49 vs. H + Ex9-39 + GCGRant + G49, $***p < 0.0001$. One-way ANOVA with Bonferroni post hoc test. **G** BAT *Ucp1* ($n = 6$ except H + Ex9-39 + G49, $n = 7$) and *Th* (HFD, $n = 8$; H + G49, $n = 9$; H + Ex9-39 + G49, $n = 6$; H + GCGRant + G49 and H + Ex9-39 + GCGRant + G49, $n = 7$) at 1 week. *Ucp1*: HFD vs. H + G49, $**p = 0.0029$; H + G49 vs. H + Ex9-39 + G49, $**p = 0.0032$; H + G49 vs. H + GCGRant + G49, $***p = 0.0008$; H + G49 vs. H + Ex9-39 + GCGRant + G49, $**p = 0.0043$. One-way ANOVA with Bonferroni post hoc test. *Th*: HFD vs. H + G49, $***p = 0.0007$; HFD vs. H + GCGRant + G49, $**p = 0.0092$; H + G49 vs. H + Ex9-39 + G49, $**p = 0.0073$; H + G49 vs. H + Ex9-39 + GCGRant + G49, $*p = 0.0101$. Kruskal–Wallis with Dunn's post hoc test. **H** EE at 1 week ($n = 4$ except in H + G49 in dark $n = 5$). Light: H + G49 vs. H + Ex9-39 + G49: day 2, $*p = 0.0306$; day 3, $***p < 0.0001$; day 4, $***p < 0.0001$; H + G49 vs. H + GCGRant + G49: day 2, $**p = 0.0084$; day 3, $***p = 0.0003$; day 4, $***p < 0.0001$; day 0 vs. day 4: H + G49, $**p = 0.0054$. Dark: H + G49 vs. H + Ex9-39 + G49: day 4, $***p < 0.0001$; H + G49 vs. H + GCGRant + G49: day 3, $*p = 0.0388$; day 4, $***p < 0.0001$; day 0 vs. day 4: H + G49, $***p < 0.0001$. Two-way ANOVA with Bonferroni post hoc test. Data are mean \pm SEM. Source data are provided as a Source Data file.

In this regard, we found elevations in plasma FGF21 from 12 up to 72 h post-G49 injection. Of interest, our experiments administering G49 to mice lacking hepatocyte FGF21 in which *Fgf21* expression was found elevated upon G49 treatment revealed an extra-hepatic contribution to plasma FGF21 by eWAT and iWAT as reported⁵⁹. This rise in plasma FGF21 by G49 in *FGF21^{Alb-KO}* mice is likely a compensatory mechanism triggered by G49 since it was absent in those mice under basal conditions.

FGF21 is a potent inducer of BAT thermogenesis and iWAT browning and also improves insulin sensitivity and weight loss⁶⁰. FGF21 decreases postprandial TG-rich lipoproteins by enhancing their catabolism in both WAT and BAT⁶¹. Similarly, the rise in FGF21 in G49-injected mice concurred with a decrease in plasma TGs and subsequent elevations in EE, BAT temperature and UCP1 in WAT and BAT. Our data in *FGF21^{Alb-KO}* mice revealed that liver FGF21 is necessary to achieve the full effect of G49 in BAT activation and body weight loss since the eWAT/iWAT-derived FGF21 is not able to fully compensate the effects of hepatic FGF21. These results were strongly supported by the in vivo FGF21 rescue experiment. Our study also provides mechanistic evidences on the role of adiponectin in G49 actions in weight loss by promoting hepatic FAO as reported³². Therefore, although the FGF21-mediated effects are significant, a contribution of FGF21 to adiponectin secretion⁶² cannot be excluded.

Notably, the increase in BAT temperature and EE was totally suppressed by GCGR or GLP-1R antagonism, as well as by pharmacological ATGL inhibition or its deficiency in adipose tissue in parallel to a reduction in UCP1 levels. Regarding GCGR-mediated G49 action, the results could be explained by inhibition of the early inter-organ crosstalk driven by eWAT lipolysis which is supported by the results in *ATGL^{adipoCre}* mice and by previous data demonstrating the requirement of WAT lipolysis to release FFAs for energy combustion during fasting and cold exposure⁶³. In support of these results, a study from Drucker's laboratory found that *Gcgr* deficiency in BAT does not impact on EE⁶⁴. On the other hand, the contribution of GLP-1R to BAT activation is likely secondary to G49 actions in the central nervous system (CNS) (i.e., *Th* mRNA) where GLP-1Rs are highly expressed in the hypothalamus⁵⁴ and to the activation of GLP-1R-mediated pancreatic insulin secretion-driven de novo lipogenesis and the subsequent series of metabolic events discussed above. In addition to the inter-organ crosstalk orchestrated by G49 that

ultimately leads to UCP-1-dependent BAT activation, our results provide evidence of cell-autonomous effects in differentiated BA that were manifested by increases in lipolysis, brown-related gene expression profile, UCP1 protein levels, increased respiratory capacity and FAO.

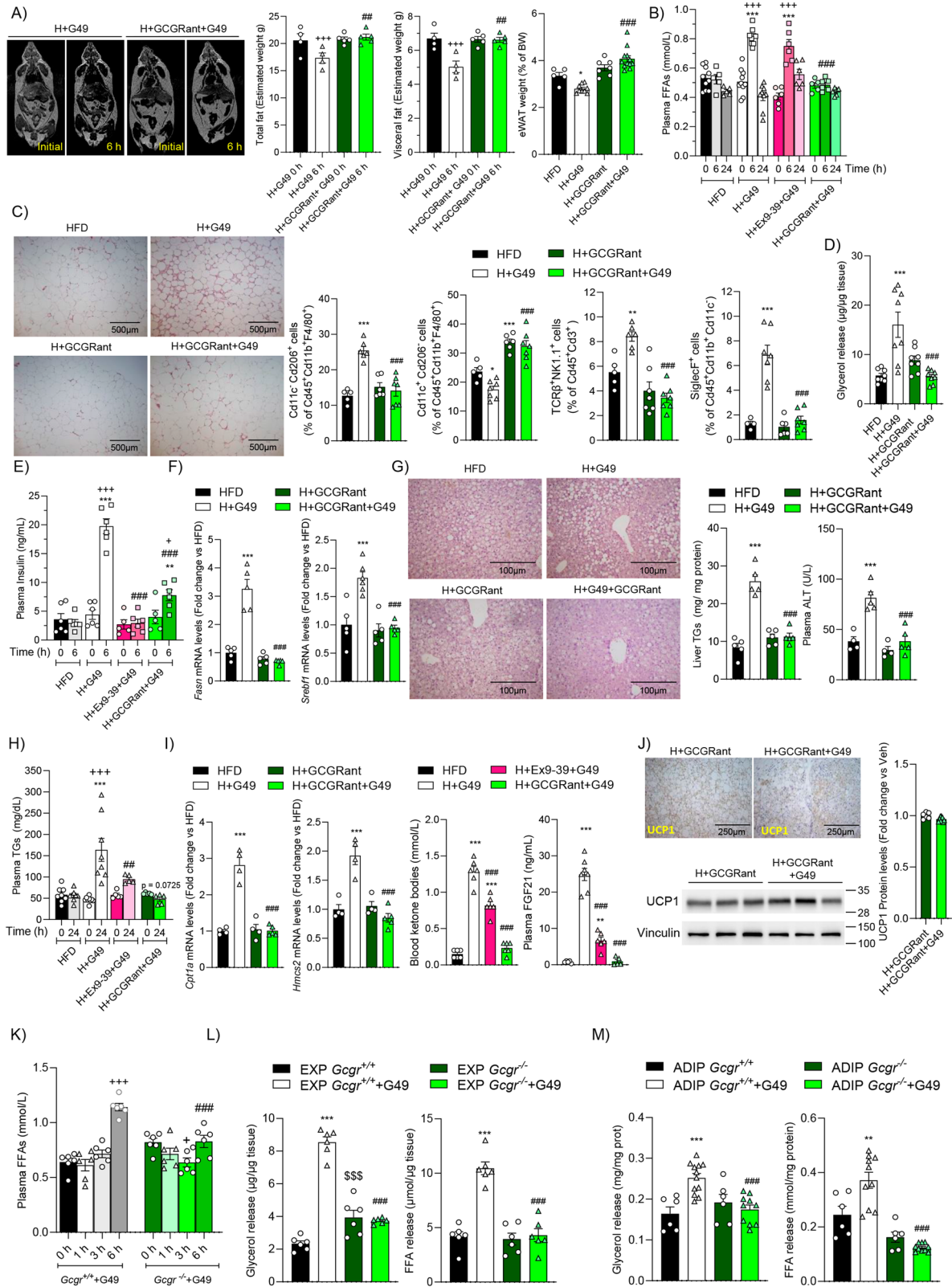
Intriguingly, we found similarities in the metabolic reprogramming induced by G49 treatment and metabolic bariatric surgery in humans. In this regard, the translational relevance of this preclinical study was demonstrated in patients with obesity by correlation of: (1) circulating FGF21 levels 4 weeks after mRYGB with the initial fat mass and one-year body weight reduction, (2) circulating FFAs with 4 week-body weight loss in mRYGB patients and (3) circulating adiponectin and OXM with weight loss. Of note, among different bariatric surgery procedures, mRYGB has superior efficacy in reducing body weight, being the choice for highly obese patients.

In summary, this study demonstrates that the superior efficacy of dual GLP-1R/GCGR agonism versus single GLP-1 agonism in reducing obesity in DIO mice involves WAT lipolysis and remodeling towards beige and UCP-1-dependent BAT activation. These data support an inter-organ crosstalk driven by WAT lipolysis, likely through cooperative GCGR and FGF21-mediated lipolysis, adiponectin secretion and liver-derived FGF21, in favoring EE and body weight loss. However, cooperation with GLP-1R-related effects, both peripheral (i.e., insulin secretion) or CNS-mediated is necessary to achieve G49 full pharmacological effects (Fig. S13). Thus, treatment with balanced dualAGs could deliver metabolic improvements comparable with mRYGB bariatric surgery but devoid of its complications.

Methods

Ethical information

In the human studies, the design and conduct complied with all relevant regulations regarding the use of human study participants in accordance with the criteria set by the Declaration of Helsinki. The patients recruited from Bellvitge University Hospital and included in this study provided written informed consent, as approved by the corresponding ethics committee of the institution (CEIC code PRI43/11 to NV). For the study of lipolysis in hMSC, hMSC were obtained from subcutaneous abdominal adipose tissue from subjects undergoing elective laparoscopic surgery that was approved by the local Committee of the Aragón regional government (CEIC-A, 20/2014 to JM A-M) and an informed consent was signed by all donors. For the study of



lipolysis in explants, human adipose tissue samples were obtained from the National Adipose Tissue Collection, registered under reference C.0003609 in the National Biobank Registry of the Instituto de Salud Carlos III (<https://biobancos.isciii.es/ListadoColecciones.aspx?id=C.0001665>) and with University Hospital Joan XXIII Ethics Committee approval number CEIC 54c/2009 (to JV). All donors signed an informed consent. All animal procedures conformed to European

Union Directive 2010/63/EU and Recommendation 2007/526/EC regarding the protection of animals used for experimental and other scientific purposes, enforced in Spanish law under Real Decreto 53/2013. Protocols were approved by the Consejo Superior de Investigaciones Científicas (CSIC) Ethics Committee (PROEX 325/15, 007/19, 026.5/24, 083.5/24) and the Spanish National Center for Cardiovascular Research (CNIC, PROEX 215/18).

Fig. 8 | GCGR-mediated effects of G49 in the inter-organ crosstalk between WAT and liver. **A** Representative MRI images, total and visceral fat (H + G49, $n = 4$; H + GCGRAnt + G49, $n = 5$) and eWAT weight (HFD, $n = 5$; H + G49, $n = 9$; H + GCGRAnt, $n = 7$; H + GCGRAnt + G49, $n = 12$). Total fat: H + G49 vs. H + GCGRAnt + G49: 6 h, $^{***}p = 0.0077$; $t0$ h vs. 6 h: H + G49, $^{***}p = 0.0001$. Visceral fat: H + G49 vs. H + GCGRAnt + G49: 6 h, $^{**}p = 0.0022$; $t0$ h vs. 6 h: H + G49, $^{***}p < 0.0001$. eWAT weight: HFD vs. H + G49, $^{*}p = 0.0186$; H + G49 vs. H + GCGRAnt + G49, $^{***}p < 0.0001$. For total and visceral fat, Two-way RM ANOVA with Bonferroni post hoc test. For eWAT, Two-way ANOVA with Bonferroni post hoc test. **B** Plasma FFAs (HFD $t0$ h, $n = 10$, 6 h, 24 h, $n = 5$; H + G49, $t0$ h, $n = 10$, 6 h, 24 h, $n = 9$; H + Ex9-39 + G49, $n = 6$; H + GCGRAnt + G49, $t0$ h, $n = 5$, 6 h, 24 h, $n = 6$). HFD vs. H + G49: 6 h, $^{***}p < 0.0001$; HFD vs. H + Ex9-39 + G49: 6 h, $^{***}p < 0.0001$. 0 h vs. 6 h: H + G49, $^{***}p < 0.0001$; H + Ex9-39 + G49, $^{***}p < 0.0001$; H + G49 vs. H + GCGRAnt + G49: 6 h, $^{***}p < 0.0001$. **C** eWAT representative H&E images (Scale bar 500 μ m) and immune cells in SVF at 6 h (Cd11c⁺Cd206⁺: HFD, $n = 5$; H + G49, $n = 6$; H + GCGRAnt, $n = 6$; H + GCGRAnt + G49, $n = 7$; Cd11c⁺Cd206⁺: HFD, $n = 5$; H + G49, $n = 7$; H + GCGRAnt, $n = 6$; H + GCGRAnt + G49, $n = 7$; TCR β ⁺NK1.1⁺: HFD, $n = 5$; H + G49, $n = 6$; H + GCGRAnt, $n = 7$; H + GCGRAnt + G49, $n = 7$; SiglecF⁺: HFD, $n = 4$; H + G49, $n = 7$; H + GCGRAnt, $n = 6$; H + GCGRAnt + G49, $n = 7$). Cd11c⁺Cd206⁺: HFD vs. H + G49, $^{***}p < 0.0001$; H + G49 vs. H + GCGRAnt + G49, $^{***}p < 0.0001$. Cd11c⁺Cd206⁺: HFD vs. H + G49, $^{*}p = 0.0189$; HFD vs. H + GCGRAnt, $^{***}p = 0.0004$; H + G49 vs. H + GCGRAnt + G49, $^{***}p < 0.0001$. TCR β ⁺NK1.1⁺: HFD vs. H + G49, $^{**}p = 0.0043$; H + G49 vs. H + GCGRAnt + G49, $^{***}p < 0.0001$. SiglecF⁺: HFD vs. H + G49, $^{***}p < 0.0001$; H + G49 vs. H + GCGRAnt + G49, $^{***}p < 0.0001$. **D** Glycerol in eWAT explants (500 nM G49, 4 h) without or with GCGR antagonist (1 μ M) ($n = 8$, explants from independent mice). HFD vs. H + G49, $^{***}p < 0.0001$; H + G49 vs. H + GCGRAnt + G49, $^{***}p < 0.0001$. **E** Plasma insulin ($n = 6$ in HFD and H + G49, H + Ex9-39 + G49 and H + GCGRAnt + G49, 0 h, $n = 5$, 6 h, $n = 6$). HFD vs. H + G49: 6 h, $^{***}p < 0.0001$; HFD vs. H + GCGRAnt + G49: 6 h, $^{**}p = 0.0048$; $t0$ h vs. 6 h: H + G49, $^{***}p < 0.0001$; H + GCGRAnt + G49, $^{*}p = 0.0351$. H + G49 vs. H + Ex9-39 + G49: 6 h, $^{***}p < 0.0001$; H + G49 vs. H + GCGRAnt + G49: 6 h, $^{***}p < 0.0001$. **F** mRNAs at 6 h (*Fasn*; $n = 5$, *Srebf1*, $n = 5$ except in H + G49, $n = 6$). *Fasn*: HFD vs. H + G49, $^{***}p < 0.0001$; HFD + G49 vs. H + GCGRAnt + G49, $^{***}p < 0.0001$. *Srebf1*: HFD vs. H + G49, $^{***}p = 0.0002$; H + G49 vs. H + GCGRAnt + G49, $^{***}p < 0.0001$.

G Representative H&E images (Scale bar 100 μ m), liver TGs ($n = 5$) and plasma ALT at 6 h ($n = 4$ HFD and H + GCGRAnt; $n = 5$ H + G49 and H + GCGRAnt + G49). TGs: HFD vs. H + G49, $^{***}p < 0.0001$; H + G49 vs. H + GCGRAnt + G49, $^{***}p < 0.0001$. ALT: HFD vs. H + G49, $^{***}p = 0.0001$; H + G49 vs. H + GCGRAnt + G49, $^{***}p < 0.0001$. **H** Plasma TGs (HFD, $n = 8$; H + G49 $t0$, $n = 9$, $t24$ h, $n = 8$; H + Ex9-39 + G49 and H + GCGRAnt + G49, $n = 5$). HFD vs. H + G49: 24 h, $^{***}p = 0.0002$; $t0$ h vs. 24 h: H + G49, $^{***}p < 0.0001$; H + G49 vs. H + Ex9-39 + G49: 24 h, $^{***}p = 0.0031$; H + G49 vs. H + GCGRAnt + G49: 24 h, $p = 0.0725$. **I** *Cpt1a* and *Hmcs2* (HFD, H + G49, H + GCGRAnt, $n = 4$; H + GCGRAnt + G49, $n = 5$), blood ketone bodies ($n = 6$) and plasma FGF21 at 72 h (HFD, $n = 5$; H + G49 $n = 7$; H + Ex9-39 + G49, $n = 6$; H + GCGRAnt + G49, $n = 5$). *Cpt1a*: HFD vs. H + G49, $^{***}p < 0.0001$. H + G49 vs. H + GCGRAnt + G49, $^{***}p < 0.0001$. *Hmcs2*: HFD vs. H + G49, $^{***}p < 0.0001$; H + G49 vs. H + GCGRAnt + G49, $^{***}p < 0.0001$. Ketone bodies: HFD vs. H + G49, $^{***}p < 0.0001$; HFD vs. H + Ex9-39 + G49, $^{***}p < 0.0001$; H + G49 vs. H + Ex9-39 + G49, $^{***}p < 0.0001$; H + G49 vs. H + GCGRAnt + G49, $^{***}p < 0.0001$. FGF21: HFD vs. H + G49, $^{***}p < 0.0001$; HFD vs. H + Ex9-39 + G49, $^{**}p = 0.0082$; H + G49 vs. H + Ex9-39 + G49, $^{***}p < 0.0001$; H + G49 vs. H + GCGRAnt + G49, $^{***}p < 0.0001$. **J** Representative BAT UCPI images ($n = 3$). Scale bar 250 μ m. Western Blot and quantification (H + GCGRAnt, $n = 6$; H + GCGRAnt + G49, $n = 9$). **K** Plasma FFAs ($n = 6$ *Gcgr*^{+/+}; *Gcgr*^{-/-}, individual mice were analyzed at each time). *Gcgr*^{+/+} vs. *Gcgr*^{-/-}: 6 h, $^{***}p < 0.0001$. *Gcgr*^{+/+}: $t0$ h vs. 6 h, $^{***}p < 0.0001$. *Gcgr*^{-/-}: $t0$ h vs. 3 h, $^{*}p = 0.0497$. Two-way RM ANOVA with Bonferroni post hoc test. **L** Glycerol and FFAs in eWAT explants (500 nM G49, 4 h) ($n = 6$, explants from independent mice). Glycerol: Vehicle vs. G49: EXP *Gcgr*^{+/+}, $^{***}p < 0.0001$; EXP *Gcgr*^{+/+} vs. EXP *Gcgr*^{-/-}: Vehicle, $^{***}p = 0.0010$; G49, $^{***}p < 0.0001$. FFAs: Vehicle vs. G49: EXP *Gcgr*^{+/+}, $^{***}p < 0.0001$; EXP *Gcgr*^{+/+} vs. EXP *Gcgr*^{-/-}: G49, $^{***}p < 0.0001$. **M** Glycerol (ADIP *Gcgr*^{+/+}, $n = 6$; ADIP *Gcgr*^{+/+} + G49, $n = 12$; ADIP *Gcgr*^{-/-}, $n = 6$; ADIP *Gcgr*^{-/-} + G49, $n = 10$) and FFAs (ADIP *Gcgr*^{+/+}, $n = 6$; ADIP *Gcgr*^{+/+} + G49, $n = 10$; ADIP *Gcgr*^{-/-}, $n = 6$; ADIP *Gcgr*^{-/-} + G49, $n = 10$) released by adipocytes (500 nM G49, 4 h). Glycerol: Vehicle vs. G49: ADIP *Gcgr*^{+/+}, $^{***}p = 0.0002$; ADIP *Gcgr*^{+/+} vs. ADIP *Gcgr*^{-/-}: G49, $^{***}p = 0.0002$. FFAs: Vehicle vs. G49: ADIP *Gcgr*^{+/+}, $^{**}p = 0.0017$; ADIP *Gcgr*^{+/+} vs. ADIP *Gcgr*^{-/-}: G49, $^{***}p < 0.0001$. **C, D, F, G, L, M** Two-way ANOVA with Bonferroni post hoc test. **B, E, H, I** One-way ANOVA with Bonferroni post hoc test. Data are mean \pm SEM. Source data are provided as a Source Data file.

Human studies

Sex was not considered in the human studies. Age was only considered for inclusion and exclusion criteria.

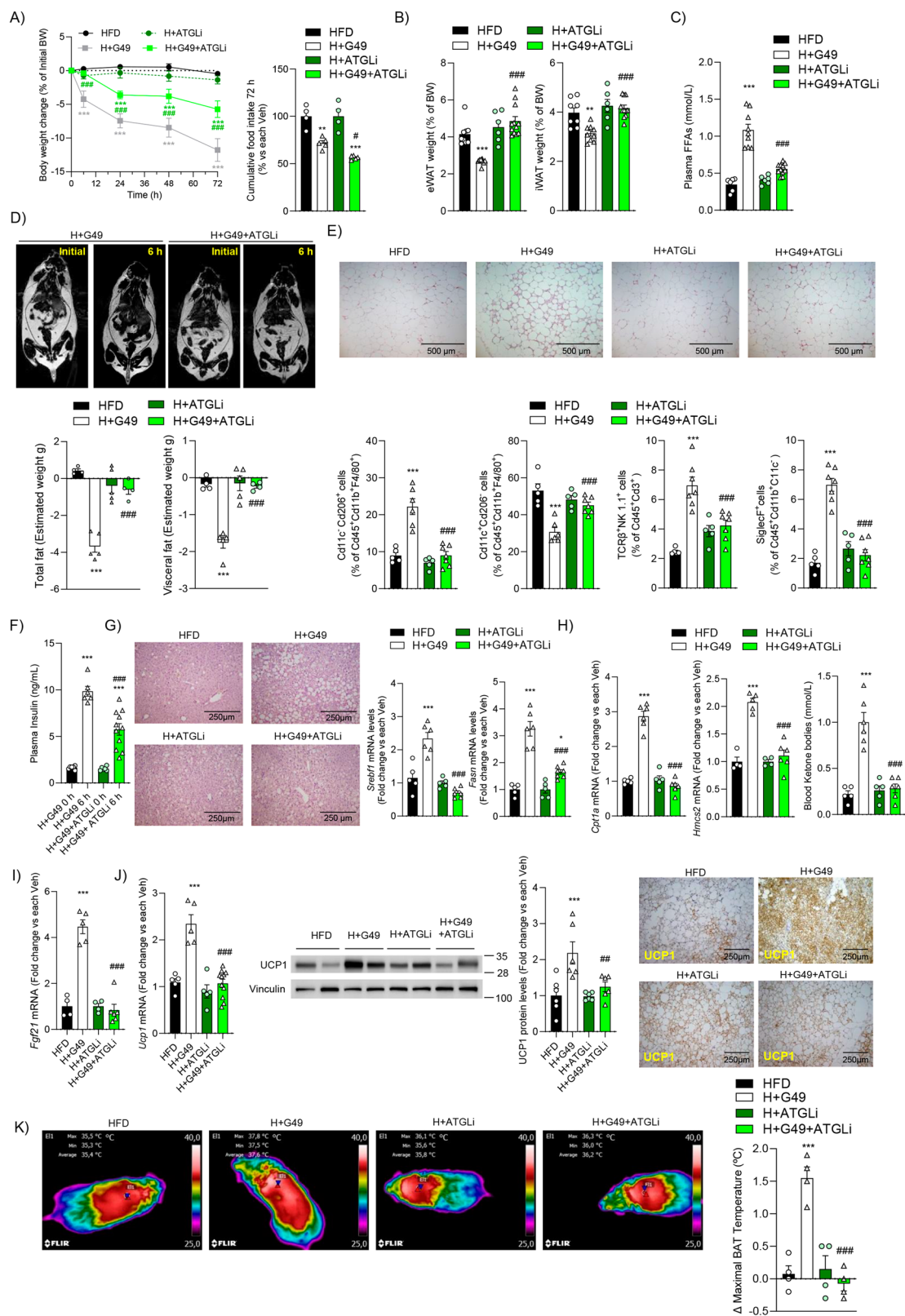
The participants in the bariatric surgery study recruited at Bellvitge University Hospital were enrolled in a registered clinical trial (ISRCTN14104758, <https://doi.org/10.1186/ISRCTN14104758>) and the primary outcomes have been published in Casajoana et al.³⁰. Briefly, patients were consecutively recruited from the diabetes outpatient clinic of the hospital. Inclusion criteria were as follows: age between 18 and 60 years, BMI 35–43 kg/m², type 2 diabetes on hypoglycemic agents alone, insulin or both. Exclusion criteria were as follows: type 1 diabetes or positivity for anti-glutamic acid decarboxylase autoantibodies, secondary forms of diabetes, acute metabolic complications, liver disease, renal dysfunction or patients under anticoagulant treatment, previous bariatric surgery, congenital or acquired abnormalities of the digestive tract, pregnancy, nursing or desired pregnancy in the 12 months following inclusion, and corticoid use by oral or intravenous route for more than 14 consecutive days in the last 3 months. In the first cohort (interventional study), patients (15 men, 30 women) were randomly assigned 1:1:1 to undergo metabolic Roux-en-Y gastric bypass (mRYGB), Sleeve gastrectomy (SG), or Greater curvature plication (GCP) (the latter two referred as restrictive). The randomization process was performed using a computer software program that generates a random sequence. Allocation of patients was assigned by simple randomization with stratification according to baseline levels of HbA_{1c} (greater or lower/equal to 7%). In the confirmatory cohort (observational study), all patients (4 men and 9 women) were submitted to mRYGB surgery.

Metabolic RYGB combines restriction, by creating a small (100 mL) gastric pouch, with hypo-absorption, accomplished by creating a 200 cm biliopancreatic limb and a 100 cm alimentary limb. In classic RYGB the gastric pouch is smaller, with approximately 30 to

45 mL, and the biliopancreatic limb is shorter of 60-cm and alimentary limb of 150-cm. SG is a restrictive technique consisting of a gastric volume reduction to 150 mL by resecting the stomach over a 36 French catheter beginning 4 cm from the pylorus and ending at the angle of His. GCP is a reversible restrictive technique with no stomach resection, in which an invagination of the greater gastric curvature is performed with two running non-absorbable sutures, calibrated over a 36 French catheter. A physical examination with determination of anthropometrical parameters and a complete biochemical analysis was performed before bariatric surgery and at months 1, 3, 6, and 12 following the procedure. Body composition was analyzed by dual-energy X-ray absorptiometry (Hologic QDR 4500; Hologic Inc., Waltham, MA) before and 12 months after surgery. Blood was collected before and 4 weeks after surgery and frozen at -80° C.

Before and 4 weeks after mRYGB a Meal Tolerance Test (MTT) was performed in the confirmatory cohort in the morning after an overnight fast, with no food or drink (except for water) after 8 p.m. of the preceding day. Diabetes treatment excluding insulin was withdrawn 1 week before the test. An intravenous line was established in the antecubital vein for venous blood sampling. Patients ingested a standardized liquid meal beverage (16% proteins, 49% carbohydrates, and 30% lipids [320 kcal]; Iso-source, Nestle Health Science) over 5 min. Blood was sampled before meal ingestion (time 0 min) and 30, 60, and 120 min after meal ingestion and plasma OXM was analyzed as described⁶⁵.

For analyzing lipolysis in human explants, omental fat pads (from 2 men and 2 women) were collected in ice-cold Dulbecco's Modified Eagle Medium (DMEM) containing penicillin (100 U/mL) and streptomycin (100 μ g/mL). Explants were placed under sterile conditions in 60 cm plates with prewarmed (37 $^{\circ}$ C) DMEM containing penicillin and streptomycin. Connective tissue and blood vessels were removed by dissection before cutting the tissue into small pieces (approx. 5 mg). Explants



were cultured in DMEM with 2 mM L-glutamine, penicillin, streptomycin and 2% FFA-free bovine serum albumin (BSA) in the presence or absence of G49 (500 nM) for 24 h. Supernatants were collected, and the amount of glycerol was quantified spectrophotometrically at 540 nm with the free glycerol reagent colorimetric kit.

Drug description

G49 (HSQGTFTSDYSKYLEEAVRLFIC (40 kDa PEG) WLMNT-amide acetate salt, (AstraZeneca), is a PEGylated analog of OXM exhibiting dual GLP-1R/GCGR agonist activity. The peptide is PEGylated with a 40 kDa polyethylene glycol moiety to extend circulation lifetime¹³.

Fig. 9 | ATGLi blocks G49-mediated BAT activation and reduces its effect in body weight loss. **A** BW evolution (HFD, $n = 4$; H + G49, $n = 11$; H + ATGLi, $n = 6$; H + G49 + ATGLi, $n = 16$). Two-way RM ANOVA with Bonferroni post hoc test. p values are detailed in Source data file. Cumulative food intake (HFD, $n = 4$; H + G49, $n = 5$; H + ATGLi, $n = 4$; H + G49 + ATGLi, $n = 5$). HFD vs. H + G49, $**p = 0.0010$; H + ATGLi vs. H + G49 + ATGLi, $***p < 0.0001$; H + G49 vs. H + G49 + ATGLi, $\#p = 0.0447$. **B** eWAT (HFD, $n = 9$; H + G49, $n = 9$; H + ATGLi, $n = 6$; H + G49 + ATGLi, $n = 12$) and iWAT (HFD, $n = 8$; H + G49, $n = 9$; H + ATGLi, $n = 6$; H + G49 + ATGLi, $n = 11$) weight at 72 h. eWAT: HFD vs. H + G49, $***p = 0.0001$; H + G49 vs. H + G49 + ATGLi, $***p < 0.0001$. iWAT: HFD vs. H + G49, $**p = 0.0022$; H + G49 vs. H + G49 + ATGLi, $***p < 0.0001$. **C** Plasma FFAs at 6 h (HFD, $n = 6$; H + G49, $n = 9$; H + ATGLi, $n = 6$; H + G49 + ATGLi, $n = 11$). HFD vs. H + G49, $***p < 0.0001$; H + G49 vs. H + G49 + ATGLi, $***p < 0.0001$. **D** Representative MRI images (upper panel) and total and visceral fat (HFD, $n = 4$; H + G49, $n = 5$; H + ATGLi, $n = 5$; H + G49 + ATGLi, $n = 4$) (lower panel). Total fat: HFD vs. H + G49, $***p < 0.0001$; H + G49 vs. H + G49 + ATGLi, $***p < 0.0001$. Visceral fat: HFD vs. H + G49, $***p < 0.0001$; H + G49 vs. H + G49 + ATGLi, $***p < 0.0001$. **E** Representative eWAT H&E images (scale bar 500 μm) ($n = 5$) and immune cells in SVF at 6 h (Cd11c⁺Cd206⁺ and Cd11c⁺Cd206⁻: HFD, $n = 5$; H + G49, $n = 6$; H + ATGLi, $n = 5$; H + G49 + ATGLi, $n = 7$; TCR β ⁺NK1.1⁺ and SiglecF⁺: HFD, $n = 5$; H + G49, $n = 7$; H + ATGLi, $n = 5$; H + G49 + ATGLi, $n = 7$). Cd11c⁺Cd206⁺: HFD vs. H + G49, $***p < 0.0001$; H + G49 vs. H + G49 + ATGLi, $***p < 0.0001$. Cd11c⁺Cd206⁻: HFD vs. H + G49, $***p < 0.0001$; H + G49 vs. H + G49 + ATGLi, $***p = 0.0006$. TCR β ⁺NK1.1⁺: HFD vs. H + G49, $***p < 0.0001$; H + G49 vs. H + G49 + ATGLi, $***p = 0.0002$. SiglecF⁺: HFD vs. H + G49, $***p < 0.0001$;

H + G49 vs. H + G49 + ATGLi, $***p < 0.0001$. **F** Plasma insulin (H + G49, $t0$, 6 h, $n = 6$; H + G49 + ATGLi $t0$ h, $n = 6$, $t6$ h, $n = 11$). 0 h vs. 6 h: H + G49, $***p < 0.0001$; H + G49 + ATGLi, $***p < 0.0001$; H + G49 vs. H + G49 + ATGLi: 6 h, $***p < 0.0001$. **G** Representative H&E images (scale bar 250 μm) ($n = 4$) and mRNAs in liver at 6 h (*Srebf1*: HFD, $n = 5$; H + G49, $n = 6$; H + ATGLi, $n = 5$; H + G49 + ATGLi, $n = 6$; *Fasn*: HFD, $n = 5$; H + G49, $n = 6$; H + ATGLi, $n = 5$; H + G49 + ATGLi, $n = 7$). *Srebf1*: HFD vs. H + G49, $***p < 0.0001$; H + G49 vs. H + G49 + ATGLi, $***p < 0.0001$. *Fasn*: HFD vs. H + G49, $***p < 0.0001$; H + ATGLi vs. H + G49 + ATGLi, $\#p = 0.0233$; H + G49 vs. H + G49 + ATGLi, $***p < 0.0001$. **H** *Cpt1a* (HFD, $n = 5$; H + G49, $n = 6$; H + ATGLi, $n = 5$; H + G49 + ATGLi, $n = 6$), *Hmcs2* (HFD, $n = 4$; H + G49, $n = 5$; H + ATGLi, $n = 4$; H + G49 + ATGLi, $n = 6$) and blood ketone bodies (HFD, $n = 5$; H + G49, $n = 6$; H + ATGLi, $n = 5$; H + G49 + ATGLi, $n = 6$) at 72 h. *Cpt1a*: HFD vs. H + G49, $***p < 0.0001$; H + G49 vs. H + G49 + ATGLi, $***p < 0.0001$. *Hmcs2*: HFD vs. H + G49, $***p < 0.0001$; H + G49 vs. H + G49 + ATGLi, $***p < 0.0001$. Blood ketone bodies: HFD vs. H + G49, $***p < 0.0001$; H + G49 vs. H + G49 + ATGLi, $***p < 0.0001$. **I** *Fgf21* at 72 h (HFD, $n = 4$; H + G49, $n = 5$; H + ATGLi, $n = 4$; H + G49 + ATGLi, $n = 6$) HFD vs. H + G49, $***p < 0.0001$; H + G49 vs. H + G49 + ATGLi, $***p < 0.0001$. **J** BAT *Ucp1* ($n = 5$ except H + G49 + ATGLi $n = 11$), representative UCPI Western blot and quantification ($n = 6$ in all groups) and representative BAT UCPI images (Scale bar 250 μm) ($n = 3$) at 72 h. *Ucp1*: HFD vs. H + G49, $***p < 0.0001$; H + G49 vs. H + G49 + ATGLi, $***p < 0.0001$. UCPI protein levels: HFD vs. H + G49, $***p = 0.0007$; H + G49 vs. H + G49 + ATGLi, $\#p = 0.0058$. **K** Representative thermographic images and quantification of Δ maximal BAT temperature ($n = 4$ in **A** (right)–**K** Two-way ANOVA with Bonferroni post hoc test. Source data are provided as a Source Data file.

Fc-GLP1 is a Fc-amide derived peptide based on naïve GLP-1 (GLP-1(7-36) NH₂ sequence HGEFTTSDVSSYLEGQAQAEFIKLVKGG-linker-Fc⁶⁶.

Mice and treatments

C57BL/6J male and female mice were purchased from Charles River (San Cugat del Valles, Spain). For the generation of FGF21^{Alb-KO} mice, the FGF21loxP (B6.129S6(SJL)-Fgf21tm1.2Djm/J) line was crossed with B6.Cg-Tg(Alb-cre)21Mgn/J (Alb^{Cre}) mice (Jackson laboratory). Alb^{Cre} mice were used as controls. The generation of ATGL^{adipoCre} was previously described⁶³. ATGL^{fllox/fllox} and Adiponectin-Cre (Adipo^{Cre}) mice were used as controls. Adiponectin KO (Adipoq^{-/-}) (B6.129-Adipoqt1Chan/J), UCPI KO (UCPI^{-/-}) (B6.129-*Ucp1*^{tm1kz/J}) mice and their respective wild type controls were purchased from the Jackson Laboratory. All mice were backcrossed to the C57BL/6J background for 10 generations. Experiments with genetically modified mice were performed in male mice. Both male and female mice were housed under controlled conditions of 12 h:12 h light-dark cycles and at 22 °C temperature and 45–55% humidity and fed ad libitum a standard rodent chow diet (CHD) or high fat diet (HFD) (60% of calories from fat) for 12 (males) or 24 (females) weeks starting at week 8 of age. In the experiments using both CHD and HFD-fed mice, CHD-fed mice were age-matched to HFD-fed mice. We also used global *Gcgr*^{+/-} and *Gcgr*^{-/-} mice, kindly provided by D. Perez-Tilve (University of Cincinnati, USA)⁶⁷, fed a CHD. One cohort of HFD-fed C57BL/6J male mice was housed at 30 °C to conduct the treatment at thermoneutrality. Another cohort of DIO mice was treated on reversed light/dark cycle.

Mice received subcutaneous (s.c.) injections of G49 (20–500 nmol/kg) or vehicle (50 mM sodium phosphate, 300 mM mannitol, pH 6.9) or Fc-GLP1 (50 nmol/kg) or vehicle (saline) every 2 days for the indicated time-periods up to 1 week. In the experiments with GLP-1R or GCGR antagonists, DIO C57BL/6J male mice were randomized in groups to receive the different treatments. One group was treated daily via i.p. with des-His1-[Glu9]-Glucagon (1-29) amide, a glucagon receptor antagonist (GCGRant), at 1 mg/kg as reported⁶⁸ in the absence or presence of G49 for 1 week. The first injection was administered 1 h before the first dosing of G49. Other cohort was treated daily with the GLP-1R antagonist (GLP-1ant) Ex9-39 (25 nmol/kg, i.p.)⁶⁹ in the absence or presence of G49. A third cohort of mice was co-treated with both antagonists in the absence or presence of G49. In experiments with GLP-1R and GCGR blocking monoclonal antibodies, DIO mice were treated 24 h

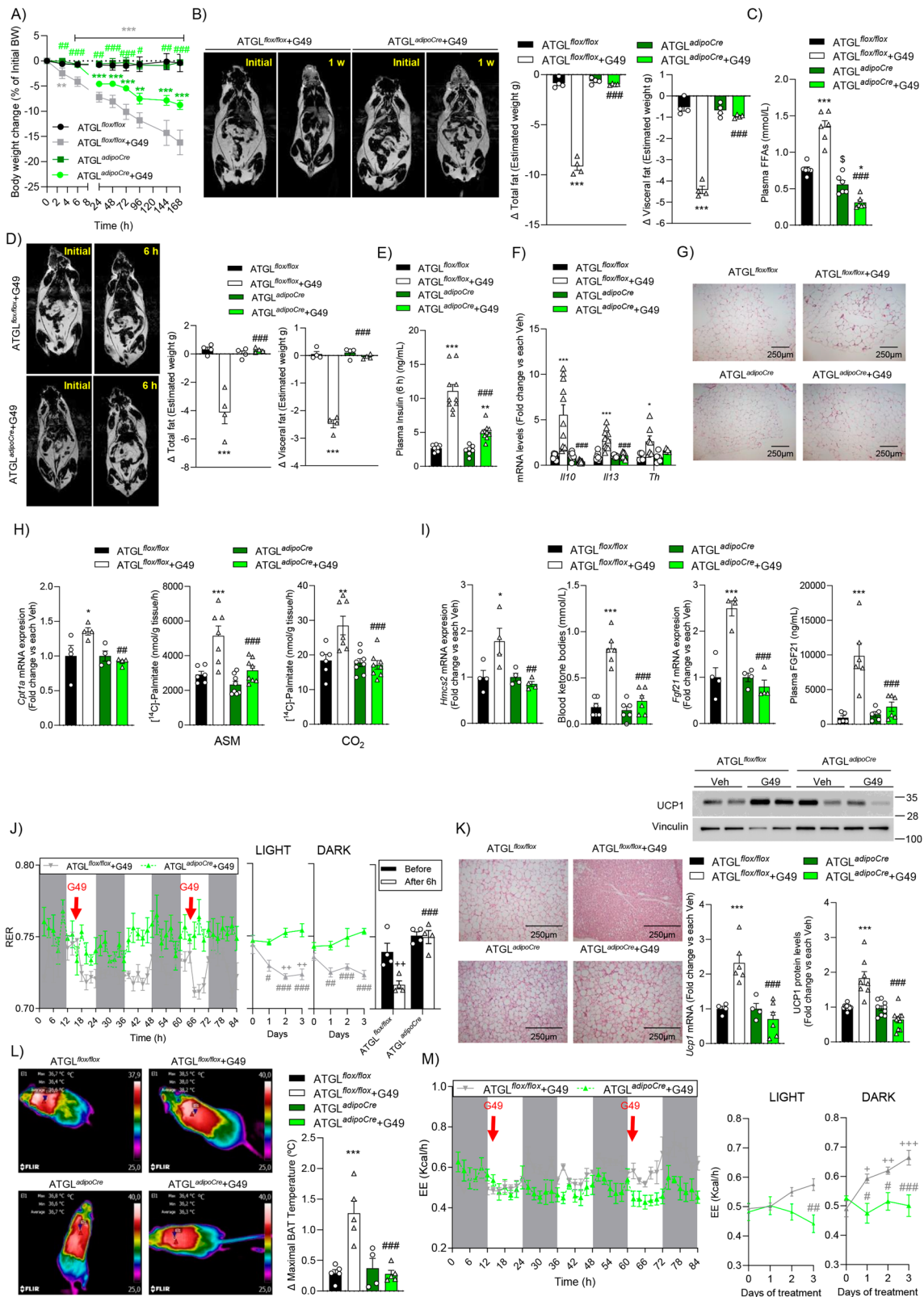
before G49 treatment with GCGRmAb (6 mg/kg, i.p.) and/or with GLP-1RmAb (19.2 mg/kg, i.p.)⁷⁰ and further injected G49 every 2 days for 1 week. In experiments with the ATGLi, mice received Atglistatin, dissolved in olive oil (1.25 mg/mice), by oral gavage 3 h before G49 injection³⁵. Another cohort of DIO mice was irradiated with a dose of 900 rads (9 Gy) by a cesium γ -source as described⁷¹. After 24 h mice were injected 200 μl of clodronate- or buffer phosphate saline (PBS)-loaded liposomes (www.clodronateliposomes.com) by retroorbital injection. Animals were injected cefovecin (0.04 mg/g) two days before and after irradiation. The circulating immune population was analyzed at 4 days post-irradiation in a hemocytometer (Elements HT5, Heska). Then, mice received a single G49 injection (s.c.) and were sacrificed at 6 h.

Measurement of drug concentration in plasma

The concentration of Fc-GLP1 and G49 present in mouse plasma samples was estimated from the cAMP accumulation assay for agonist activity against the human GLP-1R expressing CHO cell line. Reference Fc-GLP1 and G49 peptides were spiked into a 0.2% final concentration of naïve mouse plasma in assay buffer (pH 7.4 HBSS supplemented with 25 mM HEPES, 0.1% BSA, and 0.5 mM 3-isobutyl-1-methylxanthine (IBMX)) at a known concentration to generate a standard curve to determine the amount of active peptide in each related plasma test sample. All samples were serially diluted in assay buffer in duplicate and incubated with the cells for 30 min at room temperature (RT) before detection with the cAMP dynamic 2 HTRF assay as described previously⁷². Plasma test samples were plotted using the same top concentration as the equivalent reference. EC50 values obtained using this method were then used to calculate: sample ratio = sample EC50/EC50 reference peptide-spiked plasma sample and estimated concentration = Known top concentration of peptide-spiked plasma sample/sample ratio.

cAMP accumulation agonist potency assay

cAMP accumulation assays for G49 and Fc-GLP1 were performed as described above. In brief, serial dilutions of G49 and Fc-GLP1 in assay buffer (as above) were added in duplicate to CHO cells recombinantly expressing human GLP-1R and incubated for 30 min at RT before detection with the cAMP dynamic 2 HTRF assay. EC50 values were determined by 4-parameter non-logistical fit analysis.



Indirect calorimetry

Indirect calorimetry was carried out using a 16-chamber TSE PhenoMaster monitoring system (TSE Systems GmbH, Germany). Mice were placed in acclimatization cages with one mouse per cage. Acclimation started 72h before the beginning of the experiment and the recording was monitored for 5 consecutive days. During the experiment mice were on a 12h light-dark

cycle and RT was maintained at 22 ± 2 °C. Food and water were provided ad libitum in appropriated devices that allow measurement of cumulative food intake and drink consumption. Oxygen consumption (VO₂) and carbon dioxide production (VCO₂) of individual mice were recorded every 30 or 60 min over 5 days and EE and RER were calculated using the TSA Systems software.

Fig. 10 | Deletion of ATGL in WAT suppresses the effects of G49 in BAT activation and reduces its efficacy in weight loss. A BW evolution (ATGL^{flax/flax}, $n = 11$; ATGL^{flax/flax} + G49, $n = 13$; ATGL^{adipoCre}, $n = 8$; ATGL^{adipoCre} + G49, $n = 12$). Mixed-effect analysis test with Bonferroni post hoc test. p values are detailed in Source data file. **B** Representative MRI images and total and visceral fat ($n = 4$ ATGL^{flax/flax}, $n = 4$ ATGL^{adipoCre}, same mice analyzed before and after 1 week of treatment). Total fat: ATGL^{flax/flax} vs. ATGL^{flax/flax} + G49, $***p < 0.0001$; ATGL^{flax/flax} + G49 vs. ATGL^{adipoCre} + G49, $###p < 0.0001$. Visceral fat: ATGL^{flax/flax} vs. ATGL^{flax/flax} + G49, $***p < 0.0001$; ATGL^{flax/flax} + G49 vs. ATGL^{adipoCre} + G49, $###p < 0.0001$. **C** Plasma FFAs at 6 h ($n = 6$ ATGL^{flax/flax}; ATGL^{flax/flax} + G49; ATGL^{adipoCre}, ATGL^{adipoCre} + G49). ATGL^{flax/flax} vs. ATGL^{flax/flax} + G49, $***p < 0.0001$; ATGL^{adipoCre} vs. ATGL^{adipoCre} + G49, $*p = 0.0102$; ATGL^{flax/flax} vs. ATGL^{adipoCre}, $^{\$}p = 0.0295$; ATGL^{flax/flax} + G49 vs. ATGL^{adipoCre} + G49, $###p < 0.0001$. **D** MRI analysis of total and visceral fat ($n = 4$ ATGL^{flax/flax}; ATGL^{flax/flax} + G49; ATGL^{adipoCre}; ATGL^{adipoCre} + G49, each mouse was analyzed before and 6 h post-G40 injection). Δ Total fat: ATGL^{flax/flax} vs. ATGL^{flax/flax} + G49, $***p < 0.0001$; ATGL^{flax/flax} + G49 vs. ATGL^{adipoCre} + G49, $###p < 0.0001$. Δ Visceral fat: ATGL^{flax/flax} vs. ATGL^{flax/flax} + G49, $***p < 0.0001$; ATGL^{flax/flax} + G49 vs. ATGL^{adipoCre} + G49, $###p < 0.0001$. **E** Plasma insulin at 6 h (ATGL^{flax/flax}, $n = 8$; ATGL^{flax/flax} + G49, $n = 10$; ATGL^{adipoCre}, $n = 7$; ATGL^{adipoCre} + G49, $n = 10$). ATGL^{flax/flax} vs. ATGL^{flax/flax} + G49, $***p < 0.0001$; ATGL^{adipoCre} vs. ATGL^{adipoCre} + G49, $**p = 0.0097$; ATGL^{flax/flax} + G49 vs. ATGL^{adipoCre} + G49, $###p < 0.0001$. **F** mRNAs in eWAT SVF at 6 h (*Il10*, ATGL^{flax/flax}, $n = 8$; ATGL^{flax/flax} + G49, $n = 11$; ATGL^{adipoCre}, $n = 9$; ATGL^{adipoCre} + G49, $n = 11$; *Il13*, ATGL^{flax/flax}, $n = 8$; ATGL^{flax/flax} + G49, $n = 10$; ATGL^{adipoCre}, $n = 8$; ATGL^{adipoCre} + G49, $n = 9$; *Th*, ATGL^{flax/flax}, $n = 5$; ATGL^{flax/flax} + G49, $n = 7$; ATGL^{adipoCre}, $n = 5$; ATGL^{adipoCre} + G49, $n = 5$). *Il10*: ATGL^{flax/flax} vs. ATGL^{flax/flax} + G49, $***p < 0.0001$; ATGL^{flax/flax} + G49 vs. ATGL^{adipoCre} + G49, $###p < 0.0001$. *Il13*: ATGL^{flax/flax} vs. ATGL^{flax/flax} + G49, $***p < 0.0001$; ATGL^{flax/flax} + G49 vs. ATGL^{adipoCre} + G49 vs. ATGL^{adipoCre} + G49, $###p < 0.0001$. *Th*: ATGL^{flax/flax} vs. ATGL^{flax/flax} + G49, $*p = 0.0142$. **G** Representative eWAT H&E images at 6 h (Scale bar 250 μ m) ($n = 4$). **H** Hepatic *Cpt1a* expression at 72 h ($n = 4$ in ATGL^{flax/flax}; ATGL^{flax/flax} + G49; ATGL^{adipoCre}; ATGL^{adipoCre} + G49) and FAO (ATGL^{flax/flax}, $n = 6$; ATGL^{flax/flax} + G49, $n = 7$; ATGL^{adipoCre}, $n = 8$; ATGL^{adipoCre} + G49, $n = 8$). *Cpt1a*: ATGL^{flax/flax} vs. ATGL^{flax/flax} + G49, $*p = 0.0312$; ATGL^{flax/flax} + G49 vs. ATGL^{adipoCre} + G49, $##p = 0.0090$. ASM: ATGL^{flax/flax} vs. ATGL^{flax/flax} + G49, $***p = 0.0003$; ATGL^{flax/flax} + G49 vs. ATGL^{adipoCre} + G49,

$###p = 0.0005$. CO₂: ATGL^{flax/flax} vs. ATGL^{flax/flax} + G49, $**p = 0.0015$; ATGL^{flax/flax} + G49 vs. ATGL^{adipoCre} + G49, $###p = 0.0002$. **I** *Hmcs* mRNA ($n = 4$ in each group), blood ketone bodies ($n = 6$ in each group), *Fgf21* mRNA ($n = 4$ in each group) and plasma FGF21 (ATGL^{flax/flax}, $n = 5$; ATGL^{flax/flax} + G49, $n = 6$; ATGL^{adipoCre}, $n = 5$; ATGL^{adipoCre} + G49, $n = 6$) at 72 h. *Hmcs2*: ATGL^{flax/flax} vs. ATGL^{flax/flax} + G49, $*p = 0.0129$; ATGL^{flax/flax} + G49 vs. ATGL^{adipoCre} + G49, $##p = 0.0041$. Blood ketone bodies: ATGL^{flax/flax} vs. ATGL^{flax/flax} + G49, $***p < 0.0001$; ATGL^{flax/flax} + G49 vs. ATGL^{adipoCre} + G49, $###p < 0.0001$. *Fgf21*: ATGL^{flax/flax} vs. ATGL^{flax/flax} + G49, $***p < 0.0001$; ATGL^{flax/flax} + G49 vs. ATGL^{adipoCre} + G49, $###p < 0.0001$. Plasma FGF21: ATGL^{flax/flax} vs. ATGL^{flax/flax} + G49, $***p < 0.0001$; ATGL^{flax/flax} + G49 vs. ATGL^{adipoCre} + G49, $###p < 0.0002$. **J** RER during 3 days of treatment and before and 6 h after first and second injections ($n = 4$ in ATGL^{flax/flax} and ATGL^{adipoCre}). Light: ATGL^{flax/flax} + G49 vs. ATGL^{adipoCre} + G49: day 1, $^{\#}p = 0.0236$; day 2 and day 3, $###p < 0.0001$; ATGL^{flax/flax} + G49: day 0 vs. day 2, $^{++}p = 0.0025$; day 0 vs. day 3, $^{++}p = 0.0052$. Dark: ATGL^{flax/flax} + G49 vs. ATGL^{adipoCre} + G49: day 1, $^{\#}p = 0.0024$; day 2, $###p = 0.0009$; day 3, $###p < 0.0001$. RER (6 h): ATGL^{flax/flax} vs. ATGL^{adipoCre}: 6 h, $###p = 0.0003$; t_0 h vs. 6 h: ATGL^{flax/flax}, $^{++}p = 0.0048$. **K** Representative BAT H&E images (Scale bar 250 μ m) ($n = 4$), *Ucp1* (ATGL^{flax/flax}, $n = 4$; ATGL^{flax/flax} + G49, $n = 6$; ATGL^{adipoCre}, $n = 4$; ATGL^{adipoCre} + G49, $n = 6$) and representative UCP1 Western blot and quantification (ATGL^{flax/flax}, $n = 10$; ATGL^{flax/flax} + G49, $n = 8$; ATGL^{adipoCre}, $n = 9$; ATGL^{adipoCre} + G49, $n = 10$). *Ucp1*: ATGL^{flax/flax} vs. ATGL^{flax/flax} + G49, $***p = 0.0006$; ATGL^{flax/flax} + G49 vs. ATGL^{adipoCre} + G49, $###p < 0.0001$. UCP1 protein levels: ATGL^{flax/flax} vs. ATGL^{flax/flax} + G49, $***p < 0.0001$; ATGL^{flax/flax} + G49 vs. ATGL^{adipoCre} + G49, $###p < 0.0001$. **L** Representative thermography images and Δ maximal BAT temperature at 1 week (ATGL^{flax/flax}, $n = 5$; ATGL^{flax/flax} + G49, $n = 5$; ATGL^{adipoCre}, $n = 4$; ATGL^{adipoCre} + G49, $n = 5$). ATGL^{flax/flax} vs. ATGL^{flax/flax} + G49, $***p = 0.0002$; ATGL^{flax/flax} + G49 vs. ATGL^{adipoCre} + G49, $###p = 0.0002$. **M** Energy expenditure at 1 week ($n = 4$). Light: ATGL^{flax/flax} + G49 vs. ATGL^{adipoCre} + G49: day 3, $^{\#}p = 0.0024$. Dark: ATGL^{flax/flax} + G49 vs. ATGL^{adipoCre} + G49: day 1, $^{\#}p = 0.0129$; day 2, $^{\#}p = 0.0317$; day 3, $###p = 0.0006$. ATGL^{flax/flax} + G49: day 0 vs. day 1, $^{\#}p = 0.0264$; day 0 vs. day 2, $^{++}p = 0.0044$; day 0 vs. day 3, $^{+++}p = 0.0002$. **B–F, H–M** Two-way ANOVA with Bonferroni post hoc test. Data are mean \pm SEM. Source data are provided as a Source Data file.

Measurement of BAT temperature

The skin temperature surrounding BAT was recorded with an infrared camera (FLIR B335: Compact-Infrared-Thermal-Imaging-Camera). Pictures were captured and temperature measured at different time-points of treatment and analyzed with a specific software package (FLIR-Tools-Software, FLIR).

Analysis of body composition

Images were acquired in a Bruker Biospec 47/40 spectrometer (Bruker Biospin GmbH) located at the Bioimaging Center (Bioimac) (Complutense University of Madrid, Spain). The MRI system works at a 4.7 Teslas and is equipped with a 12 cm shielded gradient coil with a maximum gradient strength of 450 mT/m. A 70-mm volume radio-frequency (RF) coil, acting as a transmitter and receiver, was used for these experiments. Mice were anaesthetized with a mixture of oxygen and isoflurane and placed in prone position inside the RF coil. Animal respiration and temperature were monitored throughout the experiment using a 1035 MR-compatible monitor system (SA Instruments Inc., Stony Brook).

First, 2D spin-echo T1 weighted (TIWI) images covering the whole body of the mouse were acquired. The parameters for this sequence were: repetition time (TR) = 1 s; echo time (TE) = 10 ms; slice thickness = 1.0 mm; field of view (FOV) = 10 \times 5 cm²; matrix size = 256 \times 128; number of averaged experiments (NA) = 2. Thirty coronal slices were acquired in 4 min. Then, the spectrometer frequency was centered on the fat signal, and the same images as above were acquired, but a water suppression sequence, consisting of three narrow-band saturation pulses each followed by a spoiling gradient, was applied on the water signal, so only the fat signal was visible in the images. Images were processed using the ImageJ 1.52 package (NIH). First, the fat tissue was segmented from the water-suppressed images to determine the

weight of the fat. Next, the fat tissue volume was calculated by multiplying the total number of voxels representing this fat tissue by the volume of each voxel. Subsequently, this fat volume was multiplied by the fat density to estimate the weight of the fat.

Immortalized brown preadipocytes and differentiation

Briefly, primary brown preadipocytes were isolated from interscapular BAT of C57BL/6J lactating mice. BAT was chopped in 0.2% (w/v) collagenase type I solution dissolved in DMEM supplemented with penicillin (100 U/mL), streptomycin (100 μ g/mL), 2 mM glutamine, 10 mM HEPES, and 1.5% BSA, incubated at 37 °C for 30 min in a stirring bath and filtered through a 250 μ m silk filter. Then, the infranatant was poured through a 25- μ m silk filter and centrifuged at 720 \times g for 10 min. The pellet was washed with culture medium (DMEM supplemented with penicillin, streptomycin, 2 mM glutamine, 10 mM of HEPES, 10% newborn calf serum (NCS), and 3 nM insulin) and cells were plated. Once the brown preadipocytes reached 70–80% confluence, they were infected with retroviral particles encoding SV40 Large T antigen in culture medium containing 20% heat-inactivated fetal bovine serum (FBS) and polybrene (8 μ g/mL) for 48 h. Selection with puromycin (1 μ g/mL) was performed in 10% FBS culture medium. Immortalized brown preadipocytes were maintained in DMEM supplemented with penicillin, streptomycin, 10 mM HEPES, 2 mM glutamine and 10% heat-inactivated FBS. For differentiation, cells were plated in 10% FBS-DMEM (as above) supplemented with 1 nM T₃ and 20 nM insulin (medium 1) until reaching the confluence. Next, cells were cultured during 2 days in induction medium containing medium 1 plus 0.5 μ M dexamethasone, 0.5 mM IBMX, 0.125 M indomethacin and 1 μ M rosiglitazone. Then, cells were switched to medium 1 for 5 additional days after which they

exhibited a fully differentiated phenotype and were used for experiments.

hMSC culture and treatment

hMSC were obtained from subcutaneous abdominal adipose tissue of 2 obese obese male subjects (BMI: 30–41 kg/m²) undergoing elective laparoscopic surgery. Fat biopsies from washed in PBS, minced with a scalpel and disaggregated with digestion medium containing low glucose DMEM, 10 mg/ml BSA, 1.5 mg/ml type IV collagenase and 0.6% antibiotic mixture for 40–50 min at 37 °C and agitation. After centrifugation, the pellet was resuspended in red cell lysis buffer (150 mM NaH₄Cl, 10 mM NaHCO₃, 1.27 mM EDTA) and incubated for 2 min at RT with gentle manual agitation and centrifuged again. The pellet was washed with PBS, resuspended in low glucose DMEM medium supplemented with 10% FBS and 1% antibiotic mixture, plated in 25 cm² cell culture flasks and expanded. Isolated hMSC were tested by fluorescence-activated cell sorting analysis using specific antibodies to detect mesenchymal markers⁷³ and then frozen. For experiments, 5 independent vials of hMSC were thawed in 10% FBS-low glucose DMEM medium at 37 °C and 5% CO₂. When reaching confluence, hMSC were differentiated into adipocytes using an adipogenic cocktail containing 500 μM IBMX, 1.67 μM insulin, 1 μM dexamethasone, 1 μM rosiglitazone and 10% FBS-high glucose DMEM medium for 6 days, removing the media after 3 days and adding new adipogenic cocktail. After 9 days, cells were incubated with 10% FBS-high glucose DMEM medium for 3 days. Adipocytes were then treated with G49 (500 nM) for 4 h.

Primary mouse hepatocytes

Primary mouse hepatocytes were isolated from non-fasting male C57BL/6j mice after 12 weeks fed on a HFD and receiving or not G49 treatment by a two-step collagenase perfusion. Livers were cannulated through the inferior vena cava via the right atrium and perfused with a calcium- and magnesium-free HBSS containing 10 mM HEPES, 0.5 mM EGTA followed by perfusion with Williams E medium containing 50 mM HEPES and type IV collagenase. The liver was removed, minced in DMEM and Ham's F-12 medium (1:1) supplemented with 2 mM glutamine, 15 mM glucose, 20 mM HEPES, 100 U/ml penicillin, 100 μg/ml streptomycin and 1 mM sodium pyruvate (attachment medium) and the hepatocytes were filtered through a 100 μm cell strainer. After centrifugation at 60 × g for 5 min at RT, the hepatocyte pellet was resuspended in attachment medium and mixed with an isotonic Percoll solution (1:1) followed by centrifugation at 230 × g for 10 min at RT. After washing, cells were seeded on collagen-coated plates and cultured in attachment medium in 6-well plates under humidity conditions in 95% air and 5% CO₂ at 37 °C for 24 h before treatment.

Isolation and culture of pancreatic islets

Mice were sacrificed by cervical dislocation and the pancreas was excised after infusing the animal in the common bile duct with 3–4 mL of Collagenase P solution (13.5 U/mL) derived from *Clostridium histolyticum* mixed with HBSS (1:14) following the procedure reported by Carter et al.⁷⁴. The perfusion was performed with a 30-gauge needle secured to a 5 mL syringe. After successful infusion and removal of the pancreas from the mouse, pancreata were further incubated in a 50 mL Falcon tube with the collagenase solution for 10–12 min at 37 °C in a water bath. Following incubation, 10 mL of ice-cold HBSS medium were added to the tubes and pancreata were mechanically digested by vigorous shaking. Then, pancreatic tissue was divided into different tubes and washed in several steps with ice-cold HBSS isolation medium. Islets were then handpicked under a stereomicroscope (Leica M80; Leica microsystems) using a 10 μL pipette. Freshly isolated islets were transferred into Falcon 35 mm sterile dishes and cultured o/n in Roswell Park Memorial Institute medium (RPMI-1640) containing 5.6 mM glucose supplemented with 10% FBS, 100 U/mL penicillin, 100 μg/mL streptomycin, 10 mM HEPES, 2 mM L-glutamine, 1 mM

sodium pyruvate and 50 μM β-mercaptoethanol. The islets were plated at a density of 100 islets in 3 mL of medium. The day after, islets were treated with 500 nM of G49 for 1 or 24 h.

Isolation of mature adipocytes from eWAT

Floating mature adipocytes were isolated from eWAT depots of DIO mice or global *Gcgr*^{+/+} and *Gcgr*^{-/-} mice. Briefly, eWAT was weighted and placed in ice-cold phosphate buffer (PB). The tissue was transferred to a petri dish with PBS, blood vessels were removed, and tissue was minced with scissors to obtain pieces around 1 mm. Then, tissue fragments were transferred to a conical tube with digestion buffer (PB, 2.5 mM glucose, 2.5 mg/g of Type I collagenase and 0.1% FFA-free BSA) and incubated for 20 min at 37 °C on a bath shaker. Following tissue digestion, the suspension was passed through a 150-μm mesh CellTrics filter followed by an equal volume of PB and centrifuged at 400 × g for 1 min. After centrifugation, the adipocytes formed a layer at the top of the liquid. This layer was collected and washed twice with 3 volumes of PB. Finally, floating adipocytes were collected and treated with G49 in PBS-0.1% BSA for 4 h at 37 °C on a bath shaker. After treatment, the reaction was stopped on ice for 15 min. Culture media were collected and glycerol and FFAs were quantified spectrophotometrically with colorimetric kits and normalized to the protein amount of each sample.

Preparation of protein lysates and Western blot

For BAT samples, a piece of tissue was lysed in lysis buffer (50 mM HEPES pH 7.5, 1% Triton X-100, 50 mM tetrabasic sodium pyrophosphate, 100 mM sodium fluoride, 10 mM EDTA, 10 mM sodium o-vanadate, 1 mM phenylmethanesulfonyl fluoride and 10 μg/mL protease inhibitors pH 7.4–7.6, using a tissue homogenizer (0003737000; IKA). After centrifugation at 98,560 × g for 40 min at 4 °C, the supernatant was centrifuged at 16,000 × g for 20 min at 4 °C. The resulting supernatant was centrifuged at 16,000 × g for 7 min at 4 °C and the final supernatant was collected. For eWAT and iWAT samples, a piece of tissue was chopped with scissors in ice-cold lysis buffer and homogenized passing the lysate through a 23G syringe 5–10 times. The homogenate was centrifuged as in BAT samples. Liver tissue was lysed with the buffer used for BAT tissue. The homogenates were centrifuged twice at 98,560 × g for 40 min at 4 °C and the resulting supernatants were collected. Protein content was quantified using the BCA dye method.

For cell samples, BA and hepatocytes were lysed in lysis buffer (10 mM Tris pH 7.5, 5 mM EDTA, 50 mM HCl, 30 μM sodium pyrophosphate, 50 mM NaF, 100 mM sodium o-vanadate, 1% Triton X-100, 1 mM PMSF and 10 μg/mL protease inhibitors), pH 7.4–7.6. Then, cells were centrifuged twice at 11,200 × g for 20 min at 4 °C. Protein content was quantified using the Bradford dye method.

Protein extracts (15–75 μg) were boiled at 95 °C for 5 min in loading buffer (100 mM Tris pH 6.8, 10% glycerol, 4% sodium dodecyl sulfate (SDS), 0.2% bromophenol blue and 2 mM β-mercaptoethanol) and subjected to 8–12% SDS polyacrylamide gel electrophoresis (SDS-PAGE) and then transferred to polyvinylidene difluoride (PVDF) membranes. Once transferred, Ponceau solution (0.1% Ponceau and 5% acetic acid in water) was added to the membranes to visualize protein loading. After washing with Tris-buffered saline (TBS)-0.05% Tween-20 (TBS-T), membranes were blocked with 6% skimmed milk powder in TBS-T buffer for 2 h at RT and incubated with primary antibodies (Supplementary Data 1) at 4 °C waving o/n. After 4–5 washes with TBS-T, membranes were incubated with the corresponding secondary antibody for 1 h waving at RT. Membranes were developed with chemiluminescent substrate and different exposure times were performed for each primary antibody with radiographic films in a radiology cassette (AGFA, Mortsel, Belgium) or developed in a ChemiDoc imager (Bio-Rad Laboratories). Blots were normalized using antibodies against housekeeping proteins. Densitometry values were

determined using ImageJ 1.52 or ImageLab Software (version 6.0.1, Bio-Rad Laboratories). The original Western blots are included as Source Data File.

Histological and morphometric analysis, oil red O (ORO) staining and immunostaining

Hematoxylin and eosin (H&E) staining was performed in paraffin sections of BAT, eWAT, iWAT and liver from mice. The tissue was fixed in 4%-paraformaldehyde (PFA) for 24 h, washed twice with PBS and dehydrated with ascending ethanol solutions, incubated with xylene and then embedded in paraffin. Blocks were cut in 5 μ m sections. Prior to H&E staining or immunohistochemistry, sections were deparaffinized in xylene and hydrated in descending ethanol solutions and distilled water. The slides were stained with Mayer's hematoxylin for 15–20 min and eosin for 1 min. After dried and mounted, images were captured with an Axiophot light microscope (Zeiss, Oberkochen, Germany).

For immunohistochemistry, sections were heated for 20 min in 100 mM sodium citrate buffer (pH 6.0) and 0.05% Tween-20. After washing with PBS, endogenous peroxidase was blocked by incubation with a solution of 9% H₂O₂ in 10% methanol for 10 min at RT. Tissue sections were then incubated in 6% BSA and 2% horse serum in PBS-0.1% Triton X-100 for 1 h at RT to block nonspecific binding. Sections were incubated with primary antibodies at 4 °C o/n. The sections were washed with PBS and incubated with biotinylated secondary antibodies for 1 h at RT. After washing with PBS, the slides were incubated with DAB-immunoperoxidase staining. After washing 5 min with water, sections were counterstained with hematoxylin solution for 10 s and rinsed again with water. After dehydrated and xylene incubation, the sections were assembled with Depex, covered with coverslips and dried o/n. After dried and mounted, images of the samples were captured with an Axiophot light microscope (Zeiss).

For ORO staining pieces of liver were fixed o/n in 4%-PFA and cryoprotected in subsequent gradients of 15% and 30% sucrose in PBS at 4 °C. Samples were quickly frozen in Tissue-Tek® Optimum Cutting Temperature (OCT) compound and sectioned at 5 μ m using a Leica CM3050 S cryostat. Tissue slices were fixed in ice cold 10% formaldehyde for 10 min and washed twice in distilled water. Then, samples were fixed in 1,2 propylene glycol for 10 min at RT. Slices were stained in 0.7% ORO solution shaking for 7 min. After washing twice in 87% glycerol, sections were counterstained with hematoxylin solution for 5 s, rinsed again with tap water and mounted in Aquatex. Tissue slides were then left at RT for 10 min and the remaining OCT was washed with PBS. Slides were then placed in 60% isopropanol for 15 s before being placed in filtering ORO solution (60% isopropanol in water) for 15 min. After washing the slides with PBS, they were stained with Carazzi's hematoxylin for 1 min. The excess of the hematoxylin was washed with PBS, after which the slides were mounted in 50% glycerol (in PBS) and sealed. After drying, the images were captured with an Axiophot light microscope (Carl Zeiss).

Brain slice immunofluorescence

Mice were anesthetized with ketamine/xylazine 80/5 mg/kg (i.p.) and transcardially perfused with ice-cold PBS followed by 4% PFA in PBS. Brains were extracted and post-fixed overnight in 4% PFA at 4 °C, and then exposed to 30% sucrose in PBS. Brains were sectioned to a thickness of 40 μ m using a sliding freezing microtome (Leica SM2010 R) and preserved in cryoprotectant solution (25% glycerol and 30% ethylene glycol in PBS). Free-floating brain slices were washed in PBS. For immunostaining, slices were then incubated in 10 mM sodium citrate (pH 8) in PBS at 60 °C for 30 min and washed in PBS. Thereafter, all slices were incubated for 2 h in blocking buffer (1% BSA and 0.1% Triton-X-100 in PBS) at RT, and incubated overnight at 4 °C with primary antibodies diluted in blocking buffer.

Anti-POMC and anti-c-Fos antibodies were used (Supplementary Data 1). Slices were then washed in PBS and incubated for 2 h at RT with secondary antibodies diluted in 1% BSA in PBS under light-protected conditions. Goat anti-guinea pig IgG conjugated to Alexa Fluor™ 488 and donkey anti-rabbit IgG conjugated to Alexa Fluor™ 546 antibodies were used. After a final washing in PBS for 10 min, cells were mounted with DAPI Fluoromount-G® Mounting Media. All images were acquired using a confocal laser scanning microscope (LSM 800 with Airyscan, Zeiss), and the ZEN 2 Blue Edition software (Zeiss).

TUNEL analysis

Paraffin-embedded eWAT biopsy sections were stained using Dead-End™ Fluorimetric TUNEL system according to the manufacturer's instructions. After immunostaining, eWAT sections were mounted with fluorescent mounting medium and images were taken using a confocal microscope LSM710.

Quantitative real time polymerase chain reaction

Total RNA from tissues or cells was extracted using TRIzol Reagent. Reverse transcription was performed using the High-Capacity cDNA Reverse Transcription Kit according to the manufacturer's instructions. Quantitative PCR (qPCR) was performed with 50 ng of cDNA mixed with Power SYBR Green Master Mix for primers or with Taqman Universal Master Mix II for Taqman probes. Amplification was conducted in a 7900HT Fast-Real Time PCR System (Life Technologies). Primer sequences and TaqMan probes are listed in Supplementary Data 1. The relative changes in gene expression were calculated using the 2^{- $\Delta\Delta$ Ct} (cycle threshold) quantification method, normalized to expression levels of the *RplpO* (Ribosomal protein, large, P0). Data analysis is based on the $\Delta\Delta$ Ct method with normalization of the raw data to housekeeping genes.

Lipolysis assay in brown and white adipocytes and WAT explants

Differentiated BA were treated for 4 h with or without 500 nM G49 in Krebs-Ringer Modified Buffer (KRB) (118.5 mM NaCl, 4.75 mM KCl, 1.92 mM CaCl₂, 1.19 mM KH₂PO₄, 1.19 mM MgSO₄(H₂O)₇, 25 mM NaHCO₃, 10 mM HEPES, 6 mM D-Glucose, 4% BSA pH 7.4). Isolated white adipocytes were stimulated for 4 h with or without 500 nM G49 in PBS-0.1% BSA. Culture media were collected and glycerol and FFAs were quantified spectrophotometrically with the free glycerol reagent colorimetric kit and NEFAs assay kit and normalized to the protein amount of each sample.

Epididymal fat pads from mice were placed in 60 cm plates with prewarmed (37 °C) DMEM containing 100 U/mL penicillin and 100 μ g/mL streptomycin. Connective tissue and blood vessels were removed by dissection before cutting the tissue into small pieces. Explants were cultured in DMEM with L-glutamine (2 mM), 100 U/mL penicillin, 100 μ g/mL streptomycin and 2% FFA-BSA in presence or absence of G49 (500 nM) for 4 h. Supernatants were collected and the amount of glycerol was quantified spectrophotometrically with the free glycerol reagent colorimetric kit.

Biochemical determinations

For human studies, serum levels of human FGF21, and plasma levels of OXM, adiponectin, GLP-1, insulin and glucagon were analyzed in a subsample of patients included in each surgical group by ELISA immunoassay according to the instructions of manufacturer. Plasma GGT levels were measured colorimetrically using automated tests. FFAs were measured as detailed above.

In animal studies, serum levels of mouse FGF21 and plasma levels of adiponectin, insulin and glucagon were measured by ELISA immunoassay according to the instructions of manufacturer. Plasma TG levels were measured using a colorimetric assay, plasma ALT levels were determined using Reflotron strips accordingly with the

manufacturer's instructions and plasma FFAs were measured as detailed above. All measurements were performed according to the manufacturer's instructions. Glucose and ketone bodies were measured in blood collected from the tail vein.

Determination of intrahepatic triglyceride content

Mouse livers were collected and immediately frozen and stored at -80°C . Liver samples were thoroughly homogenized for 30 s in 500 μL of 20 mM phosphate buffer (equimolar mix of K_2HPO_4 and KH_2PO_4) and then 400 μL were mixed with 1 mL of a 1:1 v/v chloroform/methanol mixture, vortexed and then samples were rotated in a wheel for 60 min at RT for 30 min. After adding 500 μL chloroform and 165 μL 0.74% KCl to each sample, the samples were manually mixed for 30 s and centrifuged for 5 min at $500 \times g$ at RT. The bottom organic phase was separated and 500 μL 1:1 v/v chloroform/methanol was added to the samples, vortexed, and centrifuged. Again, the bottom organic layer was isolated and evaporated at RT in a hood. The following day, the pellets were resuspended in isopropyl alcohol and TGs were quantified with a colorimetric kit.

Isolation and analysis of liver neutrophils by flow cytometry

Non-parenchymal liver cells (NPCs) were isolated based on the protocol reported by González-Rodríguez et al.⁷⁵ with slight modifications. Briefly, mice were sacrificed by cervical dislocation and livers were removed, washed in PBS at 37°C and then transferred to 5 mL of HBSS. After, livers were grinded with syringe plunged in a 100 μm cell strainer and the homogenate was centrifuged at $500 \times g$ for 5 min at RT. The pellets were resuspended in 36% Percoll solution in HBSS supplemented with heparin at 100 U/mL, transferred to another tube and centrifuged at $800 \times g$ for 20 min without break at RT. Supernatant was discarded and pellets were incubated in Ammonium-Chloride-Potassium buffer (ACK) (0.15 mM NH_4Cl , 10 mM KHCO_3 and 0.5 M EDTA, pH 7.3) for 5 min at RT and centrifuged at $500 \times g$ for 5 min at 4°C . Pellets were washed twice with ice cold HBSS and finally resuspended in 80 μL HBSS. Cells were incubated with Cd45-FITC (rat IgG), Cd11b-(Mac1)-PECy7 (rat IgG2b, κ), and Ly6g-PE (rat IgG2a, κ) antibodies (Supplementary Data 1) for 20 min at RT. Flow cytometry data were acquired with a FACSCanto II (BD Biosciences, Madrid, Spain) and data analysis was performed using Cytomics FC500 with the CXP program and Kaluza Analysis Software.

Isolation and analysis of eWAT stromal vascular fraction by flow cytometry

Mice were sacrificed by cervical dislocation and eWAT was isolated. One gram of tissue was collected and washed in ice-cold PBS. Then, tissue samples were chopped with scissors in digestion buffer (HBSS supplemented with Ca and Mg and 0.5% FFA-BSA), transferred to a conical tube and mixed (10:1 v/v) with collagenase solution (10 mg/mL Collagenase Type II) and incubated at 37°C in a water bath for 20–45 min with orbital shaking until the digestion was completed. Then, 50 μL of 10 mM EDTA was added and incubation continued for a further 10 min. The homogenates were filtered through 100 μm cell strainers and filters were washed twice with FACS buffer (1 mM EDTA, 25 mM HEPES, 1% FBS in PBS) and centrifuged at $500 \times g$ for 10 min at 4°C . Pellets were incubated in 0.5 mL of ACK buffer for 5 min and centrifuged at $500 \times g$ for 10 min at 4°C . Pellets were then resuspended in FACS buffer and incubated with Cd45-FITC (rat IgG2b), Cd45-Brilliant Violet 570 (rat IgG2b, κ), Cd11b-APC (rat IgG2b, κ), Cd11b-(Mac1)-PERCy5.5 (rat IgG2b, κ), F4/80-PECy7 (rat IgG2a, κ), Ly6g-APC-Cy7 (rat IgG2a, κ), Cd11c-PE (hamster IgG), Cd11c-APC (hamster IgG), Cd206-FITC (rat IgG2a, κ), Cd3-PECy7 (hamster IgG), SiglecF-PCy7 (rat IgG2a, κ),

NK1.1-APC (mouse IgG2a, κ), Cd8-Brilliant Violet 421 (rat IgG2a, κ), Cd4-PERCy5.5 (rat IgG2b, κ), TCR β -FITC (hamster IgG) and IL4-PE (rat IgG1) antibodies (Supplementary Data 1) or their corresponding isotype controls for 20 min at RT. Flow cytometry data were acquired with a FACSCanto II (BD Biosciences, Madrid, Spain) and data analysis was performed using Cytomics FC500 with the CXP program. Gating strategy is detailed in Fig. S14.

Ex vivo glucose-stimulated insulin secretion (GSIS) in pancreatic islets

After G49 treatment, pancreatic islets were incubated in KRB with 2.8 mM glucose and 0.25% BSA, pH 7.4 for 1 h at 37°C in an atmosphere of 5% CO_2 . Thereafter, batches of 3 islets per condition were transferred into a 96-well plate containing 200 μL KRB per well followed by the addition of 2.8 and 16.7 mM glucose (final concentrations) and the plate was incubated at 37°C for 1 h. After that, 100 μL of the supernatant (medium) was collected and stored at -20°C until the analysis. Insulin concentration was determined with the mouse insulin ELISA kit following manufacturer's instructions and values were normalized per islet number.

Measurement of cellular bioenergetics profile in BAT explants and brown adipocytes

Oxygen consumption rate (OCR) was measured in BAT explants from DIO mice treated with G49 or vehicle for 72 h with XF Seahorse technology. BAT was excised and cut using a scalpel into 9 mg pieces and then placed into a tube containing DMEM supplemented with 25 mM glucose and 25 mM HEPES. Samples were kept in this medium (wash medium) until measurement of respiration. The Seahorse capture screens (Agilent Technologies) were pre-wet in wash medium in a small petri dish to remove air bubbles. A pair of sterile forceps was used to position the screens (ring facing up) in a new empty small petri dish, and 9 mg of BAT was placed on the screen with forceps. Then, the Seahorse capture screen insert tool (Agilent Technologies) was used to pick up the tissue-containing screens from the petri dish and to place them in an XF24 Islet Capture Microplate (Agilent Technologies). Once in position, 450 μL of assay medium (DMEM supplemented with 25 mM glucose) was added to the samples. For a typical bioenergetic profile, a set of inhibitors of key components of cellular respiration was added: 24 $\mu\text{g}/\text{mL}$ oligomycin A, 0.8 μM of the uncoupler FCCP and a mix of 5 μM rotenone and 15 μM antimycin A.

For analysis of OCR in BA, cells were differentiated in customized Seahorse 24-well plates and then treated with G49 or vehicle for 16 h. Before any measurement, cells were incubated for one hour with XF Assay Medium (Seahorse Bioscience) plus 5 mM glucose. We followed the protocol and injection strategies of the Mito Stress Assay (Seahorse Bioscience). The concentrations of the inhibitors were: 2 μM oligomycin A, 2 μM uncoupler FCCP and a mix of 10 μM rotenone and 10 μM antimycin. OCR was calculated by plotting the O_2 tension of media as a function of time (pmol/min) and data were normalized by the protein concentration measured in each individual well by the Bradford method. Calculations were performed using the Seahorse Wave Pro Software (Agilent).

Fatty acid oxidation assay in mouse hepatocytes and brown adipocytes

Palmitate oxidation to CO_2 and acid-soluble material (ASM), essentially acyl-carnitine, Krebs cycle intermediates and acetyl-CoA, were measured in primary mouse hepatocytes and differentiated BA in presence or absence of 500 nM G49. The day of the assay, cells were washed in KRB-HEPES buffer (KRBH buffer: 135 mM NaCl, 3.6 mM KCl, 0.5 mM NaH_2PO_4 , 0.5 mM MgSO_4 , 1.5 mM CaCl_2 , 2 mM NaHCO_3 , and 10 mM HEPES, pH 7.4) and 0.1% BSA,

preincubated at 37 °C for 30 min in KRBH-1% BSA and washed again in KRBH-0.1% BSA. Cells were then incubated for 3 h at 37 °C with fresh KRBH containing 25 mM glucose and 8 mM carnitine, 2.5 mM palmitate and 1 $\mu\text{Ci}/\text{mL}$ [^{14}C] palmitate bound to BSA. Oxidation measurements were performed as previously described⁷⁶ with minor modifications by trapping the radioactive CO_2 in a 1 cm^2 Whatman paper soaked with 40 μL 0.1 N KOH using parafilm-sealed system. The reaction was stopped by the addition of 40% perchloric acid through a syringe that pierced the parafilm. The following day, the system was opened and the papers were left to dry out, before transferring them into tubes with 5 mL scintillation liquid. An amount of 300 μL of the reaction mix with perchloric acid was removed and centrifuged at maximum speed for 10 min. Then, 150 μL of the supernatant, which contained the ASM, were transferred into a tube containing 5 mL scintillation liquid. After 2 h of stabilization, samples were analyzed and data for CO_2 are expressed as: $\text{nmol palmitate mg}^{-1} \text{prot h}^{-1} = (\text{cpm}_{\text{sample}} - \text{cpm}_{\text{blank}}) * 80 / (\text{total cpm} * \text{mg prot} * \text{h})$. The results for ASM are expressed as: $\text{nmol palmitate mg}^{-1} \text{prot h}^{-1} = (\text{cpm}_{\text{sample}} - \text{cpm}_{\text{blank}}) * 80 * (352/150) / (\text{total cpm} * \text{mg prot} * \text{h})$.

FAO assay in liver tissue

Frozen (liquid nitrogen) liver pieces (30 mg) were homogenized in cold homogenization STE buffer (25 mM Tris-HCl, 500 nM sucrose, 1 mM EDTA- Na_2 pH 7.4) and sonicated for 10 s. Then, the homogenates were centrifuged at 420 $\times g$ for 10 min at 4 °C and the supernatant was collected. Five hundred μg of protein from the liver homogenates were used for the assay in a volume of 60 μL . The reaction started by adding 340 μL of assay buffer containing: 0.7% BSA/500 μM palmitate/0.4 μCi (0.5 $\mu\text{Ci}/\text{ml}$) [^{14}C]-Palmitic acid, 100 mM sucrose, 10 mM Tris-HCl, 5 mM KH_2PO_4 , 0.2 mM EDTA, 80 mM KCl, 1 mM MgCl_2 , 2 mM L-carnitine, 0.1 mM malate, 0.05 mM coenzyme A, 2 mM ATP and 1 mM DTT to the samples. Samples were incubated for 30 min at 37 °C in Eppendorf tubes with a Whatman paper circle in the cap. The reaction was stopped by adding 200 μL of 3 M perchloric acid, after adding 1 M NaOH in to the Whatman cap to collect all the evaporated $^{14}\text{C}\text{CO}_2$. After 1 h, the Whatman caps were removed and the associated radioactivity to CO_2 was measured in a scintillation counter. Radioactivity associated to acid soluble metabolites (ASM) was measured after centrifugation at maximum speed for 10 min by taking the supernatant which contained ASM in a scintillation counter. Results are expressed as nmol/g liver tissue/h.

Statistical analysis

Data are expressed as the mean \pm SEM. Normal distribution was assessed by two different tests, Shapiro–Wilk and Kolmogorov–Smirnov. To determine the effects of G49 in the different experimental protocols, one-way ANOVA or Brown–Forsythe Welch ANOVA or Kruskal–Wallis, two-way ANOVA or two-way repeated measures (RM) ANOVA or Mixed-effect analysis tests, followed by Bonferroni or Dunnett T3 or Dunn’s post hoc tests was carried out. Specific statistical analysis is detailed in figure legends. To analyze the differences between two independent variables paired or unpaired two-tailed t tests were performed. In order to establish correlation between parameters a simple linear regression test was accomplished. Pearson correlation test was used for correlations. p values correspond to post hoc test. All statistical analyses were performed using the GraphPad Prism software version 10.0 (GraphPad Software Inc.). Differences were considered statistically significant at $p < 0.05$, $p < 0.01$ and $p < 0.001$. Except for repeated measure (RM) tests, measurements were taken from distinct samples. The ex vivo or in vitro experiments were conducted in independent biological samples.

Reporting summary

Further information on research design is available in the Nature Portfolio Reporting Summary linked to this article.

Data availability

The authors declare that the data generated in this study are provided within the article and its Supplementary Information files. Source data are provided with this paper.

References

- Sanchez-Garrido, M. A. et al. GLP-1/glucagon receptor co-agonism for treatment of obesity. *Diabetologia* **60**, 1851–1861 (2017).
- Nielsen, M. S. et al. Oxyntomodulin and glicentin may predict the effect of bariatric surgery on food preferences and weight loss. *J. Clin. Endocrinol. Metab.* **105**, 1064–1074 (2020).
- Perakakis, N. et al. Circulating levels of gastrointestinal hormones in response to the most common types of bariatric surgery and predictive value for weight loss over one year: evidence from two independent trials. *Metabolism* **101**, 153997 (2019).
- Baldissera, F. G., Holst, J. J., Knuhtsen, S., Hilsted, L. & Nielsen, O. V. Oxyntomodulin (glicentin-(33-69)); pharmacokinetics, binding to liver cell membranes, effects on isolated perfused pig pancreas, and secretion from isolated perfused lower small intestine of pigs. *Regul. Pept.* **21**, 151–166 (1988).
- Schjoldager, B. T., Baldissera, F. G., Mortensen, P. E., Holst, J. J. & Christiansen, J. Oxyntomodulin: a potential hormone from the distal gut. Pharmacokinetics and effects on gastric acid and insulin secretion in man. *Eur. J. Clin. Invest.* **18**, 499–503 (1988).
- Pocai, A. et al. Glucagon-like peptide 1/glucagon receptor dual agonism reverses obesity in mice. *Diabetes* **58**, 2258–2266 (2009).
- Day, J. W. et al. Optimization of co-agonism at GLP-1 and glucagon receptors to safely maximize weight reduction in DIO-rodents. *Biopolymers* **98**, 443–450 (2012).
- Di Prospero, N. A. et al. Efficacy and safety of glucagon-like peptide-1/glucagon receptor co-agonist JNJ-64565111 in individuals with type 2 diabetes mellitus and obesity: a randomized dose-ranging study. *Clin. Obes.* **11**, e12433 (2021).
- Day, J. W. et al. A new glucagon and GLP-1 co-agonist eliminates obesity in rodents. *Nat. Chem. Biol.* **5**, 749–757 (2009).
- Zimmermann, T. et al. BI 456906: discovery and preclinical pharmacology of a novel GCGR/GLP-1R dual agonist with robust anti-obesity efficacy. *Mol. Metab.* **66**, 101633 (2022).
- Jungnik, A. et al. Phase I studies of the safety, tolerability, pharmacokinetics and pharmacodynamics of the dual glucagon receptor/glucagon-like peptide-1 receptor agonist BI 456906. *Diabetes Obes. Metab.* **25**, 1011–1023 (2023).
- Pei, Z. et al. Design and characterization of novel oxyntomodulin derivatives with potent dual GLP-1/glucagon receptor activation and prolonged antidiabetic effects. *Life Sci.* **253**, 117651 (2020).
- Valdecantos, M. P. et al. A novel glucagon-like peptide 1/glucagon receptor dual agonist improves steatohepatitis and liver regeneration in mice. *Hepatology* **65**, 950–968 (2017).
- Boland, M. L. et al. Resolution of NASH and hepatic fibrosis by the GLP-1R/GcgR dual-agonist Cotadutide via modulating mitochondrial function and lipogenesis. *Nat. Metab.* **2**, 413–431 (2020).
- Marcondes-de-Castro, I. A. et al. Cotadutide effect in liver and adipose tissue in obese mice. *J. Mol. Endocrinol.* **70**, e220168 (2023).
- Ambery, P. et al. MEDIO382, a GLP-1 and glucagon receptor dual agonist, in obese or overweight patients with type 2 diabetes: a randomised, controlled, double-blind, ascending dose and phase 2a study. *Lancet* **391**, 2607–2618 (2018).
- Parker, V. E. R. et al. Efficacy, safety, and mechanistic insights of cotadutide, a dual receptor glucagon-like peptide-1 and glucagon agonist. *J. Clin. Endocrinol. Metab.* **105**, dgz047 (2020).

18. Nahra, R. et al. Effects of cotadutide on metabolic and hepatic parameters in adults with overweight or obesity and type 2 diabetes: a 54-week randomized phase 2b study. *Diabetes Care* **44**, 1433–1442 (2021).
19. Jastreboff, A. M. et al. Tirzepatide once weekly for the treatment of obesity. *N. Engl. J. Med.* **387**, 205–216 (2022).
20. Coskun, T. et al. LY3437943, a novel triple glucagon, GIP, and GLP-1 receptor agonist for glycemic control and weight loss: from discovery to clinical proof of concept. *Cell Metab.* **34**, 1234–1247.e1239 (2022).
21. Knerr, P. J. et al. Next generation GLP-1/GIP/glucagon triple agonists normalize body weight in obese mice. *Mol. Metab.* **63**, 101533 (2022).
22. Jastreboff, A. M., Kaplan, L. M. & Hartman, M. L. Triple-hormone-receptor agonist retatrutide for obesity. Reply. *N. Engl. J. Med.* **389**, 1629–1630 (2023).
23. Boland, B. B. et al. Peptide-YY(3-36)/glucagon-like peptide-1 combination treatment of obese diabetic mice improves insulin sensitivity associated with recovered pancreatic beta-cell function and synergistic activation of discrete hypothalamic and brainstem neuronal circuitries. *Mol. Metab.* **55**, 101392 (2022).
24. Qiu, Y. et al. Eosinophils and type 2 cytokine signaling in macrophages orchestrate development of functional beige fat. *Cell* **157**, 1292–1308 (2014).
25. Lynch, L. et al. iNKT cells induce FGF21 for thermogenesis and are required for maximal weight loss in GLP1 therapy. *Cell Metab.* **24**, 510–519 (2016).
26. Heine, M. et al. Lipolysis triggers a systemic insulin response essential for efficient energy replenishment of activated brown adipose tissue in mice. *Cell Metab.* **28**, 644–655 e644 (2018).
27. Badman, M. K. et al. Hepatic fibroblast growth factor 21 is regulated by PPARalpha and is a key mediator of hepatic lipid metabolism in ketotic states. *Cell Metab.* **5**, 426–437 (2007).
28. Alonge, K. M., Mearns, G. P. & Hillgartner, F. B. Glucagon and insulin cooperatively stimulate fibroblast growth factor 21 gene transcription by increasing the expression of activating transcription factor 4. *J. Biol. Chem.* **292**, 5239–5252 (2017).
29. Keipert, S. et al. Endogenous FGF21-signaling controls paradoxical obesity resistance of UCP1-deficient mice. *Nat. Commun.* **11**, 624 (2020).
30. Casajoana, A. et al. Predictive value of gut peptides in T2D remission: randomized controlled trial comparing metabolic gastric bypass, sleeve gastrectomy and greater curvature plication. *Obes. Surg.* **27**, 2235–2245 (2017).
31. Thompson, A. C. et al. Fibroblast growth factor 21 is not required for the reductions in circulating insulin-like growth factor-1 or global cell proliferation rates in response to moderate calorie restriction in adult mice. *PLoS ONE* **9**, e111418 (2014).
32. Yamauchi, T. et al. Targeted disruption of AdipoR1 and AdipoR2 causes abrogation of adiponectin binding and metabolic actions. *Nat. Med.* **13**, 332–339 (2007).
33. Vasileva, A., Marx, T., Beaudry, J. L. & Stern, J. H. Glucagon receptor signaling at white adipose tissue does not regulate lipolysis. *Am. J. Physiol. Endocrinol. Metab.* **323**, E389–E401 (2022).
34. Conarello, S. L. et al. Glucagon receptor knockout mice are resistant to diet-induced obesity and streptozotocin-mediated beta cell loss and hyperglycaemia. *Diabetologia* **50**, 142–150 (2007).
35. Mayer, N. et al. Development of small-molecule inhibitors targeting adipose triglyceride lipase. *Nat. Chem. Biol.* **9**, 785–787 (2013).
36. Holst, J. J. et al. Mechanisms in bariatric surgery: gut hormones, diabetes resolution, and weight loss. *Surg. Obes. Relat. Dis.* **14**, 708–714 (2018).
37. Pociu, A. Action and therapeutic potential of oxyntomodulin. *Mol. Metab.* **3**, 241–251 (2014).
38. Alexiadou, K. et al. Proglucagon peptide secretion profiles in type 2 diabetes before and after bariatric surgery: 1-year prospective study. *BMJ Open Diabetes Res. Care* **8**, 1076 (2020).
39. Gelling, R. W. et al. Lower blood glucose, hyperglucagonemia, and pancreatic alpha cell hyperplasia in glucagon receptor knockout mice. *Proc. Natl Acad. Sci. USA* **100**, 1438–1443 (2003).
40. Tura, A., Pacini, G., Yamada, Y., Seino, Y. & Ahren, B. Glucagon and insulin secretion, insulin clearance, and fasting glucose in GIP receptor and GLP-1 receptor knockout mice. *Am. J. Physiol. Regul. Integr. Comp. Physiol.* **316**, R27–R37 (2019).
41. Leitner, B. P. et al. Mapping of human brown adipose tissue in lean and obese young men. *Proc. Natl Acad. Sci. USA* **114**, 8649–8654 (2017).
42. Maida, A., Lovshin, J. A., Baggio, L. L. & Drucker, D. J. The glucagon-like peptide-1 receptor agonist oxyntomodulin enhances beta-cell function but does not inhibit gastric emptying in mice. *Endocrinology* **149**, 5670–5678 (2008).
43. Komatsu, M. et al. Augmentation of Ca²⁺-stimulated insulin release by glucose and long-chain fatty acids in rat pancreatic islets: free fatty acids mimic ATP-sensitive K⁺ channel-independent insulinotropic action of glucose. *Diabetes* **48**, 1543–1549 (1999).
44. Gravholt, C. H., Moller, N., Jensen, M. D., Christiansen, J. S. & Schmitz, O. Physiological levels of glucagon do not influence lipolysis in abdominal adipose tissue as assessed by microdialysis. *J. Clin. Endocrinol. Metab.* **86**, 2085–2089 (2001).
45. Schneider, S. H., Fineberg, S. E. & Blackburn, G. L. The acute metabolic effects of glucagon and its interactions with insulin in forearm tissue. *Diabetologia* **20**, 616–621 (1981).
46. Arafat, A. M. et al. Glucagon increases circulating fibroblast growth factor 21 independently of endogenous insulin levels: a novel mechanism of glucagon-stimulated lipolysis? *Diabetologia* **56**, 588–597 (2013).
47. Pereira, M. J. et al. Direct effects of glucagon on glucose uptake and lipolysis in human adipocytes. *Mol. Cell Endocrinol.* **503**, 110696 (2020).
48. Nason, S. R. et al. Glucagon receptor signaling regulates weight loss via central KLB receptor complexes. *JCI Insight* **6**, e141323 (2021).
49. Kinoshita, K. et al. Glucagon is essential for adaptive thermogenesis in brown adipose tissue. *Endocrinology* **155**, 3484–3492 (2014).
50. Fabbiano, S. et al. Caloric restriction leads to browning of white adipose tissue through type 2 immune signaling. *Cell Metab.* **24**, 434–446 (2016).
51. Kosteli, A. et al. Weight loss and lipolysis promote a dynamic immune response in murine adipose tissue. *J. Clin. Invest.* **120**, 3466–3479 (2010).
52. Zizzo, G., Hilliard, B. A., Monestier, M. & Cohen, P. L. Efficient clearance of early apoptotic cells by human macrophages requires M2c polarization and MerTK induction. *J. Immunol.* **189**, 3508–3520 (2012).
53. Crespo, M. et al. Neutrophil infiltration regulates clock-gene expression to organize daily hepatic metabolism. *Elife* **9**, e59258 (2020).
54. Richards, P. et al. Identification and characterization of GLP-1 receptor-expressing cells using a new transgenic mouse model. *Diabetes* **63**, 1224–1233 (2014).
55. Welles, J. E., Dennis, M. D., Jefferson, L. S. & Kimball, S. R. Glucagon-dependent suppression of mTORC1 is associated with upregulation of hepatic FGF21 mRNA translation. *Am. J. Physiol. Endocrinol. Metab.* **319**, E26–E33 (2020).
56. Inagaki, T. et al. Endocrine regulation of the fasting response by PPARalpha-mediated induction of fibroblast growth factor 21. *Cell Metab.* **5**, 415–425 (2007).
57. Markan, K. R. et al. Circulating FGF21 is liver derived and enhances glucose uptake during refeeding and overfeeding. *Diabetes* **63**, 4057–4063 (2014).

58. Habegger, K. M. et al. Fibroblast growth factor 21 mediates specific glucagon actions. *Diabetes* **62**, 1453–1463 (2013).
59. van Baak, M. A. et al. Adipose tissue contribution to plasma fibroblast growth factor 21 and fibroblast activation protein in obesity. *Int J. Obes.* **44**, 544–547 (2020).
60. BonDurant, L. D. & Potthoff, M. J. Fibroblast growth factor 21: a versatile regulator of metabolic homeostasis. *Annu. Rev. Nutr.* **38**, 173–196 (2018).
61. Schlein, C. et al. FGF21 lowers plasma triglycerides by accelerating lipoprotein catabolism in white and brown adipose tissues. *Cell Metab.* **23**, 441–453 (2016).
62. Holland, W. L. et al. An FGF21-adiponectin-ceramide axis controls energy expenditure and insulin action in mice. *Cell Metab.* **17**, 790–797 (2013).
63. Schreiber, R. et al. Cold-induced thermogenesis depends on ATGL-mediated lipolysis in cardiac muscle, but not brown adipose tissue. *Cell Metab.* **26**, 753–763.e757 (2017).
64. Beaudry, J. L. et al. The brown adipose tissue glucagon receptor is functional but not essential for control of energy homeostasis in mice. *Mol. Metab.* **22**, 37–48 (2019).
65. Astiarraga, B. et al. Impaired succinate response to a mixed meal in obesity and type 2 diabetes is normalized after metabolic surgery. *Diabetes Care* **43**, 2581–2587 (2020).
66. Chodorge, M. et al. Engineering of a GLP-1 analogue peptide/anti-PCSK9 antibody fusion for type 2 diabetes treatment. *Sci. Rep.* **8**, 17545 (2018).
67. Rivero-Gutierrez, B. et al. Deletion of the glucagon receptor gene before and after experimental diabetes reveals differential protection from hyperglycemia. *Mol. Metab.* **17**, 28–38 (2018).
68. Unson, C. G., Gurzenda, E. M. & Merrifield, R. B. Biological activities of des-His1[Glu9]glucagon amide, a glucagon antagonist. *Peptides* **10**, 1171–1177 (1989).
69. Green, B. D. et al. Chronic treatment with exendin(9-39)amide indicates a minor role for endogenous glucagon-like peptide-1 in metabolic abnormalities of obesity-related diabetes in ob/ob mice. *J. Endocrinol.* **185**, 307–317 (2005).
70. Biggs, E. K. et al. Development and characterisation of a novel glucagon like peptide-1 receptor antibody. *Diabetologia* **61**, 711–721 (2018).
71. Povinelli, B. J. et al. Standard sub-thermoneutral caging temperature influences radiosensitivity of hematopoietic stem and progenitor cells. *PLoS ONE* **10**, e0120078 (2015).
72. Naylor, J., Rossi, A. & Hornigold, D. C. Acoustic dispensing preserves the potency of therapeutic peptides throughout the entire drug discovery workflow. *J. Lab. Autom.* **21**, 90–96 (2016).
73. Perez-Diaz, S. et al. Knockdown of PTRF ameliorates adipocyte differentiation and functionality of human mesenchymal stem cells. *Am. J. Physiol. Cell Physiol.* **312**, C83–C91 (2017).
74. Carter, J. D., Dula, S. B., Corbin, K. L., Wu, R. & Nunemaker, C. S. A practical guide to rodent islet isolation and assessment. *Biol. Proced. Online* **11**, 3–31 (2009).
75. Gonzalez-Rodriguez, A. et al. Dual role of protein tyrosine phosphatase 1B in the progression and reversion of non-alcoholic steatohepatitis. *Mol. Metab.* **7**, 132–146 (2018).
76. Herrero, L. et al. Alteration of the malonyl-CoA/carnitine palmitoyltransferase I interaction in the beta-cell impairs glucose-induced insulin secretion. *Diabetes* **54**, 462–471 (2005).
- 0001 (CIBERobn, ISCIII, Spain) and 2021SGR00367 (Government of Catalonia) to L.H., grants PID2019-106982RB-I00 funded by MICIU/AEI/10.13039/501100011033 and CB12/03/30002 (CIBERobn, ISCIII, Spain) to M.J.M.-A., grants AECC PROYE19047SABI, PMP21/00057 Infraestructura de Medicina de Precisión asociada a la Ciencia y Tecnología IMPACT-2021, Instituto de Salud Carlos III, PDC2021-121147-I00 funded by MICIU/AEI/10.13039/501100011033 and the “European Union NextGeneration/PRTR” and PID2022-138525OB-I00 funded by MICIU/AEI/10.13039/501100011033 and ERDF/EU to G.S., grant PID2021-122480OB-I00 funded by MICIU/AEI/10.13039/501100011033 and by ERDF/EU, and 2021 SGR 01409 (Generalitat de Catalunya) to S.F.V., grant PID2021-128737NB-I00 funded by MICIU/AEI/10.13039/501100011033 and by ERDF/EU to M.S., grants PI20/00338, PI23/01133 (ISCIII, Spain), and 2021 SGR 00829 (Government of Catalunya) to J.V., grants PI17/01556 and PI22/01773 (ISCIII, Spain) to N.V., grants IT1476-22 funded by Basque Government, Department of Education and PID2021-124425OB-I00 funded by MICIU/AEI/10.13039/501100011033 and by ERDF/EU to P.A. and F7302 SFB-Lipid-Hydrolysis from the Austrian Science Fund FWF and 12CVDO4 from the Leducq Foundation both to R.Z. C.F. was funded by EASO/Novo Nordisk New Investigator Award in Basic Sciences 2023, EFSD/Novo Nordisk Rising Star 2024 and IBSA Foundation Fellowship Endocrinology 2023. V.F. was supported by “Albert Renold Travel Fellowship” grant from EFSD. Magnetic resonance imaging studies were performed at BiolmaC (Biolmagen Complutense), a node of the ICTS ReDIB. We acknowledge F. Gribble and F. Reimann (Institute of Metabolic Science, Addenbrooke’s Hospital, Cambridge, UK) for the GLP-1R mAb, E. Fernández Valle and David Moreno Molera (BiolmaC, UCM, Madrid) for assisting in the body composition analysis and Angela Montes-San Lorenzo for technical assistance. We also acknowledge all members of A.M.V.’s laboratory for helpful discussions.

Author contributions

Conceptualization: A.M.V., M.P.V. and J.G.; Funding acquisition: A.M.V., G.S., L.H., D.S., S.F.-V., J.V., N.V., R.Z., R.S., P.A., M.S. and M.J.M.-A.; Investigation: M.P.V., L.R., C.F., P.R., B.G., M.S., A.B.H., J.F., V.F., C.E.-G., S.Z., M.C.-D., P.M., I.G.-M., E.M.-M., D.G., R.A., A.M., N.S., I.V.-U., N.V., J.M.A.-M., C.Z. and D.H.; Supervision: A.M.V., M.P.V., C.M.R. and J.G.; Writing—original draft: A.M.V., M.P.V. and J.G. and Review and editing: C.F., P.R., B.G., M.S., V.F., E.M.-M., A.M., N.S., I.V.-U., N.V., J.M.A.-M., M.J.M.-A., P.A., S.F.-V., J.V., D.S., L.H., R.S., R.Z., G.S., D.H., C.M.R., L.J., J.G. and A.M.V.

Competing interests

D.H., C.M.R., L.J., J.F., and J.G. declare relationships with AstraZeneca (employee/shareholder). The remaining authors declare no competing interests.

Additional information

Supplementary information The online version contains supplementary material available at <https://doi.org/10.1038/s41467-024-54080-w>.

Correspondence and requests for materials should be addressed to M. Pilar Valdecantos or Ángela M. Valverde.

Peer review information *Nature Communications* thanks Joseph Gordon, Yong-ho Lee and the other, anonymous, reviewer(s) for their contribution to the peer review of this work. A peer review file is available.

Reprints and permissions information is available at <http://www.nature.com/reprints>

Publisher’s note Springer Nature remains neutral with regard to jurisdictional claims in published maps and institutional affiliations.

Acknowledgements

This work was funded by grants RTI2018-094052-B-100 funded by MICIU/AEI/10.13039/501100011033/ and by ERDF “A way of making Europe” and PID-2021-122766OB-I00 funded by MICIU/AEI/10.13039/501100011033 and by ERDF/EU, P2022/BMD-7227 (Comunidad de Madrid, Spain) and CIBERdem (ISCIII) to A.M.V. and M.P.V., grants PID2020-114953RB-C21 funded by MICIU/AEI/10.13039/501100011033 to L.H. and D.S., CB06/03/

Open Access This article is licensed under a Creative Commons Attribution-NonCommercial-NoDerivatives 4.0 International License, which permits any non-commercial use, sharing, distribution and reproduction in any medium or format, as long as you give appropriate credit to the original author(s) and the source, provide a link to the Creative Commons licence, and indicate if you modified the licensed material. You do not have permission under this licence to share adapted material derived from this article or parts of it. The images or other third party material in this article are included in the article's Creative Commons licence, unless indicated otherwise in a credit line to the material. If material is not included in the article's Creative Commons licence and your intended use is not permitted by statutory regulation or exceeds the permitted use, you will need to obtain permission directly from the copyright holder. To view a copy of this licence, visit <http://creativecommons.org/licenses/by-nc-nd/4.0/>.

© The Author(s) 2024

M. Pilar Valdecantos ^{1,2,3,26} ✉, **Laura Ruiz**^{1,2,25}, **Cintia Folgueira** ^{4,5,6,25}, **Patricia Rada** ^{1,2,25}, **Beatriz Gomez-Santos** ^{7,8}, **Maite Solas** ^{9,10}, **Ana B. Hitos**^{1,2}, **Joss Field** ¹¹, **Vera Francisco**¹, **Carmen Escalona-Garrido**^{1,2}, **Sebastián Zagmutt**¹², **María Calderon-Dominguez**¹², **Paula Mera**¹², **Irma Garcia-Martinez**^{1,2}, **Elsa Maymó-Masip**^{2,13}, **Diana Grajales**^{1,2}, **Rosa Alen**^{1,2}, **Alfonso Mora** ^{4,5}, **Neira Sáinz**¹⁴, **Irene Vides-Urrestarazu**¹⁴, **Nuria Vilarrasa**^{2,15}, **José M. Arbones-Mainar**^{6,16}, **Carlos Zaragoza** ^{17,18}, **María J. Moreno-Aliaga**^{6,10,14}, **Patricia Aspichueta** ^{7,8,19}, **Sonia Fernández-Veledo** ^{2,13,20}, **Joan Vendrell** ^{2,13,20}, **Dolors Serra** ^{6,12}, **Laura Herrero** ^{6,12}, **Renate Schreiber** ²¹, **Rudolf Zechner**²¹, **Guadalupe Sabio**^{4,5}, **David Hornigold** ¹¹, **Cristina M. Rondinone**^{22,23}, **Lutz Jermutus** ¹¹, **Joseph Grimsby**^{22,24} & **Ángela M. Valverde** ^{1,2,26} ✉

¹Instituto de Investigaciones Biomédicas Sols-Morreale (IIBM), Consejo Superior de Investigaciones Científicas-Universidad Autónoma de Madrid, Madrid, Spain. ²Centro de Investigación Biomédica en Red de Diabetes y Enfermedades Metabólicas Asociadas (CIBERdem), Instituto de Salud Carlos III, Madrid, Spain. ³Faculty of Experimental Science, Universidad Francisco de Vitoria, Pozuelo de Alarcón, Madrid, Spain. ⁴Centro Nacional de Investigaciones Cardiovasculares (CNIC), Instituto de Salud Carlos III, Madrid, Spain. ⁵Centro Nacional de Investigaciones Oncológicas (CNIO), Madrid, Spain. ⁶Centro de Investigación Biomédica en Red de Fisiopatología de la Obesidad y la Nutrición (CIBERobn), Instituto de Salud Carlos III, Madrid, Spain. ⁷Department of Physiology, Faculty of Medicine and Nursing, University of the Basque Country UPV/EHU, Leioa, Spain. ⁸BioBizkaia Health Research Institute, Barakaldo, Spain. ⁹Department of Pharmaceutical Sciences, Division of Pharmacology, University of Navarra, Pamplona, Spain. ¹⁰IdISNA, Navarra Institute for Health Research, Pamplona, Spain. ¹¹Bioscience Metabolism, Research and Early Development, Cardiovascular, Renal and Metabolism (CVRM), BioPharmaceuticals R&D, AstraZeneca, Cambridge, UK. ¹²Department of Biochemistry and Physiology, School of Pharmacy and Food Sciences, Institut de Biomedicina de la Universitat de Barcelona (IBUB), Universitat de Barcelona, Barcelona, Spain. ¹³Department of Endocrinology and Nutrition, Hospital Universitari de Tarragona Joan XXIII, Institut d'Investigació Sanitària Pere Virgili (IISPV), Tarragona, Spain. ¹⁴University of Navarra, Center for Nutrition Research and Department of Nutrition, Food Science and Physiology, 31008 Pamplona, Spain. ¹⁵Obesity Unit and Endocrinology and Nutrition Departments, Hospital Universitari de Bellvitge, IDIBELL, L'Hospitalet de Llobregat, Barcelona, Spain. ¹⁶Adipocyte and Fat Biology Laboratory (AdipoFat), Unidad de Investigación Traslacional, Instituto Aragonés de Ciencias de la Salud (IACS), Hospital Universitario Miguel Servet, Zaragoza, Spain. ¹⁷Centro de Investigación Biomédica en Red en Enfermedades Cardiovasculares (CIBERcv), Instituto de Salud Carlos III, Madrid, Spain. ¹⁸Unidad de Investigación Cardiovascular, Universidad Francisco de Vitoria/Servicio de Cardiología, Instituto Ramón y Cajal de Investigaciones Sanitarias (IRYCIS), Madrid, Spain. ¹⁹Centro de Investigación Biomédica en Red de Enfermedades Hepáticas y Digestivas (CIBERehd), Madrid, Spain. ²⁰Rovira i Virgili University (URV), Tarragona, Spain. ²¹Institute of Molecular Biosciences, University of Graz, 8010 Graz, Austria. ²²Research and Early Development, Cardiovascular, Renal and Metabolic Diseases, BioPharmaceuticals R&D, AstraZeneca Ltd, Gaithersburg, MD, USA. ²³Present address: Pep2Tango Therapeutics Inc., Potomac, MD, USA. ²⁴Present address: Regeneron Pharmaceuticals, Inc., Internal Medicine, Tarrytown, NY, USA. ²⁵These authors contributed equally: Laura Ruiz, Cintia Folgueira, Patricia Rada. ²⁶These authors jointly supervised this work: M. Pilar Valdecantos, Ángela M. Valverde. ✉ e-mail: pvaldecantos@iib.uam.es; avalverde@iib.uam.es